2022

Changing Snowmelt Conditions in the Western Canadian Arctic

Matthew Y. T. Tsui
Wilfrid Laurier University, tsui2680@mylaurier.ca

Changing Snowmelt Conditions in the Western Canadian Arctic

By

Matthew Y. T. Tsui

Bachelor of Arts in Mathematics, Wilfrid Laurier University, 2017

THESIS

Submitted to the Laurier-Waterloo Graduate Program in Geography
Faculty of Arts / Faculty of Graduate and Postdoctoral Studies
in partial fulfilment of the requirements for
Master of Science in Geography
Wilfrid Laurier University

Acknowledgements

Many people have supported since the start of my Master's research application. I would like first like to thank my fiancé, Susan Sham. Thank you for your unconditional support and encouragement all these years from when I first started as an undergraduate research assistant. If not for your love and patience, I would not have to accomplish this project.

Secondly, I would like to thank my mentor and supervisor, Dr. Philip Marsh. Thank you for the opportunity and time you have invested in me, regardless of the diverse background that I came from. Thank you for your appreciation from a mathematical background with limited knowledge in hydrology. Thank you for your mentorship.

Thirdly, much appreciation to Dr. Kevin Shook, who taught me the CRHM and R scripts with incredible patience. Thank you for all the detailed feedback and suggestions that you would always provide me.

Lastly, thank you to Marsh lab group for all your assistance in and out of the field. Thank you for the Catan nights to make lockdown days that much more enjoyable.

Table of Contents

Acknowledgements i
Table of Contents ii
Index of Figures iv
Index of Tables vi
Index of Appendix vii
CHAPTER 1: Introduction 1
1.1 Research Background 1
1.1.1 Climate Change 1
1.1.2 Arctic Warming 2
1.1.3 Changing Snow Cover 3
1.1.4 Snow Albedo 5
1.1.5 Hydrological Modeling 6
1.1.6 The Energy Balance 8
1.1.7 Hydrological Implications 12
1.2 Research Objectives 14
References 15
CHAPTER 2: Multidecadal Changes in Spring Snowmelt in the Western Canadian Arctic 26
Abstract 27
2.1 Introduction 28
2.2 Study Site and Meteorological Data 30
2.2.1 Study Site 30
2.2.2 Dataset and Data Processing 32
2.2.3 Extended Air Temperature 34
2.2.4 Onset, End and Duration of Snowmelt 35
2.2.5 Refreeze Events 36
2.2.6 Numerical and Statistical Analyses 37
2.3 Results 38
2.3.1 Start of Snowmelt (1957 – 2019) 38
2.3.2 Changes in the Start, End and Duration of Snowmelt (1999 – 2019) 39
2.3.3 Meteorological Conditions during the Snowmelt Period 41
2.4 Summary and discussion 47
References 52
CHAPTER 3: Changing Snowmelt Energy Balance in the Western Canadian Arctic 58
Abstract 59
3.1 Introduction 60
3.2 Methods 61
3.2.1 Study Site 61
3.2.2 Model Overview 64
3.2.3 Model Implementation 67
3.2.4 Model Performance Evaluation and Statistical Analyses 69
3.3 Results and Discussion 72
3.4 Conclusion 83
References 86
CHAPTER 4: Conclusion and Recommendations 92

4.1 Summary 92
4.2 Future Implications 93
References 95
Appendix 96

Index of Figures

Figure 2.1: The location of the Trail Valley creek (TVC) main meteorological station (TMM) and upper plateau station (TUP), located 50 km north of Inuvik-A. TVC drains towards an Arctic estuary, the Husky Lakes (Roux et al., 2015). 31

Figure 2.2: The onset of snowmelt at TMM in the period 1957 to 2019 has occurred earlier by 1.4 days/decade. The average start of melt on May 19th is indicated by the horizontal dotted line. 39

Figure 2.3: Over the study period 1999 to 2019, (a) the onset of snowmelt has occurred earlier by seven days/decade, and the end of melt has occurred earlier by 10 days/decade. As a result, (b) the duration of snowmelt in TMM has significantly shortened by 2.5 days/decade. 40

Figure 2.4: The end of winter SWE over the footprint of TMM snow survey measurements have no significant trend. The average SWE is indicated by the horizontal dotted line. 42

Figure 2.5: The meteorological conditions of (a) mean spring air temperature, and (b) refreeze days were averaged from 1957 to 2019 during the snowmelt period. Mean spring air temperature has increased by 0.3 °C/decade, while no significant changes were found in refreeze events. 43

Figure 2.6: Over the melt period, additional meteorological conditions investigated includes (a) relative humidity, (b) wind speed, (c) downward shortwave and longwave radiation, and (d) precipitation. TMM has experienced more humid conditions by 4.3 %/decade. No trends were detected for the remaining four conditions. 45

Figure 2.7: Precipitation phase partitioned based on Kienzle's (2008) method with the default values of hourly temperature threshold $Tt = 1.5\ °C$ and temperature range $Tr = 7.8\ °C$ over the study period from 1999 to 2019. 47

Figure 3.1: The location of the Trail Valley creek (TVC) main meteorological station (TMM) and upper plateau station (TUP), located 50 km north of Inuvik-A. TVC drains towards an Arctic estuary, the Husky Lakes (Roux et al., 2015). 63

Figure 3.2: The end of winter SWE over the footprint of TMM snow survey measurements have no significant trend. The average SWE is indicated by the horizontal dotted line 72

Figure 3.3: (a) The estimated end of melt has occurred earlier by 8.5 days/decade. (b) The estimated duration of the snowmelt period in TMM has significantly shortened by 2.5 days/decade. However, no trends were detected for the simulated duration of snowmelt [CRHM]. 74

Figure 3.4: The comparison for (a) end of the snow-covered period albedo and (b) the duration of snowmelt between observation values and CRHM estimations, based on observed onset of melt. CRHM is evaluated using the coefficient of determination, and complemented by the NSE measure of 0.8 and -0.28 which explains the predictability and sensitivity of the estimation values for albedo and duration of melt, respectively. 76

Figure 3.5: The sum of the energy balance from 1999 to 2019 of net radiation (red), sensible heat flux (grey), latent heat flux (blue), and heat from rainfall (yellow) as a percentage of the total energy required for snowmelt (white) during the snowmelt period. 77

Figure 3.6: The changes to the energy balance during the snowmelt period from 1999 to 2019. No trends were detected from radiative fluxes, and turbulent fluxes of sensible and latent heat, while the energy from precipitation had no apparent changes. 78

Figure 3.7: The average rate of snowmelt (dotted line) estimated from a physically based energy balance snowmelt model in CRHM over a 10-day snowmelt period. There were no significant trends found. 80

Figure 3.8: The energy balance with a high end of winter SWE (h-SWE) of net radiation (h-Qn), sensible heat flux (h-Qh), latent heat flux (h-Qe), and heat from rainfall (h-Qp) as a percentage of the total energy required for melt (h-Qm), with a SWE of 370 mm over a large drift in TMM. 81

Figure 3.9: (a) A positive relationship between the end of winter SWE and Qm over the snowmelt period. (b) The comparison between the energy available for melt from the observed SWE and h-SWE of a nearby big drift site. 82

Index of Tables

Table 2.1: A Summary of trends for the onset of snowmelt, end of the snow-covered period, duration of snowmelt and climate conditions. The MK trend test was used to detect for monotonic trends, accompanied by Theil Sen's slope estimator to calculate for the magnitude of the trend. Significant trends are noted with bolded p-values. 49

Table 3.1: A summary of trends for the onset of snowmelt, end of the snow-covered period, duration of snowmelt and energy balance components. The MK trend test was used to detect for monotonic trends, accompanied by Theil Sen's slope estimator to calculate for the magnitude of the trend. The NSE, MB, and coefficient of determination were used to test the model. Significant trends are noted with bolded p-values. 83

Index of Appendix

Appendix A: A catalog of meteorological instruments used at TMM and TUP, followed by descriptive specifications of each parameter. For this study, data began recording on August 1998 with the Campbell 21X datalogger. In 2006, the datalogger was updated to a CR23X and again to a CR1000 in 2017. Each parameter were measured every half-hour. 96

Appendix B: Model parameter values used for the albedo, PBSM, and EBSM module..... 97

CHAPTER 1: Introduction

1.1 Research Background

1.1.1 Climate Change

Numerous observation data that are supported by climate and surface hydrology models, show that climate change over the northern high latitudes affects the extent, duration, distribution (Comiso et al., 2008; Liston & Hiemstra, 2011; Serreze et al., 2007), and mass of seasonal snow cover (Hansen et al., 2011), which generally leads to a reduction of snow cover on a global (Sessa & Dolman, 2008) and regional (Dietz et al., 2013) scale. However, very little is known about the associated hydrological impacts (Shi et al., 2015). Climate change is a direct result of the increases in concentrations of atmospheric greenhouse gases (IPCC, 2013), this has led to substantial changes to many Earth systems and processes (Debeer et al., 2015). One of the major impacts of climate change is the increasing surface temperatures (Assmann et al., 2019) that may shift precipitation from snowfall to rainfall (Nayak et al., 2010; Shook & Pomeroy, 2012), and changing snow conditions in the 20th century (Lemke et al., 2007). Other changes include shrinking of snow, sea ice, and permafrost, and increasing frequency of extreme events such as heat waves and heavy precipitation (Debeer et al., 2015). Bonsal & Kochtubajda's (2009) climate projections revealed a considerable change in the temperature distribution of less extreme cold months and more warm months. This significantly alters the physical and biological systems, particularly in the high latitudes. For this reason, high latitude regions are more susceptible to climate variations and are expected to experience the greatest impacts due to climate change (Bonsal & Kochtubajda, 2009; Sturm et al., 2005).

1.1.2 Arctic Warming

The Earth surface temperature is a key indicator of climate warming (Debeer et al., 2015; Serreze et al., 2000). The strongest Arctic warming occurred since early 1970s with warming at nearly double the global rate (Fouché et al., 2017; Hinzman et al., 2005; Overland et al., 2004; White et al., 2007), where recent warming appeared strongest in the winter and the spring (~+3 °C) (Bonsal & Kochtubajda, 2009; Shi et al., 2015). Warming above the freezing point melts snow and ice, which exposes surface that are more susceptible in absorbing solar radiation. This increases warming, which leads to the melting of snow and hence furthers warming. The first occurrence of above freezing air temperature and the date after which air temperature remains above 0 °C are important indicators from the winter to spring season. It signifies the end of the winter accumulation period and the beginning of the spring snowmelt period (Marsh et al., 2002). Average annual temperatures have increased approximately 2 °C since the 1930s over the northwestern parts of North America (Dettinger & Cayan, 1995; Karl et al., 1993; Lettenmaier et al.,1994). Serreze and Barry (2012) showed similar results using the Goddard Institute for Space Science temperature dataset over North America. And so, rapid warming in the Arctic has produced significant environmental changes (Hinzman et al., 2005; Krogh & Pomeroy, 2018; Wanishsakpong et al., 2016). Warmer temperatures are driving earlier melt, however, there are many other potential processes that are a consequence of earlier melt, which are poorly understood. For example, how snowmelt rates will respond to climate change (Musselman et al., 2017).

Air temperature ultimately controls the precipitation phase, resulting in either rain or snow. The volume of local precipitation are generally affected by the interaction of the terrain with the local weather and climate (Beniston et al., 2003). Warmer temperatures reduce

snowpack volume (Mote et al., 2005) by shifting precipitation from snowfall to rainfall, resulting in an earlier onset of snowmelt. The separation of precipitation into snowfall or rainfall is one of the most sensitive parameterizations in simulating cold regions hydrological processes (Loth et al., 1993). Therefore, it is critical to partition precipitation phase, especially during the snowmelt period. The changes in precipitation caused by climate change can effectively amplify or diminish spring snowmelt rates (Musselman et al., 2017). In addition to changing physical properties of the snow (Grenfell & Putkonen, 2008; Zhang et al., 2001), rain on snow events cause considerable heating to the snow surface, and would induce earlier snowmelt. Surface temperatures are controlled locally by net radiation and the turbulent fluxes of heat and moisture (Wang & Dickinson, 1995). Therefore, temperature and state of the surface, whether frozen or thawed, would be vital to the change of the energy fluxes between the land and the atmosphere (Hobbie et al., 2000; Molotch & Bales, 2006; Monson et al., 2006).

1.1.3 Changing Snow Cover

Snow covered area greatly influences the surface energy fluxes through its effects on the albedo fraction and temperature of the surface (Debeer & Pomeroy, 2009). Snow cover is known for its distinctive feature of the arctic and subarctic environment, covering the land surface for up to nine months of the year which yields a significant importance to climatology, hydrology, and ecology (Derksen et al., 2009). Each of these systems have an interdependent role connecting processes in the tundra. For example, the interaction between snow and shrubs, driven by wind transport controls snow depth distributions and affects the surface energy balance and spring snowmelt runoff (Sturm et al., 2001). Snow plays an extremely important role to the water and energy fluxes of Arctic regions (Marsh & Pomeroy, 1996), and as well, to water resource management (Seidel et al., 2016). Snow is generally assumed to accumulate when precipitation

as snow coincides with sub-freezing daily mean air temperature, which becomes a primary source of water around the world. While snow also acts as a water storage reservoir where snow is released in a liquid form during the spring snowmelt, the amount of water stored in a snowpack and its spatial distribution has a crucial impact to the timing, duration, and rate of snowmelt (Lehning et al., 2006; Pomeroy et al., 1998). The melting of snow plays a vital role in the hydrological cycle for irrigation and for the regulation of water supply (Albert & Krajeski, 1998). Therefore, melt water is beneficial to domestic livestock supplies, wildlife habitats, and for recharging soil water resources (Gray & Landine, 1988).

The timing of spring snowmelt is a quantifiable indicator of climate change and plays a crucial role in the feedbacks that amplify Arctic warming (Mioduszewski et al., 2014). Snow cover across the Northern Hemisphere has shown similar earlier trends of snow loss, as a result of warmer temperature and changes in atmospheric circulation (Déry & Brown, 2007; Dye, 2002). Other previous studies over western North America have also shown earlier timing of snowmelt onset (Burn et al., 2004; Moore et al., 2007; Stewart et al. 2005). Brown and Braaten (1998) have shown significant trends to earlier snowmelt in northern and western Canada with the onset of melt shifting earlier each year by 0.2 to 0.6 days per year, while snowmelt end dates shifting earlier by 0.5 to 2.0 days per year. This leads to a shorter snowmelt period (Bavay et al., 2013), which would partly suggest higher melt rate over the spring snowmelt period. Derksen et al. (2014) has observed a decrease in spring snow cover duration at high latitudes over the Canadian tundra. Progressively earlier snowmelt will increasingly challenge many water resource management systems with respect to predictability and seasonal snowmelt and runoff (Stewart et al., 2005). Increased variation of the snowmelt period has significant influence in developing water resources management strategies, and will have extensive hydrological and ecological

impacts, however, this would also depend on the changes in melt rates (Musselman et al., 2017). Monitoring continuous changes of spring snow cover over the Arctic region is a major challenge due to strong local controls on snow cover, and large gaps and biases in surface observational data (Brown et al., 2010). As such, reliable data on spring snow cover change is needed to understand the Arctic climate and to evaluate the representation of snow cover and snow cover feedbacks (Fernandes et al., 2009; Fletcher et al., 2009; Roesch, 2006).

1.1.4 Snow Albedo

The main processes of snow metamorphism are phases that changes from ice to water vapour (sublimation), from ice to liquid water (melting), from water vapor to ice (condensation), and from liquid water to ice (freezing) (Berteaux et al., 2017). Snow is one of the most reflective surfaces and is considered one of the main interfaces between the atmosphere and land surfaces (Pederson et al., 2015), especially during the springtime (Allen & Zender, 2010; Fletcher et al., 2009; Randall, 1994). Surface albedo play a vital role in the surface to atmosphere interactions, as it largely affects the amount of shortwave radiation absorbed. Albedo is defined as the ratio of downward and upward shortwave radiation, which is in the range of 0.3 to 3.0 μm (Colbeck, 1988). Snow generally reflects 70 % to 90 % of downward shortwave radiation in the 0.3 to 2.5 μm range (e.g. the albedo range from 0.7 to 0.9) (Gardner & Sharp, 2010). During the snowmelt season, the albedo of a snow cover is influenced by three factors (Barry, 1996): (1) snow cover characteristics such as surface roughness, snow grain size and shape, liquid water content and snow impurities (Warren, 1982), such as dust and black carbon (Seidel et al., 2016), (2) the solar zenith angle and cloud conditions, and (3) the surface albedo.

Fresh snow with smaller grains typically have higher albedo values, while older snow have lower albedo values (Warren & Wiscombe, 1980) due to thawing and refreezing processes

that would consequently reduce the albedo. Increases of liquid water content in a snowpack and wet snow have lower albedo in comparison to dry snow (Blumthaler & Ambach, 2008). Higher albedo values also have significant impact on the surface energy budget (Meinander et al., 2008). The high albedo reflects more downward solar radiation back to space than snow free surfaces, influencing air temperature and atmospheric circulation patterns (Liston & Elder, 2006). For this reason, the upper surface is subjected to rapidly changing atmospheric conditions (Colbeck, 1988). The loss of snow cover leads to removal of snow earlier, which reduces surface albedo due to increased net radiation (Adam et al., 2009). This feedback mechanism would strongly impact the climate on all temporal and spatial scales (Seidel et al., 2016). Therefore, changes in surface energy can significantly influence snow cover variations over the Arctic (Serreze et al., 2000; Shi et al., 2011).

1.1.5 Hydrological Modeling

Models can be used to quantify the interactions between the atmospheric, terrestrial, and human interference of the Arctic system (Serreze et al., 2000). Hock (2003) found that temperature index models were the most common method for snowmelt modeling due to four main reasons: (1) the availability of air temperature data, (2) air temperature can easily be interpolated and predicted, (3) simple and efficient computation, and (4) good model performance. The temperature index model is based on a melt coefficient, and the temperature difference between the daily average temperature and a base temperature, generally 0 °C (Van Mullem & Garen, 2004). However, the coefficient varies seasonally and by location, and therefore it must change with the changing conditions. This approach is acceptable due to the strong correlation between air temperature and the energy balance (Hock et al., 2006), and has shown to be generally sufficient for the prediction of snow accumulation and snow ablation

(Daly et al., 2000). However, the temperature index method does not perform well due to their lack of physical basis, the need for calibration on a regular basis due to limited snowmelt observations, and neglects sublimation contributions to the snowpack (Pomeroy et al., 2014; Walter et al., 2005). Therefore, multi-decadal changes in snowmelt cannot be explained solely by temperature variations, additional information is required. Further complex approaches can describe the variability in melt as a function of land type, slope and aspect, and other factors. Rango and Martinec (1995) noted the need to replace temperature index models with energy balance models for snowmelt estimations. And so, energy balance models can provide better estimates due to their greater physical basis (Vehviläinen, 1991).

Physically based hydrological models are effective approaches to examine the hydrological response to climate change and can better describe the complex hydrological processes (Fang & Pomeroy, 2020) like the Cold Regions Hydrological Model (CRHM). In contrast to many other hydrological models, CRHM is highly flexible and follows a modular modeling object-oriented structure (Leavesley et al., 1996; Leavesley et al., 2002). A library of process modules can be selected and linked to simulate the hydrological cycle of Hydrological Response Unit (HRU). HRU are spatial units of mass that are normally defined by soil types, vegetation, hillslope or valley bottom. Process modules includes snow transport, interception, evaporation, snowmelt, infiltration, flow, and etc. (Pomeroy et al., 2007). This wide selection of modules permits users to adapt the model to the appropriate complexity based on the objective and available information from the study basin. Each model are described by sets of parameters, state variables and fluxes which includes horizontal fluxes. Due to the flexibility of spatial representation in CRHM from lumped to distributed approaches, it is suitable for data availability and for the purpose of the simulation. Good simulations of model state variables also increase the

confidence of snowmelt estimations and emphasize the value of the physically based approach to represent tundra landscapes (Cordeiro et al., 2017). However, an incorrectly simulated melt event may not only incorrectly predict snowmelt runoff, but also when the actual melt occurs (Walter et al., 2005). A key drawback in hydrological modelling at larger scales is the availability of applicable input data including, precipitation, temperature, and radiation (Marsh et al., 2008; Thorne et al., 2007).

1.1.6 The Energy Balance

The energy balance of a snowpack includes net radiative fluxes, turbulent fluxes of sensible and latent heat, ground heat fluxes, and the energy transfer due to rainfall. The energy available for melt, net shortwave radiation, and change in the internal energy of the snowpack can be distributed throughout the whole vertical extent of the snowpack (Kuusisto, 1986). Snowmelt is generally influenced by physiographic properties such as enhancing turbulent and radiative fluxes (Kumar et al., 2013). Early in the snowmelt period, Mioduszewski et al. (2014) found that snowmelt is primarily controlled by higher levels of radiative energy, followed by turbulent heat fluxes (Marks & Dozier, 1992), while local advection of sensible heat can increase the fluxes at the upwind edge of the snow patches (Marsh et al., 2008). Positive radiation and turbulent heat fluxes imply a gain of energy in the snowpack (Cline, 1997), while negative energy balance will cool the snowpack, increasing its cold content (Marks & Dozier, 1992).

Radiation emitted by the sun is received as shortwave radiation, and emitted by the surface and the atmosphere as longwave radiation (Cotton et al., 2011). The increase in net radiation is well correlated with increased shortwave, whereas longwave radiation does not change much since temperature of the snowpack is mostly isothermal during the snowmelt period. The increased shortwave radiation levels during the spring results in sufficient absorption

within a snowpack to trigger melt, which further reduces surface albedo (Gleason et al., 2019). Therefore, snowmelt may still occur due to shortwave radiation, even when the temperature of the snow surface remains below freezing (Kuusisto, 1986). Longwave radiation dominate the radiative process during the winter and early spring. Under clear sky conditions, downward longwave radiation is dependent on the changes in air temperature and relative humidity (Wang & Dickinson, 1995). Humidity fluctuations typically are associated with different weather systems on a seasonal cycle that is controlled by temperature (Wood et al., 2019). While, under heavy cloud cover, longwave radiation is less negative or even positive and shortwave radiation is reduced due to high cloud albedo and by cloud absorption.

Turbulent fluxes of sensible and latent heat flux are also dominate on cloudy or rainy days over the snowmelt period (Kuusisto, 1986). Sensible heat flux depends on the vertical exchange between snow surface and the overlying atmosphere (Sicart et al., 2008). Direction is primarily defined by the sign of the vertical temperature gradient, upward, when temperature decreases with height, and downward, when temperature increases with height. Energy transported downward where it may be transferred to the snow cover, results in an increased melt on the snowpack (Liston, 1995; Marsh & Pomeroy, 1996). When the snow cover is patchy, and the bare ground warms due to lower albedo, this results in significant transfer of longwave radiation and sensible heat flux from the bare ground to the overlying atmosphere. During the spring snowmelt period, sensible heat flux is generally larger than latent heat fluxes, and as such latent heat has only a minor influence on snow cover (Shi et al., 2013). Latent heat flux is extracted from the snowpack due to evaporation or sublimation during the early stages of snowmelt. Conversely, energy is released during a phase change from water vapor to liquid to solid when condensation onto the snowpack occurs (Van Mullem & Garen, 2004). During cold

nights, when the snow temperature is below 0 °C and refreezes, ice layers are formed. As such, latent heat is released, which enhances snowpack warming. Therefore, increases in turbulent heat fluxes can significantly increase the snowmelt contribution (Marks et al., 2001).

In addition to radiative and turbulent fluxes, advection heat by rainfall has an important influence on the water retention characteristics of snow, however, it has low effects in comparison other energy fluxes (Male & Granger, 1981). When rain falls onto snow surface that is below the freezing point, rainfall cools to the freezing point and sensible heat is released, this would produce melt. Ground heat flux is another small component of the energy balance of the changes in the snowpack. Therefore, it's influence can safely be ignored (Gray & Prowse, 1993). The temperature underlying the snowpack generally increase downward, and as such, heat is transferred upwards to the base of the snowpack.

The cold content of a snow is the amount of energy required to bring its temperature to 0 °C (Marks et al., 2001). For deeper snowpacks, it would require more energy input to overcome the cold content and liquid water holding capacity to initiate snowmelt (Colbeck, 1976), but undergoes a relatively damped diurnal variation of internal energy due to its greater thermal mass (DeBeer & Pomeroy, 2010). On the other hand, shallow snow cover tends to go through larger diurnal variations in internal energy due to overnight cooling and refreezing (Gray & Landine, 1988). The liquid water content increases when air temperatures rise or rainfall occurs (Bartsch et al., 2010). During the warming phase, the absorbed energy raises the average snowpack temperature where it is isothermal at 0 °C. Once the entire snow cover is isothermal, a positive change in snow cover energy must result in snowmelt (Marks & Dozier, 1992). However, it is not realistic to expect the entire snowpack to be always isothermal, for example, temperature at the base, is the same as the surface of the snow (Tuttle & Jacobs, 2019).

Since the first successful study to estimate snowmelt using an energy balance approach by Anderson (1976), various snowmelt models have been developed (e.g. Energy Balance Snowmelt Model (EBSM) (Gray & Landine, 1988), SNTHERM (Jordan, 1991), SHAW (Flerchinger & Saxton, 1989), SnowModel (Liston & Elder, 2006), SNOWPACK (Lehning et al., 2002), and Snobal (Marks et al., 1999)). Due to the differences in objectives specific to each model, there are considerable variations to which snow energetics may be described, as well as forcing data and parameterization requirements (Ellis et al., 2010). In general, more complex snowmelt models require additional information that may limit their success in remote environments, where forcing data and parameter information is restricted or poorly approximated. Understanding and predicting hydrological responses within snowmelt dominated basins to climate variability and change, requires a comprehensive understanding of the energy transfers between the snow surface and the atmosphere that lead to changes in the internal energy of the snowpack, which eventually cause snow to melt (Cline, 1997).

EBSM is based on an energy budget snowmelt model that follows an equation in the energy balance model which governs the energy and mass conservation for the accumulated snow, and are solved together to obtain snowmelt (Kumar et al., 2013). EBSM is capable of estimating snowmelt and streamflow utilizing empirical procedures for estimating radiative, convective, advective, and internal energy terms from daily measurements of air temperature, precipitation, snow cover depth and density, wind speed, shortwave radiation and sunshine hours. The snowmelt model provides better estimates of the occurrences of snowmelt and quantity of melt over a simple temperature index model (Gray & Landine, 1988). One key drawback of EBSM is that the snowmelt model requires a large database of hourly measurements, such as, relative humidity, wind speed, and maximum and minimum air temperature (Gray & Landine,

1988). However, the offset to this disadvantage is that these observations can be measured with relatively simple instruments at meteorological stations.

1.1.7 Hydrological Implications

The melting of snow usually occurs at the surface (Li et al., 2009) during the daytime, whereas nighttime cooling can delay diurnal melting (Sicart et al., 2008). Shallow snowpack may entirely disappear before the areas with a deeper snowpack begin to produce melt (Male & Gray, 1975). Snowmelt is the period of rapid ablation that leads to the disappearance of the seasonal snow cover (Gray & Landine, 1987). When this occurs, snow cover influences evaporation and precipitation (Groisman et al., 2004; Roesch, 2006), which can enhance snowmelt runoff (Fuka et al., 2012). In high latitude, high altitude parts of the world consider snowmelt runoff as the most important component of the hydrological cycle (Gray & Male, 1981). Snowmelt runoff can cause local flooding, soil erosion, and drainage problems (Ohmura, 2001). In the case of extreme precipitation events such as droughts and floods, these events have the greatest impact on human life and the environment, and can be associated with large anomalies in the atmospheric circulation (Trenberth & Guillemot, 1996). As such, snowmelt runoff is expected to intensify as a result of climate change (Matonse et al., 2011; Pradhanang et al., 2013).

The detection of past trends, long term changes and variations are indicators and controls of climate change over the majority of the Northern Hemisphere (Frei & Robinson, 1999; Gray & Male, 1981; Robinson & Frei, 2000), and are necessary for the understanding of potential future changes resulting from anthropogenic activities (Zhang et al., 2001). Numerous studies have attempted to understand the relationship between snow cover observations and hydroclimatic variables, such as air temperature, radiation, precipitation, and runoff. These studies have focused on local scales over individual meteorological stations (Shi et al., 2009;

Westermann et al., 2009) and Trail Valley Creek (TVC) (Marsh & Pomeroy, 1996), regional scales over the Red Valley of North Dakota and Minnesota (Dyer & Mote, 2002), and continental scales over North America or Eurasia (Déry et al., 2005; Groisman et al., 1994a; Tan et al., 2011). Based on past studies, seasonal snowmelt at TVC generally occurs from April to June and is driven by meteorological variables of albedo, air temperature, humidity, precipitation, wind speed and radiation (Marsh et al., 2010).

Snowmelt rates and the timing of melt, which respond to climate change, are poorly known due to inadequate methods of calculations over large areas (Musselman et al., 2017). The timing and the rate of spring snowmelt are essential for the replenishment of water in soils, wetlands, lakes and streams (Pomeroy & Granger, 1997). Snowmelt rates primarily depend on three major sources of thermal energy, convective heat from a warm air mass, net radiative heat, and latent heat changes associated with evaporation or condensation of water vapour (Quick & Pipes, 1977). In a warmer environment, patchy snow cover will be exposed to high energy fluxes that drive higher rates of snowmelt. Heat can be advected horizontally, but normally vertical components of heat flux are considered (Colbeck, 1988). However, when horizontal convection from warmer surfaces does occur, the melt rate is significantly increased. Melt rate calculations can be challenging due to the prevalence of melt below the surface caused by radiative heating (Hoffman et al., 2008; Macdonell et al., 2013). Melt rates are typically non-uniform within individual terrain units (DeBeer & Pomeroy, 2010), and are found highly sensitive to vegetation, slope, and aspect (Pomeroy & Granger, 1997; Pomeroy et al., 2003). For this reason, melt rate can affect streamflow production (Westerling et al., 2006), with high melt rates resulting in higher runoff and soil infiltration (Granger & Male, 1978), which are important considerations

for water resource management. The shifts in snowmelt driven runoff are linked to warmer winters, smaller snowpacks, and the transition from snowfall to rainfall in the winter and spring.

1.2 Research Objectives

Numerous studies, using both observation data and models, have outlined that anthropogenic warming is resulting in earlier snowmelt, but there are considerable uncertainties on how snowmelt timing and rates of melt have changed in the past decades. Given these research gaps, the primary objective of this thesis is to understand and quantify details of changes in snowmelt at a representative site in the Canadian Arctic between 1999 and 2019. Specifically, the objectives are:

Objective (1): Evaluate the changes in snowmelt onset and duration, and the changes in meteorological conditions during the melt period;
Objective (2): Estimate the magnitude of snowmelt and observe the changes to the each of the energy balance components during the melt period.

References

Adam, J. C., Hamlet, A. F., & Lettenmaier, D. P. (2009). Implications of global climate change for snowmelt hydrology in the twenty-first century. *Hydrological Processes*, *23*, 962–972. https://doi.org/10.1002/hyp

Albert, M., & Krajeski, G. (1998). A fast, physically based point snowmelt model for use in distributed applications. *Hydrological Processes*, *12*(1011), 1809–1824. https://doi.org/10.1002/(sici)1099-1085(199808/09)12:10/11<1809::aid-hyp696>3.3.co;2-x

Allen, R. J., & Zender, C. S. (2010). Effects of continental-scale snow albedo anomalies on the wintertime Arctic oscillation. *Journal of Geophysical Research*, *115*(D23105), 1–20. https://doi.org/10.1029/2010JD014490

Anderson, E. A. (1976). *A point energy and mass balance model of a snow cover*. Washington, DC, USA: National Oceanic and Atmospheric Administration.

Assmann, J. J., Myers-Smith, I. H., Phillimore, A. B., Bjorkman, A. D., Ennos, R. E., Prevéy, J. S., Henry, G. H. R., Schmidt, N. M., & Hollister, R. D. (2019). Local snow melt and temperature—but not regional sea ice—explain variation in spring phenology in coastal Arctic tundra. *Global Change Biology*, *25*(7), 2258–2274. https://doi.org/10.1111/gcb.14639

Barry, R. G. (1996). The parameterization of surface albedo for sea ice and its snow cover. *Progress in Physical Geography*, *20*(1), 63–79.

Bartsch, A., Kumpula, T., Forbes, B. C., & Stammler, F. (2010). Detection of snow surface thawing and refreezing in the Eurasian arctic with QuikSCAT: Implications for reindeer herding. *Ecological Applications*, *20*(8), 2346–2358. https://doi.org/10.1890/09-1927.1

Bavay, M., Grünewald, T., & Lehning, M. (2013). Response of snow cover and runoff to climate change in high Alpine catchments of Eastern Switzerland. *Advances in Water Resources*, *55*(2013), 4–16. https://doi.org/10.1016/j.advwatres.2012.12.009

Beniston, M., Keller, F., & Goyette, S. (2003). Snow pack in the Swiss Alps under changing climatic conditions: An empirical approach for climate impacts studies. *Theoretical and Applied Climatology*, *74*, 19–31. https://doi.org/10.1007/s00704-002-0709-1

Berteaux, D., Gauthier, G., Domine, F., Ims, R. A., Lamoureux, S. F., Lévesque, E., & Yoccoz, N. (2017). Effects of changing permafrost and snow conditions on tundra wildlife: critical places and times. *Arctic Science*, *3*(2), 65–90. https://doi.org/10.1139/as-2016-0023

Blumthaler, M., & Ambach, W. (2008). SOLAR UVB-ALBEDO OF VARIOUS SURFACES. *Photochemistry and Photobiology*, *48*(1), 85–88. https://doi.org/10.1111/j.1751-1097.1988.tb02790.x

Bonsal, B. R., & Kochtubajda, B. (2009). An assessment of present and future climate in the Mackenzie Delta and the near-shore Beaufort Sea region of Canada. *International Journal of Climatology*, *29*, 1780–1795. https://doi.org/10.1002/joc.1812

Brown, R. D., & Braaten, R. O. (1998). Spatial and temporal variability of Canadian monthly snow depths, 1946-1995. *Atmosphere - Ocean*, *36*(1), 37–54. https://doi.org/10.1080/07055900.1998.9649605

Brown, R., Derksen, C., & Wang, L. (2010). A multi-data set analysis of variability and change in Arctic spring snow cover extent, 1967-2008. *Journal of Geophysical Research Atmospheres*, *115*(16). https://doi.org/10.1029/2010JD013975

Burn, D. H., Cunderlik, J. M., & Pietroniro, A. (2004). Hydrological trends and variability in the Liard River basin. *Hydrological Sciences Journal*, *49*(1), 53–67. https://doi.org/10.1623/hysj.49.1.53.53994

Cline, D. W. (1997). Snow surface energy exchanges and snowmelt at a continental, midlatitude Alpine site. *Water Resources Research*, *33*(4), 689–701. https://doi.org/10.1029/97WR00026

Colbeck, S. C. (1976). An analysis of water flow in dry snow. *Water Resources Research*, *12*(3), 523–527. https://doi.org/10.1029/WR012i003p00523

Colbeck, Samuel C. (1988). *Snowmelt increase through albedo reduction*. Washington, D.C.

Comiso, J. C., Parkinson, C. L., Gersten, R., & Stock, L. (2008). Accelerated decline in the Arctic sea ice cover. *Geophysical Research Letters*, *35*(January), 1–6. https://doi.org/10.1029/2007GL031972

Cordeiro, M. R. C., Wilson, H. F., Vanrobaeys, J., Pomeroy, J. W., & Fang, X. (2017). Simulating cold-region hydrology in an intensively drained agricultural watershed in Manitoba, Canada, using the Cold Regions Hydrological Model. *Hydrology and Earth System Sciences*, *21*(7), 3483–3506. https://doi.org/10.5194/hess-21-3483-2017

Cotton, W. R., Bryan, G., & van den Heever, S. C. (2011). Radiative Transfer in a Cloudy Atmosphere and Its Parameterization. In *Storm and cloud dynamics : the dynamics of clouds and precipitating mesoscale systems* (2nd Ed., Vol. 99, pp. 143–175). Burlington, MA: Academic Press. https://doi.org/10.1016/S0074-6142(10)09911-0

Daly, S. F., Davis, R., Ochs, E., & Pangburn, T. (2000). An approach to spatially distrubuted snow modelling of the sacramento and San Joaquin basins, California. *Hydrological Processes*, *14*(18), 3257–3271. https://doi.org/10.1002/1099-1085(20001230)14:18<3257::AID-HYP199>3.0.CO;2-Z

DeBeer, C. M., & Pomeroy, J. W. (2010). Simulation of the snowmelt runoff contributing area in a small alpine basin. *Hydrology and Earth System Sciences*, *14*(7), 1205–1219. https://doi.org/10.5194/hess-14-1205-2010

Debeer, Chris M., Wheater, H. S., Quinton, W. L., Carey, S. K., Stewart, R. E., MacKay, M. D., & Marsh, P. (2015). The Changing Cold Regions Network: Observation, diagnosis and prediction of environmental change in the Saskatchewan and Mackenzie River Basins, Canada. *Science China Earth Sciences*, *58*(1), 46–60. https://doi.org/10.1007/s11430-014-5001-6

Debeer, Christopher M, & Pomeroy, J. W. (2009). Modelling snow melt and snowcover depletion in a small alpine cirque , Canadian Rocky Mountains. *Hydrological Processes*, *23*, 2584–2599. https://doi.org/10.1002/hyp

Derksen, C., English, M., Rees, A., Silis, A., & Toose, P. (2014). Observations of late winter Canadian tundra snow cover properties. *Hydrological Processes*, *28*(12), 3962–3977. https://doi.org/10.1002/hyp.9931

Derksen, C., Silis, A., Sturm, M., Holmgren, J., Liston, G. E., Huntington, H., & Solie, D. (2009). Northwest Territories and Nunavut Snow Characteristics from a Subarctic Traverse: Implications for Passive Microwave Remote Sensing. *Journal of Hydrometeorology*, *10*(2), 448–463. https://doi.org/10.1175/2008jhm1074.1

Déry, S. J., & Brown, R. D. (2007). Recent Northern Hemisphere snow cover extent trends and implications for the snow-albedo feedback. *Geophysical Research Letters*, *34*(22), 2–7. https://doi.org/10.1029/2007GL031474

Déry, S. J., Sheffield, J., & Wood, E. F. (2005). Connectivity between Eurasian snow cover extent and Canadian snow water equivalent and river discharge. *Journal of Geophysical Research*, *110*(D23), D23106. https://doi.org/10.1029/2005JD006173

Dettinger, M. D., & Cayan, D. R. (1995). Large-scale atmospheric forcing of recent trends toward early snowmelt runoff in California. *Journal of Climate1*, *8*, 606–623.

Dietz, A. J., Kuenzer, C., & Conrad, C. (2013). Snow-cover variability in central Asia between 2000 and 2011 derived from improved MODIS daily snow-cover products. *International Journal of Remote Sensing*, *34*(11), 3879–3902. https://doi.org/10.1080/01431161.2013.767480

Dye, D. G. (2002). Variability and trends in the annual snow-cover cycle in Northern Hemisphere land areas , 1972 – 2000. *Hydrological Processes*, *16*(15), 3065–3077. https://doi.org/10.1002/hyp.1089

Dyer, J. L., & Mote, T. L. (2002). Role of energy budget components on snow ablation from a mid-latitude prairie snowpack. *Polar Geography*, *26*(2), 87–115. https://doi.org/10.1080/789610133

Ellis, C. R., Pomeroy, J. W., Brown, T., & MacDonald, J. (2010). Simulation of snow accumulation and melt in needleleaf forest environments. *Hydrology and Earth System Sciences*, *14*(6), 925–940. https://doi.org/10.5194/hess-14-925-2010

Fang, X., & Pomeroy, J. (2020). Diagnosis of future changes in hydrology for a Canadian Rocky Mountain headwater basin. *Hydrology and Earth System Sciences Discussions*, *d*(January), 1–40. https://doi.org/10.5194/hess-2019-640

Fernandes, R., Zhao, H., Wang, X., Key, J., Qu, X., & Hall, A. (2009). Controls on Northern Hemisphere snow albedo feedback quantified using satellite Earth observations. *Geophysical Research Letters*, *36*(L21702), 1–6. https://doi.org/10.1029/2009GL040057

Flerchinger, G. N., & Saxton, K. E. (1989). Simultaneous Heat and Water Model of a Freezing Snow-Residue-Soil System I. Theory and Development. *Transactions of the ASAE*, *32*(2), 565–571. https://doi.org/10.13031/2013.31040

Fletcher, C. G., Hardiman, S. C., Kushner, P. J., & Cohen, J. (2009). The dynamical response to snow cover perturbations in a large ensemble of atmospheric GCM integrations. *Journal of Climate*, *22*(5), 1208–1222. https://doi.org/10.1175/2008JCLI2505.1

Fletcher, C. G., Kushner, P. J., Hall, A., & Qu, X. (2009). Circulation responses to snow albedo feedback in climate change. *Geophysical Research Letters*, *36*, 1–4. https://doi.org/10.1029/2009GL038011

Fouché, J., Lafrenière, M. J., Rutherford, K., & Lamoureux, S. (2017). Seasonal hydrology and

permafrost disturbance impacts on dissolved organic matter composition in High Arctic headwater catchments. *Arctic Science*, *3*(2), 378–405. https://doi.org/10.1139/as-2016-0031

Frei, A., & Robinson, D. A. (1999). Northern Hemisphere snow extent: Regional variability 1972-1994. *International Journal of Climatology*, *19*(14), 1535–1560. https://doi.org/10.1002/(SICI)1097-0088(19991130)19:14<1535::AID-JOC438>3.0.CO;2-J

Fuka, D. R., Easton, Z. M., Brooks, E. S., Boll, J., Steenhuis, T. S., & Walter, M. T. (2012). A Simple Process-Based Snowmelt Routine to Model Spatially Distributed Snow Depth and Snowmelt in the SWAT Model. *Journal of the American Water Resources Association*, *48*(6), 1151–1161. https://doi.org/10.1111/j.1752-1688.2012.00680.x

Gardner, A. S., & Sharp, M. J. (2010). A review of snow and ice albedo and the development of a new physically based broadband albedo parameterization. *Journal of Geophysical Research: Earth Surface*. Blackwell Publishing Ltd. https://doi.org/10.1029/2009JF001444

Gleason, K. E., McConnell, J. R., Arienzo, M. M., Chellman, N., & Calvin, W. M. (2019). Four-fold increase in solar forcing on snow in western U.S. burned forests since 1999. *Nature Communications*, *10*(1), 1–8. https://doi.org/10.1038/s41467-019-09935-y

Granger, R. J., & Male, D. H. (1978). Melting of a Prairie Snowpack. *Journal of Applied Meteorology*, *17*, 1833–1842.

Gray, D. M., & Landine, P. G. (1987). Albedo model for shallow prairie snow covers, (Canada). *Canadian Journal of Earth Sciences*, *24*(9), 1760–1768. https://doi.org/10.1139/e87-168

Gray, D. M., & Landine, P. G. (1988). An energy-budget snowmelt model for the Canadian Prairies. *Canadian Journal of Earth Sciences*, *25*(8), 1292–1303. https://doi.org/10.1139/e88-124

Gray, D. M., & Male, D. H. (1981). *Handbook of snow : principles, processes, management & use*. Toronto, Canada: Pergamon Press.

Gray, D. M., & Prowse, T. D. (1993). Snow and Floating Ice. In *Handbook of Hydrology* (pp. 631–653). New York, New York, USA: McGraw Hill Publishing Co. Retrieved from https://www.mheducation.ca/handbook-of-hydrology-9780070397323-can

Grenfell, T. C., & Putkonen, J. (2008). A method for the detection of the severe rain-on-snow event on Banks Island, October 2003, using passive microwave remote sensing. *Water Resources Research*, *44*(3), 1–9. https://doi.org/10.1029/2007WR005929

Groisman, P. Y., Karl, T. R., Easterling, D., & Lawrimore, J. (2004). Contemporary Changes of the Hydrological Cycle Over the Contiguous United States : Trends Derived From In Situ Observations Contemporary Changes of the Hydrological Cycle over the Contiguous United States : Trends Derived from In Situ Observations. *Journal of Hydrometeorology*, *5*(1), 65–85. https://doi.org/10.1175/1525-7541(2004)005<0064

Groisman, P. Y., Karl, T. R., & Knight, R. W. (1994). Changes of snow cover, temperature, and radiative heat balance over the Northern Hemisphere. *Journal of Climate*, *7*, 1633–1656.

Hansen, B. B., Aanes, R., Herfindal, I., Kohler, J., Sæther, B. E., & Oli, M. K. (2011). Climate, icing, and wild arctic reindeer: Past relationships and future prospects. *Ecology*, *92*(10), 1917–1923. https://doi.org/10.1890/11-0095.1

Hinzman, L. D., Bettez, N. D., Bolton, R. W., Chapin, F. S., Dyurgerov, M. B., Fastie, C. L., Griffith, B., Hollister, R. D., Hope, A., Huntington, H. P., Jensen, A. M., Jia, G. J., Jorgenson, T., Kane, D. L., Klein, D. R., Kofinas, G., Lynch, A. H., Lloyd, A. H., McGuire, A. D., Nelson, F. E., …, & Yoshikawa, K. (2005). Evidence and Implications of Recent Climate Change in Northern Alaska and Other Arctic Regions, Climatic Change. *Climatic Change*, *72*, 251–298. https://doi.org/10.1007/s10584-005-5352-2

Hobbie, S. E., Schimel, J. P., Trumbore, S. E., & Randerson, J. R. (2000). Controls over carbon storage and turnover in high-latitude soils. *Global Change Biology*, *6*, 196–220. https://doi.org/10.1046/j.1365- 2486.2000.06021.x, 2000

Hock, R. (2003). Temperature index melt modelling in mountain areas. *Journal of Hydrology*, *282*(1–4), 104–115. https://doi.org/10.1016/S0022-1694(03)00257-9

Hock, R., Rees, G., Williams, M. W., & Ramirez, E. (2006). Contribution from glaciers and snow cover to runoff from mountains in different climates. *Hydrological Processes*, *20*(10), 2089–2090. https://doi.org/10.1002/hyp.6206

Hoffman, M. J., Fountain, A. G., & Liston, G. E. (2008). Surface energy balance and melt thresholds over 11 years at Taylor Glacier, Antarctica. *Journal of Geophysical Research: Earth Surface*, *113*(4). https://doi.org/10.1029/2008JF001029

IPCC. (2013). *Climate change 2013: the physical science basis. Contribution of Working Group I to the Fifth Assessment Report of the Intergovernmental Panel on Climate Change*. Cambridge University Press, Cambridge, UK.

Jordan, R. (1991). *A One-dimensional temperature model for a snow cover, technical documentation for SNTHERM. US Army Corps of Engineers Cold Regions Research and Engineering Laboratory*. Hanover, New Hampshire.

Karl, T. R., Groisman, P. Y., Knight, R. W., Richard, R., Karl, T. R., Groisman, P. Y., & Knight, R. W. (1993). Recent Variations of Snow Cover and Snowfall in North America and Their Relation to Precipitation and Temperature Variations Published by : American Meteorological Society Stable URL : https://www.jstor.org/stable/26197310 REFERENCES Linked references are. *Journal of Climate*, *6*(7), 1327–1344.

Krogh, S. A., & Pomeroy, J. W. (2018). Recent changes to the hydrological cycle of an Arctic basin at the tundra-taiga transition. *Hydrology and Earth System Sciences*, *22*(7), 3993–4014. https://doi.org/10.5194/hess-22-3993-2018

Kumar, M., Marks, D., Dozier, J., Reba, M., & Winstral, A. (2013). Evaluation of distributed hydrologic impacts of temperature-index and energy-based snow models. *Advances in Water Resources*, *56*, 77–89. https://doi.org/10.1016/j.advwatres.2013.03.006

Kuusisto, E. (1986). The energy balance of a melting snow cover in different environments (Finland). *Modelling Snowmelt-Induced Processes. Proc. Budapest Symposium, 1986*, (155), 37–45.

Leavesley, G. H., Markstrom, S. L., Brewer, M. S., & Viger, R. J. (1996). The Modular Modeling System (MMS) - The physical process modeling component of a database-centered decision support system for water and power management. *Water, Air, and Soil Pollution*, *90*(1–2), 303–311. https://doi.org/10.1007/BF00619290

Leavesley, G. H., Markstrom, S. L., Restrepo, P. J., & Viger, R. J. (2002). A modular approach to addressing model design, scale, and parameter estimation issues in distributed hydrological modelling. *Hydrological Processes*, *16*(2), 173–187. https://doi.org/10.1002/hyp.344

Lehning, M., Bartelt, P., Brown, B., & Fierz, C. (2002). A physical SNOWPACK model for the Swiss avalanche warning Part III: Meteorological forcing, thin layer formation and evaluation. *Cold Regions Science and Technology*, *35*(3), 169–184. https://doi.org/10.1016/S0165-232X(02)00072-1

Lehning, M., Völksch, I., Gustafsson, D., Nguyen, T. A., Stähli, M., & Zappa, M. (2006). ALPINE3D: a detailed model of mountain surface processes and its application to snow hydrology. *Hydrological Processes*, *20*(10), 2111–2128. https://doi.org/10.1002/hyp.6204

Lemke, P., Ren, J. F., Allison, I., & Carrasco, J. F. (2007). *Observations: Changes in Snow, Ice and Frozen Ground. In: Climate Change 2007: The Physical Science Basis. Contribution of Working Group I to the Fourth Assessment Report of the Intergovernmental Panel on Climate Change*. Cambrdige, U.K. and New York.

Lettenmaier, D. P., Wood, E. F., & Wallis, J. R. (1994). Hydro-Climatological Trends in the Continental United States , 1948 – 88. *Journal of Climate*, *7*(4), 586–607.

Li, W., Sun, S., Wang, B., & Liu, X. (2009). Numerical Simulation of Sensitivities of Snow Melting to Spectral Composition of the Incoming Solar Radiation. *Advances in Atmospheric Sciences*, *26*(3), 403–412. https://doi.org/10.1007/s00376-009-0403-7

Liston, G. E. (1995). Local advection of momentum, heat, and moisture during the melt of patchy snow covers. *Journal of Applied Meteorology*, *34*(7), 1705–1715. https://doi.org/10.1175/1520-0450-34.7.1705

Liston, Glen E., & Elder, K. (2006). A distributed snow-evolution modeling system (snowmodel). *Journal of Hydrometeorology*, *7*(6), 1259–1276. https://doi.org/10.1175/JHM548.1

Liston, Glen E., & Hiemstra, C. A. (2011). The Changing Cryosphere : Pan-Arctic Snow Trends (1979 – 2009). *Journal of Climate*, *21*(2001), 5691–5712. https://doi.org/10.1175/JCLI-D-11-00081.1

Loth, B., Graf, H. F., & Oberhuber, J. M. (1993). Snow cover model for global climate simulations. *Journal of Geophysical Research*, *98*(D6). https://doi.org/10.1029/93jd00324

Macdonell, S., Kinnard, C., Mölg, T., Nicholson, L., & Abermann, J. (2013). Meteorological drivers of ablation processes on a cold glacier in the semi-arid Andes of Chile. *Cryosphere*, *7*(5), 1513–1526. https://doi.org/10.5194/tc-7-1513-2013

Male, D. H., & Granger, R. J. (1981). Snow surface energy exchange. *Water Resources Research*, *17*(3), 609–627. https://doi.org/10.1029/WR017i003p00609

Male, D. H., & Gray, D. M. (1975). Problems in Developing A physically Based Snowmelt Model. *Canadian Journal of Civil Engineering*, *2*(4), 474–488. https://doi.org/10.1139/l75-044

Marks, D., Link, T., Winstral, A., & Garen, D. (2001). Simulating snowmelt processes during rain-on-snow over a semi-arid mountain basin. *Annals of Glaciology*, *32*, 195–202.

https://doi.org/10.3189/172756401781819751

Marks, Danny, Domingo, J., Garen, D., Link, T., & Susong, D. (1999). A spatially distributed energy balance snowmelt model for application in mountain basins. *Hydrological Processes*, *13*, 1935–1959.

Marks, Danny, & Dozier, J. (1992). Climate and energy exchange at the snow surface in the Alpine Region of the Sierra Nevada: 2. Snow cover energy balance. *Water Resources Research*, *28*(11), 3043–3054. https://doi.org/10.1029/92WR01483

Marsh, P., Bartlett, P., MacKay, M., Pohl, S., & Lantz, T. (2010). Snowmelt energetics at a shrub tundra site in the western Canadian Arctic. *Hydrological Processes*, *24*(25), 3603–3620. https://doi.org/10.1002/hyp.7786

Marsh, P., Onclin, C., & Neumann, N. (2002). Water and energy fluxes in the lower Mackenzie valley, 1994/95. *Atmosphere - Ocean*, *40*(2), 245–256. https://doi.org/10.3137/ao.400211

Marsh, P., & Pomeroy, J. (1996). Meltwater fluxes at an arctic forest-tundra site. *Hydrological Processes*, *10*(10), 1383–1400. https://doi.org/10.1002/(SICI)1099-1085(199610)10:10<1383::AID-HYP468>3.0.CO;2-W

Marsh, Philip, Pomeroy, J., Pohl, S., Quiton, W., Onclin, C., Russel, M., Neumann, N., Pietroniro, A., Davison, B., & McCartney, S. (2008). Snowmelt Processes and Runoff at the Arctic Treeline: Ten Years of MAGS Research. *Cold Region Atmospheric and Hydrologic Studies. The Mackenzie GEWEX Experience*, *2*(January), 97–123. https://doi.org/10.1007/978-3-540-75136-6

Matonse, A. H., Pierson, D. C., Frei, A., Zion, M. S., Schneiderman, E. M., Anandhi, A., Mukundan, R., & Pradhanang, S. M. (2011). Effects of changes in snow pattern and the timing of runoff on NYC water supply system. *Hydrological Processes*, *25*(21), 3278–3288. https://doi.org/10.1002/hyp.8121

Meinander, O., Kontu, A., Lakkala, K., Heikkilä, A., Ylianttila, L., & Toikka, M. (2008). Diurnal variations in the UV albedo of arctic snow. *Atmospheric Chemistry and Physics*, *8*(21), 6551–6563. https://doi.org/10.5194/acp-8-6551-2008

Mioduszewski, J. R., Rennermalm, a K., Robinson, D. a, & Mote, T. L. (2014). Attribution of snowmelt onset in Northern Canada. *Journal of Geographical Sciences*, *119*, 9638–9653. https://doi.org/10.1002/2013JD021024

Molotch, N. P., & Bales, R. C. (2006). Comparison of ground-based and airborne snow surface albedo parameterizations in an alpine watershed: Impact on snowpack mass balance. *Water Resources Research*, *42*(5), 1–12. https://doi.org/10.1029/2005WR004522

Monson, R. K., Lipson, D. L., Burns, S. P., Turnipseed, A. A., Delany, A. C., Williams, M. W., & Schmidt, S. K. (2006). Winter forest soil respiration controlled by climate and microbial community composition. *Nature*, *439*(7077), 711–714. https://doi.org/10.1038/nature04555

Moore, J. N., Harper, J. T., & Greenwood, M. C. (2007). Significance of trends toward earlier snowmelt runoff, Columbia and Missouri Basin headwaters, western United States. *Geophysical Research Letters*, *34*(16). https://doi.org/10.1029/2007GL031022

Mote, P. W., Hamlet, A. F., Clark, M. P., & Lettenmaier, D. P. (2005). Declining mountain snowpack in western North America. *American Meteorological Society*, *86*, 39–49.

Musselman, K. N., Clark, M. P., Liu, C., Ikeda, K., & Rasmussen, R. (2017). Slower snowmelt in a warmer world. *Nature Climate Change*, *7*(3), 214–219. https://doi.org/10.1038/nclimate3225

Nayak, A., Marks, D., Chandler, D. G., & Seyfried, M. (2010). Long-term snow, climate, and streamflow trends at the reynolds creek experimental watershed, Owyhee Mountains, Idaho, United States. *Water Resources Research*, *46*(6). https://doi.org/10.1029/2008WR007525

Ohmura, A. (2001). Physical Basis for the Temperature-Based Melt-Index Method. *Journal of Applied Meteorology*, *40*(4), 753–761. https://doi.org/10.1175/1520-0450(2001)040<0753:PBFTTB>2.0.CO;2

Overland, J. E., Spillane, M. C., Percival, D. B., Wang, M., & Mofjeld, H. O. (2004). Seasonal and regional variation of pan-Arctic surface air temperature over the instrumental record. *Journal of Climate*, *17*(17), 3263–3282. https://doi.org/10.1175/1520-0442(2004)017<3263:SARVOP>2.0.CO;2

Pederson, C. A., Gallet, J. C., Strom, J., Gerland, S., Hudson, S. R., Forsstrom, S., Isaksson, E., & Berntsen, T. K. (2015). In situ observations of black carbon in snow and the corresponding spectral surface albedo reduction. *Journal of Geophysical Research: Atmospheres*, *120*, 1476–1489. https://doi.org/10.1002/2014JD022407

Pomeroy, J., Fang, X., Shook, K., & Whitfield, P. (2014). Predicting in Ungauged Basins Using Physical Principles Obtained Using the Deductive, Inductive, and Abductive Reasoning Approach.

Pomeroy, J. W., & Granger, R. J. (1997). Sustainability of the western Canadian boreal forest under changing hydrological conditions. I. Snow accumulation and ablation. *IAHS-AISH Publication*, *240*, 237–242.

Pomeroy, J. W., Gray, D. M., Shook, K. R., Toth, B., Essery, R. L. H., Pietroniro, A., & Hedstrom, N. (1998). An evaluation of snow accumulation and ablation processes for land surface modelling. *Hydrological Processes*, *12*(15), 2339–2367. https://doi.org/10.1002/(SICI)1099-1085(199812)12:15<2339::AID-HYP800>3.0.CO;2-L

Pomeroy, J W, Gray, D. M., Brown, T., Hedstrom, N. R., Quinton, W. L., & Granger, R. J. (2007). The Cold Regions Hydrological Model , a Platform for Basing Process Representation and Model Structure on Physical Evidence. *Hydrological Processes*, *21*(19), 2650–2667. https://doi.org/10.1002/hyp.6787

Pomeroy, John W., Toth, B., Granger, R. J., Hedstrom, N. R., & Essery, R. L. H. (2003). Variation in surface energetics during snowmelt in a subarctic mountain catchment. *Journal of Hydrometeorology*, *4*(4), 702–719. https://doi.org/10.1175/1525-7541(2003)004<0702:VISEDS>2.0.CO;2

Pradhanang, S. M., Mukundan, R., Schneiderman, E. M., Zion, M. S., Anandhi, A., Pierson, D. C., Frei, A., Easton, Z. M., Fuka, D., & Steenhuis, T. S. (2013). Streamflow Responses to Climate Change: Analysis of Hydrologic Indicators in a New York City Water Supply Watershed. *Journal of the American Water Resources Association*, *49*(6), 1308–1326. https://doi.org/10.1111/jawr.12086

Quick, M. C., & Pipes, A. (1977). U.B.C. WATERSHED MODEL. *Hydrological Sciences Journal*, 153–162.

Randall, D. A. (1994). Analysis of snow feedbacks in 14 general circulation models. *Journal of Geophysical Research*, *99*(D10), 20757–20771. https://doi.org/10.1029/94jd01633

Rango, A., & Martinec, J. (1995). Revisiting the Degree-Day Method for Snowmelt Computations. *JAWRA Journal of the American Water Resources Association*, *31*(4), 657–669. https://doi.org/10.1111/j.1752-1688.1995.tb03392.x

Robinson, D., & Frei, A. (2000). Seasonal Variability of Northern Hemisphere Snow Extent Using Visible Satellite Data. *The Professional Geographer*, *52*(2), 307–315. https://doi.org/10.1111/0033-0124.00226

Roesch, A. (2006). Evaluation of surface albedo and snow cover in AR4 coupled climate models. *Journal of Geophysical Research Atmospheres*, *111*(15), 1–18. https://doi.org/10.1029/2005JD006473

Seidel, F. C., Rittger, K., McKenzie Skiles, S., Molotch, N. P., & Painter, T. H. (2016). Case study of spatial and temporal variability of snow cover, grain size, albedo and radiative forcing in the Sierra Nevada and Rocky Mountain snowpack derived from imaging spectroscopy. *Cryosphere*, *10*(3), 1229–1244. https://doi.org/10.5194/tc-10-1229-2016

Serreze, M. C., & Barry, R. G. (2012). *The Arctic Climate System* (Second Edi). New York, USA: Cambridge University Press.

Serreze, M. C., Walsh, J. E., Chapin III, F. S., Osterkamp, T., Dyurgerov, M., Romanovsky, V., … Barry, R. G. (2000). Observational Evidence of Recent Change in the Northern High-Latitude Environment. *Climatic Change*, *46*, 159–207.

Serreze, Mark C, Barrett, A. P., Slater, A. G., Steele, M., Zhang, J., & Trenberth, K. E. (2007). The large-scale energy budget of the Arctic. *Journal of Geophysical Research*, *112*(February), 1–17. https://doi.org/10.1029/2006JD008230

Sessa, R., & Dolman, H. (2008). *Snow Cover*. Rome. Retrieved from http://www.fao.org/3/i0197e/i0197e00.htm

Shi, X., Déry, S. J., Groisman, P. Y., & Lettenmaier, D. P. (2013). Relationships between recent pan-arctic snow cover and hydroclimate trends. *Journal of Climate*, *26*(6), 2048–2064. https://doi.org/10.1175/JCLI-D-12-00044.1

Shi, X., Groisman, P. Y., Déry, S. J., & Lettenmaier, D. P. (2011). The role of surface energy fluxes in pan-Arctic snow cover changes. *Environmental Research Letters*, *6*(3). https://doi.org/10.1088/1748-9326/6/3/035204

Shi, X., Marsh, P., & Yang, D. (2015). Warming spring air temperatures, but delayed spring streamflow in an Arctic headwater basin. *Environmental Research Letters*, *10*(6), 064003. https://doi.org/10.1088/1748-9326/10/6/064003

Shi, X., Sturm, M., Liston, G. E., Jordan, R. E., & Lettenmaier, D. P. (2009). SnowSTAR2002 transect reconstruction using a multilayered energy and mass balance snow model. *Journal of Hydrometeorology*, *10*(5), 1151–1167. https://doi.org/10.1175/2009JHM1098.1

Shook, K., & Pomeroy, J. (2012). Changes in the hydrological character of rainfall on the Canadian prairies. *Hydrological Processes*, *26*(12), 1752–1766. https://doi.org/10.1002/hyp.9383

Sicart, J. E., Hock, R., & Six, D. (2008). Glacier melt, air temperature, and energy balance in different climates: The Bolivian Tropics, the French Alps, and northern Sweden. *Journal of Geophysical Research Atmospheres*, *113*(24), 1–11. https://doi.org/10.1029/2008JD010406

Stewart, I. T., Cayan, D. R., & Dettinger, M. D. (2005). Changes toward earlier streamflow timing across western North America. *Journal of Climate*, *18*(8), 1136–1155. https://doi.org/10.1175/JCLI3321.1

Sturm, M., McFadden, J. P., Liston, G. E., Stuart Chapin, F., Racine, C. H., & Holmgren, J. (2001). Snow-shrub interactions in Arctic Tundra: A hypothesis with climatic implications. *Journal of Climate*, *14*(3), 336–344. https://doi.org/10.1175/1520-0442(2001)014<0336:SSIIAT>2.0.CO;2

Sturm, Matthew, Douglas, T., Racine, C., & Liston, G. E. (2005). Changing snow and shrub conditions affect albedo with global implications. *Journal of Geophysical Research*, *110*(G1), 1–13. https://doi.org/10.1029/2005jg000013

Tan, A., Adam, J. C., & Lettenmaier, D. P. (2011). Change in spring snowmelt timing in Eurasian Arctic rivers. *Journal of Geophysical Research*, *116*(D3), D03101. https://doi.org/10.1029/2010JD014337

Thorne, R., Armstrong, R. N., Woo, M. K., & Martz, L. W. (2007). Lessons from macroscale hydrologic modeling: Experience with the hydrologic model slurp in the mackenzie basin. In *Cold Region Atmospheric and Hydrologic Studies. The Mackenzie GEWEX Experience* (Vol. 2, pp. 397–410). Springer Berlin Heidelberg. https://doi.org/10.1007/978-3-540-75136-6_21

Todd Walter, M., Brooks, E. S., McCool, D. K., King, L. G., Molnau, M., & Boll, J. (2005). Process-based snowmelt modeling: Does it require more input data than temperature-index modeling? *Journal of Hydrology*, *300*(1–4), 65–75. https://doi.org/10.1016/j.jhydrol.2004.05.002

Trenberth, K. E., & Guillemot, C. J. (1996). Physical processes involved in the 1988 drought and 1993 floods in North America. *Journal of Climate*, *9*, 1288–1298.

Tuttle, S. E., & Jacobs, J. M. (2019). Enhanced Identification of Snow Melt and Refreeze Events From Passive Microwave Brightness Temperature Using Air Temperature. *Water Resources Research*, *55*(4), 3248–3265. https://doi.org/10.1029/2018WR023995

Van Mullem, J. A., & Garen, D. (2004). Snowmelt. In *Hydrology National Engineering Handbook* (pp. 1–21). Portland, Oregon.

Vehviläinen, B. (1991). A Physically Based Snowcover Model. In *Recent Advances in the Modeling of Hydrologic Systems* (pp. 113–135). Helsinki, Finland: Kluwer Academic. https://doi.org/10.1007/978-94-011-3480-4_6

Walter, M. T., Brooks, E. S., Mccool, D. K., King, L. G., Molnau, M., & Boll, J. (2005). Process-based snowmelt modeling : does it require more input data than temperature-index modeling ? *Journal of Hydrology*, *300*, 65–75. https://doi.org/10.1016/j.jhydrol.2004.05.002

Wang, K., & Dickinson, R. E. (1995, June 1). A review of global terrestrial evapotranspiration: Observation, modeling, climatology, and climatic variability. *Reviews of Geophysical Research Atmospheres*. Blackwell Publishing Ltd. https://doi.org/10.1029/2011RG000373

Wang, K., & Dickinson, R. E. (2013). Global atmospheric downward longwave radiation at the surface from ground-based observations, satellite retrievals, and reanalyses. *Reviews of Geophysics*, *51*(2), 150–185. https://doi.org/10.1002/rog.20009

Wanishsakpong, W., McNeil, N., & Notodiputro, K. A. (2016). Trend and pattern classification of surface air temperature change in the Arctic region. *Atmospheric Science Letters*, *17*(7), 378–383. https://doi.org/10.1002/asl.668

Warren, S. G. (1982). Optical Properties of Snow. *Review of Geophysics and Space Physics*, *20*(1), 67–89.

Warren, S., & Wiscombe, W. (1980). A model for Spectral Albedo of Snow. II: Snow Containing Atmospheric Aerosols. *Journal of Atmospheric Science*, *37*, 2734–2745. https://doi.org/0022-4928/80/122734-12$07.00

Westerling, A. L., Hidalgo, H. G., Cayan, D. R., & Swetnam, T. W. (2006). Warming and earlier spring increase Western U.S. forest wildfire activity. *Science*, *313*(5789), 940–943. https://doi.org/10.1126/science.1128834

Westermann, S., Lüers, J., Langer, M., Piel, K., & Boike, J. (2009). The annual surface energy budget of a high-arctic permafrost site on Svalbard, Norway. *The Cryosphere Discussions*, *3*(2), 631–680. https://doi.org/10.5194/tcd-3-631-2009

White, D., Hinzman, L., Alessa, L., Cassano, J., Chambers, M., Falkner, K., Francis, J., Gutowski, W. J., Holland, M., Holmes, R. M., Huntington, H., Kane, D., Kliskey, A., Lee, C., McClelland, J., Peterson, B., Rupp, T. S., Straneo, F., Steele, M., Woodgate, R., Yang, D., Yoshikawa, K., & Zhang, T. (2007). The arctic freshwater system: Changes and impacts. *Journal of Geophysical Research: Biogeosciences*, *112*(G4), n/a-n/a. https://doi.org/10.1029/2006jg000353

Wood, W. H., Marshall, S. J., & Fargey, S. E. (2019). Daily measurements of near-surface humidity from a mesonet in the foothills of the Canadian Rocky Mountains, 2005-2010. *Earth System Science Data*, *11*(1), 23–34. https://doi.org/10.5194/essd-11-23-2019

Zhang, X., David Harvey, K., Hogg, W. D., & Yuzyk, T. R. (2001). Trends in Canadian streamflow. *Water Resources Research*, *37*(4), 987–998. https://doi.org/10.1029/2000WR900357

CHAPTER 2: Multidecadal Changes in Spring Snowmelt in the Western Canadian Arctic

Matthew Y.T. Tsui and Philip Marsh. Cold Regions Research Centre, Wilfrid Laurier University, Waterloo, ON N2L 3C5, Canada

Corresponding author: Matthew Y.T. Tsui (email: tsui.myt@gmail.com)

Journal: Arctic Science

Abstract

This study investigates the changes in key aspects of snowmelt in the western Canadian Arctic. Specifically, we will look at changes in the onset of snowmelt and the duration of snowmelt between 1999 and 2019, and extended air temperature between 1957 and 2019. In addition, we will look at changes in eight meteorological variables during the melt period. It was found that the onset of snowmelt occurred 14 days earlier, while the melt period ends 20 days earlier than 20 years ago. As a result, the duration of melt period has decreased by 5 days. During this earlier and shorter melt period, the air temperature and relative humidity have both increased. While these changes were statistically significant, there were no statistically significant changes in SWE, precipitation, wind speed, downward shortwave and longwave radiation, or refreeze events. Future research will consider the effects and the variability of these changes on the snowmelt energy balance.

Keywords: Arctic, snow hydrology, snowmelt onset, snow albedo, climate change

2.1 Introduction

The Arctic snow cover has important controls on weather, climate, and hydrology through the length of snow seasons, snow cover distribution, snow water equivalent (SWE), surface albedo, the timing and rate of snowmelt, and the magnitude of energy and water fluxes (Barnett et al., 2005; Souma & Wang, 2010). Over much of the Arctic, snowmelt seldom occurs during the winter, and the end of winter snow cover is removed during a brief spring snowmelt period (Hinzman et al., 2005; Nicolaus, 2006). The first occurrence of above freezing air temperature, and the date after which air temperature remains above 0 °C, are important indicators of the transition from the winter season to the spring season. This snowmelt period is typically one to three weeks in duration (Anttila et al., 2018), and is defined by the start of melt when air temperatures transition from below to above zero. The snow cover changes from 100% to 0% coverage, and albedo decreases from over 85 % to less than 19 % (Marsh et al., 2010), this can be used as an easily measurable indicator of climate change. However, there are few locations in the Arctic with sufficient, long term data records needed to properly quantify these changes. This brief snowmelt period typically results in the largest stream discharge event of the year, in which over half of the annual precipitation melts within a few weeks (Marsh et al., 2002).

The timing of snowmelt is significant to many aspects of the environment including soil moisture dynamics, vegetation seasonality (Ling & Zhang, 2007), formation and growth of the permafrost active layer (Wilcox et al., 2019), prolonged summer drought periods (Stewart et al., 2005), increased forest fire intensity, duration and frequency (Balch et al., 2017; Dennison et al., 2014), and significant changes in the timing and magnitude of spring snowmelt runoff (Tuttle & Jacobs, 2019).

The Canadian Arctic has experienced recent climate warming, decreasing precipitation (Bush & Lemmen, 2019), and decreasing snow cover (Lesack et al., 2014). The Arctic has shifted to an earlier onset of snowmelt (Burd et al., 2017), and therefore an earlier start to the spring freshet (Burn et al., 2004; Burns et al., 2007). The pan-Arctic spring snowmelt occurred an average of two to four weeks earlier than it did three decades ago (Tedesco et al., 2009; Wang et al., 2013). Significant trends to earlier snowmelt were observed (Brown & Braaten, 1998), and the onset of melt has shifted earlier each year by approximately 0.6 days (Tedesco et al., 2009), while snowmelt end dates have shifted earlier by 0.5 to 2.0 days per year (Debeer et al., 2015). The influence of an earlier snowmelt (Shi et al., 2015) and decreasing snow cover (Brown et al., 2010), has led to a shorter melt period, which would partly suggest higher melt rates during the spring period (Debeer et al., 2015).

Although spring temperature (Assmann et al., 2019) and radiation (Mioduszewski et al., 2014) are key drivers of snowmelt, snowmelt timing is a complex function of air temperature, precipitation, humidity, wind speed, and radiation (Bjorkman et al., 2015; Cortés et al., 2014; Wheeler et al., 2016). The changes of these meteorological variables will change the timing in spring snowmelt (Shi et al., 2015). Therefore, the study of onset, length and temperature of the snowmelt period is of great significance.

Due to the importance of these influencers, we need to focus on these meteorological variables to examine snowmelt at our study site, which can be an indicator of the rest of the western Arctic. The objectives of this paper are to evaluate (1) the changes in the meteorological conditions, and (2) the changes in the onset, end, and duration of the snowmelt period.

2.2 Study Site and Meteorological Data

2.2.1 Study Site

Meteorological observations were obtained from the Trail Valley Creek (TVC) Research Station (Quinton & Marsh, 1999), located in the taiga – tundra ecotone (68.7 °N, 133.5 °W; Figure 2.1). TVC is located in the uplands east of the Mackenzie River Delta and 50 km north of the Inuvik Airport (Inuvik-A), in the Northwest Territories (NWT). The total thickness of the ice-rich continuous permafrost is up to 500 m and is overlain by an active layer ranging from 0.5 m to 0.8 m (Wilcox et al., 2019). The topography is dominated by gently rolling hills and occasional steep sided river valleys, where the overall elevation ranges from 40 m to 187 m above sea level (a.s.l.) (Pohl et al., 2006), with an average of 99 m a.s.l. The TVC watershed consists of shrub tundra, and sparse black spruce forest on hillslopes and in the valley bottoms, over an area of 57 km^2 (Marsh et al., 2002; Marsh et al., 2008).

The watershed has numerous meteorological stations, but we will focus on two of these here, that represent tundra snow cover. The TVC Main Meteorological station (TMM; 69.3 °N, 133.5°W) and the TVC Upper Plateau station (TUP; 68.7 °N, 133.7 °W). TMM is positioned at ~70 m a.s.l. and TUP is positioned at ~170 m a.s.l. (Pohl et al., 2006). The TVC landscape is comprised of 70 % tundra, 21 % shrub tundra, 8 % drift, and 1 % sparse forest (Marsh & Pomeroy, 1996). Both the TMM and TUP stations are situated over shallow tundra snow cover and have measurements of air temperature, relative humidity, wind speed, and downward and upward shortwave and longwave radiation, while TMM also measures precipitation. Missing data for TMM will be supplemented by data from TUP when available. Meteorological instrumentation details are outlined in Appendix A. Although observations began at TVC in 1991

and continues to this day, the data from 1991 to 1998 is not consistently available, and as a result we will only use data from TMM for the period 1999 to 2019.

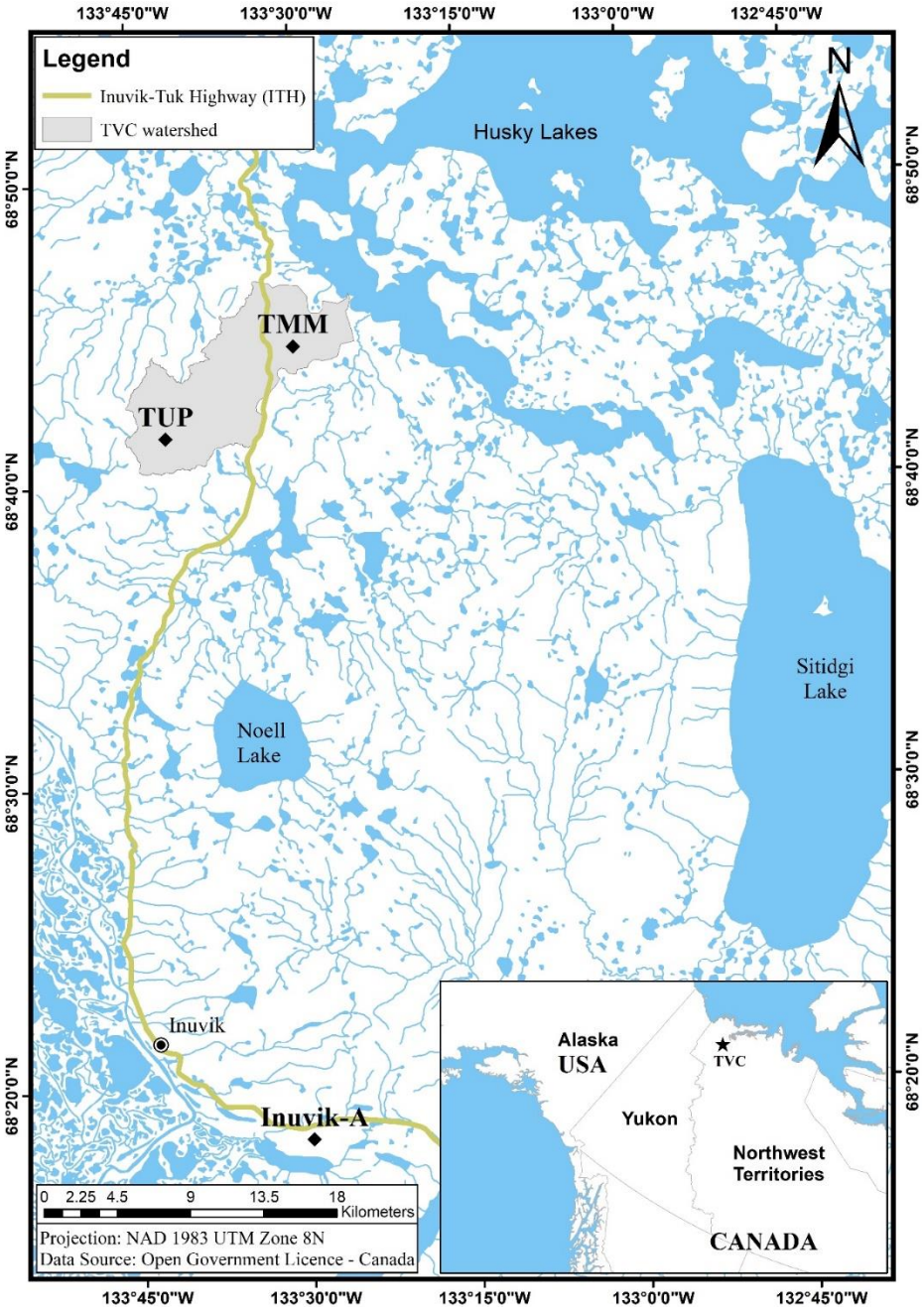

Figure 2.1: The location of the Trail Valley creek (TVC) main meteorological station (TMM) and upper plateau station (TUP), located 50 km north of Inuvik-A. TVC drains towards an Arctic estuary, the Husky Lakes (Roux et al., 2015).

The climate is characterized by short summers and long cold winters. Snowfall accumulates over eight to nine months and melts over a brief one to two week period from mid-May to early June (Pohl et al., 2007), with air temperature averaging -2.6 °C and an average precipitation of 3.1 mm over the melt period. Near the end of winter, air temperatures gradually increase and rise above 0 °C for the first time in late April or early May. This rise above the freezing point is an important indicator of the start of the spring snowmelt period. Air temperature has increased over the study region in the spring, and as a result, the onset of snowmelt has occurred earlier (Shi et al., 2015).

2.2.2 Dataset and Data Processing

A 21-year dataset, from 1999 to 2019, of hourly meteorological conditions for TMM was compiled, accessible online at https://doi.org/10.5683/SP3/MCDA2R. The primary focus is from April 1 to June 30 each year, a period that always includes the start of snowmelt period, when the watershed is 100% snow-covered, to the end of the snow-covered period (Shi et al., 2015). Meteorological conditions were processed through a series of functions written for cold regions hydrological modelling by Shook (2016). These functions included a linear interpolation function to estimate for missing gaps, a conversion of RH to vapour pressure (ea) using temperature and the saturation ratio, Geonor weighing gauge function, quality control of wind speed data, and defining the maximum and minimum thresholds for each variable. Remaining gaps in air temperature, ea, wind speed, downward/upward shortwave and longwave radiation, were gap-filled using data from TUP. TUP was suitable for TMM as they are both situated on shallow tundra snow cover and daily averages fairly similar. The linear interpolation function for this gap filling takes, at minimum, two known pairs of values, before and after, to estimate for the unknown value. The user can set the maximum gap length in timesteps. In this study we used the

default recommendation of five timesteps, as there were no gaps larger than five timesteps within the spring melt period dataset. For the maximum and minimum thresholds: temperature must be within –50 °C to +35 °C; positive wind speeds must not exceed 20 m/s; RH must be within 0 % to 100 %; positive wind speeds; and positive downward and upward shortwave radiation must not exceed 1262 Wm^{-2} and 1000 Wm^{-2} (Shook, 2016).

All precipitation data was gap-filled using the Geonor weighing gauge function (Shook, 2016). This weighing gauge function is a sequence of four main operations that infill, removes spikes, and lastly remove large signals. First, gaps in precipitation data from a weighing gauge were then infilled by linear interpolation. The second procedure removed positive and negative spikes from the decumulated weighing precipitation gauge, including resets. Removed spikes were then infilled by linear interpolation. The third procedure identified small or negative changes to remove jitters and changes due to servicing or gauge reset. Data due to servicing was removed, followed by infill using linear interpolation within the default maximum gap length of three timesteps. The last procedure converted weighing gauged cumulative precipitation to interval values. This function ensures the intervals do not contain any negative values. Any negative values will result in an error. The Geonor use a three-sensor configuration to ensure the continuation of data collection even when one sensor fail. All three sensors in the Geonor weighing gauge were processed by this sequence of functions individually and finally averaged. Lastly, a maximum and minimum test function was used on all conditions to assess whether values exceed maximum or minimum thresholds.

During the melt period, the separation of precipitation during the melt period into rainfall or snowfall, with snow adding to the snowpack can delay melt. On the other hand, rain can enhance melt, and therefore, shorten the melt period. The change of precipitation between liquid

and solid during the melt period is divided into rainfall and snowfall, based on two temperature thresholds and a temperature range. Between the two thresholds, mixed precipitation is composed of rain and partially melted snow. The approach by Kienzle (2008) was employed, as recommended from a study by Harder & Pomeroy (2013). This partitioning method was implemented for the TMM precipitation using default parameters (temperature threshold at 1.5 °C and temperature range at 7.8 °C) by Kienzle (2008). Precipitation (p) was divided by Equation 2.1:

$$p = \begin{cases} P_s, & for\ T < T_s \\ P_m, & for\ T_s < T < T_r \\ P_r, & for\ T > T_r \end{cases} \quad (2.1)$$

where $P_s,\ P_m,\ and\ P_r$ are precipitation as snowfall, mixed precipitation, and rainfall, respectively. Hourly temperature, T, were tested against two thresholds $T_s\ and\ T_r$,to identify rainfall and snowfall.

2.2.3 Extended Air Temperature

Air temperature has been recorded at Inuvik located 50 km to the south since 1957, we will use air temperature data from Inuvik-A in order to extend TMM air temperature to include the period 1957 to 1999 (Environment and Climate Change Canada, 2019). Mean daily air temperature at Inuvik-A for the period April 1 to June 30, is similar to TMM (-1.2 °C from 1999 to 2019 at TMM, compared to 0.1 °C at Inuvik-A). To account for this difference, the Inuvik-A air temperature data was gap-filled and adjusted, using the inverse distance weighting (IDW) interpolation, to be equivalent to the TMM dataset. IDW interpolation takes values from a known location to estimate values at the location of interest. The two datasets were combined to form one dataset that spans the period from 1957 to 2019, and is accessible online at https://doi.org/10.5683/SP3/MCDA2R. The linear interpolation, maximum and minimum

functions by (Shook, 2016), were applied once more to ensure no further gaps exist and was within the threshold boundaries.

2.2.4 Onset, End and Duration of Snowmelt

Although snowmelt is determined by the surface energy balance, the onset of snowmelt can be estimated from when air temperature rises above 0 °C (Malik et al., 2014; Marsh et al., 2002, 1995; Shi et al., 2015). However, using a temperature threshold for a single day may include short duration events that are characterized by small amounts of surface melt and with temperatures soon returning below 0 °C, as melt water refreezes. Such cases do not define the start of the full snowmelt season. Shi et al. (2015) avoided this issue by defining the onset of snowmelt as the first day after the last five consecutive days when the daily mean air temperature is lower than 0 °C. This approach will be used in this study.

The end of the snowmelt period is defined by the removal of the snow cover. However, the Arctic snow cover is spatially variable in depth and SWE, and becomes patchy during the melt period (Marsh et al., 2008). As most snow depth sensors, such as the SR50A used at TVC, have a small footprint (0.45 m clearance radius), they do not provide a good estimation of when the snow cover disappears across a broad area. Instead, this study will rely on the measurement of ground albedo as radiometer sensors, generally have a larger footprint (Colaizzi et al., 2010). For example, the CNR1 has a clearance radius of 1.37 m. Using albedo is a robust way to estimate the removal of the snow cover given the large differences in albedo between snow-covered and snow-free tundra. The calculation of albedo, α, is given by Equation 2.2:

$$\alpha = \frac{K_{\uparrow}}{K_{\downarrow}} \tag{2.2}$$

where $K_{\uparrow}$ is the upward shortwave radiation, and $K_{\downarrow}$ is the downward shortwave radiation. At TMM, the end of winter albedo is typically near 0.8 when the ground is fully snow covered but

with small amounts of shrubs extending above the snow surface, and 0.19 when completely snow free (Marsh et al., 2010). We will use an albedo value of 0.19, a value known to be when the ground at TVC is nearly snow free (Marsh et al., 2010; Thompson et al., 2004), to allow the estimation of the end of the snow-covered period. The duration of snowmelt is defined by the difference between the onset of snowmelt and the end of the snow-covered period. Since the end of snowmelt relies on albedo measurements from TMM, data is only available from 1999 to 2019.

2.2.5 Refreeze Events

Nighttime refreezing of the snow surface is an important control on snowmelt and duration of the melt period. The total daily melt can differ for days with the same day-time melting conditions, but with different nighttime freezing. Nighttime freezing can be attributed to differences in radiative balance which could be related to clear versus cloudy skies or cooler air mass (Sælthun, 1996). In this paper, the magnitude of the refreeze events are estimated using cumulative cooling degree days after the onset of snowmelt (discussed in the next section). Cooling degree days is a measure of how much (in degrees Celsius) and for how long (in days), the air temperature was below a freezing level. Daily temperature was assessed with a base temperature, (T_b), below freezing, and the degree days (DD) was calculated by Equation 2.3:

$$DD = \begin{cases} T_b - T_{daily}, & for\ T_{daily} < 0 \\ 0, & for\ T_{daily} \geq 0 \end{cases} \quad (2.3)$$

where T_b and T_{daily} are the base temperature and daily temperature, respectively. Each degree day was accumulated over the melt period of each year and aggregated to form a 63-year timeseries.

2.2.6 Numerical and Statistical Analyses

In order to test the hypothesis of the changes in meteorological conditions and the changes in onset, end, and duration of snowmelt period, we used the non-parametric Mann Kendall (MK) test (Kendall, 1975; Mann, 1945). This test has been extensively used to test for identifying linear trends in hydrological and meteorological variables (Burn et al., 2004; Déry & Brown, 2007; Hamed, 2008; Krogh & Pomeroy, 2018; Lettenmaier et al., 1994; Shi et al., 2013, 2011; Yip et al., 2012). In addition, we used the Theil Sen's slope estimator (Theil, 1950), and the coefficient of determination, R^2. Tests were applied with a probability level (p-value) of 0.05 (two-sided test). MK estimates are used instead of least square estimates, as it is less inclined to be affected by extreme values or outliers in the data and less sensitive to non-normally distributed variables (Moore et al., 2007). According to Mann (1945), the null hypothesis of randomness H_0 states that the data $(x_1, \dots, x_n)$ are independently and identically distributed (IID) random variables, as shown in Equation 2.4.

$$S = \sum_{k=1}^{n-1} \sum_{j=k+1}^{n} \operatorname{sgn}\left(X_j - X_k\right), \text{ where} \tag{2.4}$$

$$\operatorname{sgn}(x) = \begin{cases} 1 & if\ x > 0 \\ 0 & if\ x = 0. \\ -1 & if\ x < 0 \end{cases}$$

The alternate hypothesis H_a of a two-sided test is that the distribution of x_j and x_i are not identical for all $j, i \leq n\ with\ j \neq i$. The power of the MK test is the probability to reject the null hypothesis, detecting a monotonic (single direction) trend over time.

Theil Sen's slope method is a robust non-parametric slope estimator, used for the determination of trend magnitudes (Lettenmaier et al., 1994) based on Kendall rank correlation, τ, a common application of Kendall test for correlation (Kendall, 1975). This magnitude for

monotonic trends are based on the associated Kendall-Theil robust lines (Theil, 1950). The slope estimator is calculated based on Equation 2.5:

$$d = \frac{x_j - x_i}{j - i}, \quad (2.5)$$

where $1 \leq i < j \leq n$.

The coefficient of determination, also known as the R-squared (R^2) value is a statistical measure that represents the proportion of the variance for a dependent variable that is explained by an independent variable (Cheng et al., 2014). The correlation is statistically significant at a level of p-value of < 0.05. This is a good indicator of how much variation of a dependent variable is explained by the independent variable in a regression model, and how close the data are fitted to the regression line. The R^2 values range from 0 to 1 and is calculated from Equation 2.6:

$$R^2 = 1 - \frac{RSS}{TSS} = 1 - \frac{\sum_{i=1}^{n}(y_i - \hat{y})^2}{\sum_{i=1}^{n}(y_i - \bar{y})^2} \quad (2.6)$$

where the residual sum of squares (RSS) and the total sum of squares (TSS) can be calculated given, the actual value, y_i, the predicted value of y_i, $\hat{y}$, and the mean of the y_i values, $\bar{y}$.

2.3 Results

2.3.1 Start of Snowmelt (1957 – 2019)

For the period of 1957 to 2019, the earliest onset of melt was May 1st in 1991, and the latest was on June 1st in 1959 (Figure 2.2). A large year to year variability was observed, with a 7.1 day standard deviation relative to the mean on May 19th. The two-sided MK-trend analysis shows a significant monotonic downward trend, evaluated by a significance level (p-value) of 0.0026. Over the 63-year record period, the total change in snowmelt onset is approximately nine days, with an increase of -1.4 days per decade. This is a similar trend to that from Shi et al. (2015), for the period of 1985 to 2011.

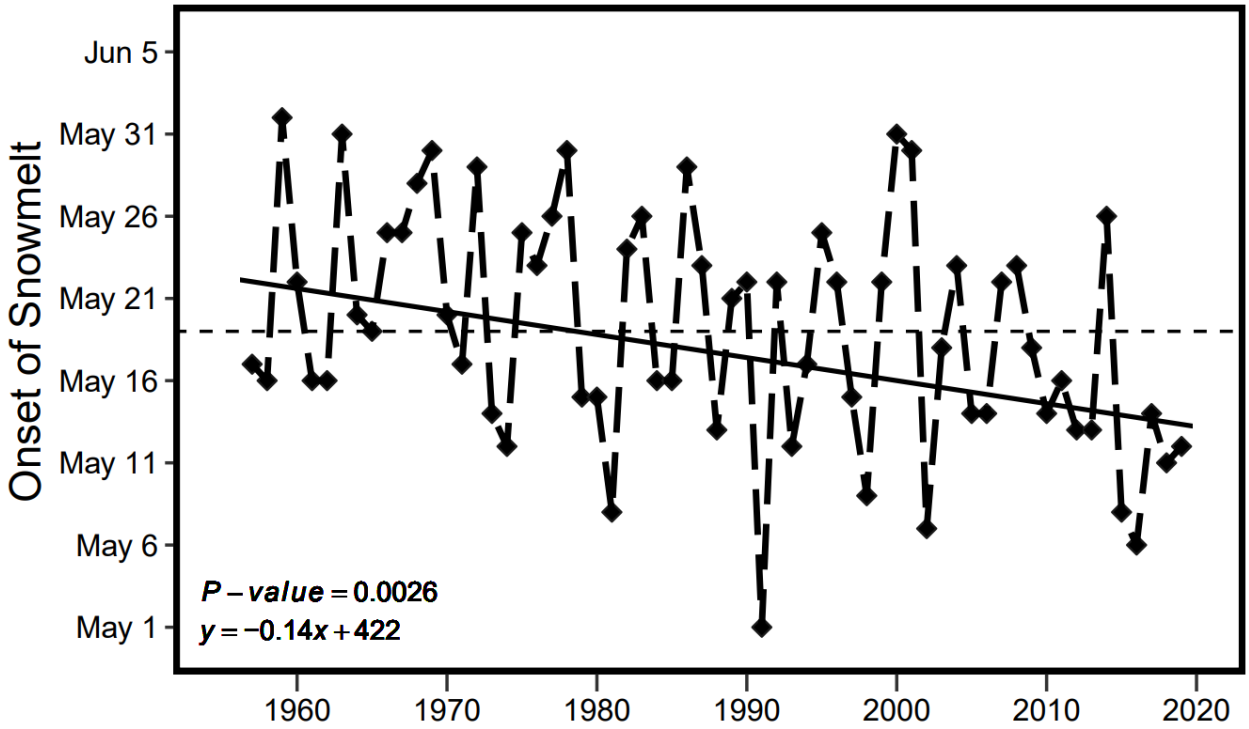

Figure 2.2: The onset of snowmelt at TMM in the period 1957 to 2019 has occurred earlier by 1.4 days/decade. The average start of melt on May 19th is indicated by the horizontal dotted line.

2.3.2 Changes in the Start, End and Duration of Snowmelt (1999 – 2019)

Over the study period 1999 to 2019, the earliest onset of melt occurred on May 5th in 2016, and the latest was on May 31st in 2000, as shown in Figure 2.3a. In contrast to the long-term record period, the average onset of melt is three days earlier on May 16th. The standard deviation for onset of melt is 7.1 days relative to the mean. The two-sided MK-trend analysis shows a significant monotonic downward trend, evaluated by a significance level of 0.0057. Over the study period, the total change in snowmelt onset is approximately 14 days, with an increase of -7 days per decade. This is also similar trend to the 63-year record period, showing a trend towards earlier onset of snowmelt.

Between 1999 and 2019, the end of melt, when snow cover is completely removed, occurs 10 days earlier on average, as shown in Figure 2.3a. The earliest end of melt was recorded on May 14th in 2016 and the latest end of melt was recorded on June 11th in 2000. The two-sided

MK-trend analysis show a significant monotonic downward trend, evaluated by a significance level of 0.00087. The end of melt has occurred earlier by approximately 10 days per decade, a larger change relative to the onset of snowmelt. Similar to the onset of snowmelt, the end of melt yields a large variability over time, with an 8.1 day standard deviation relative to the mean on May 27th.

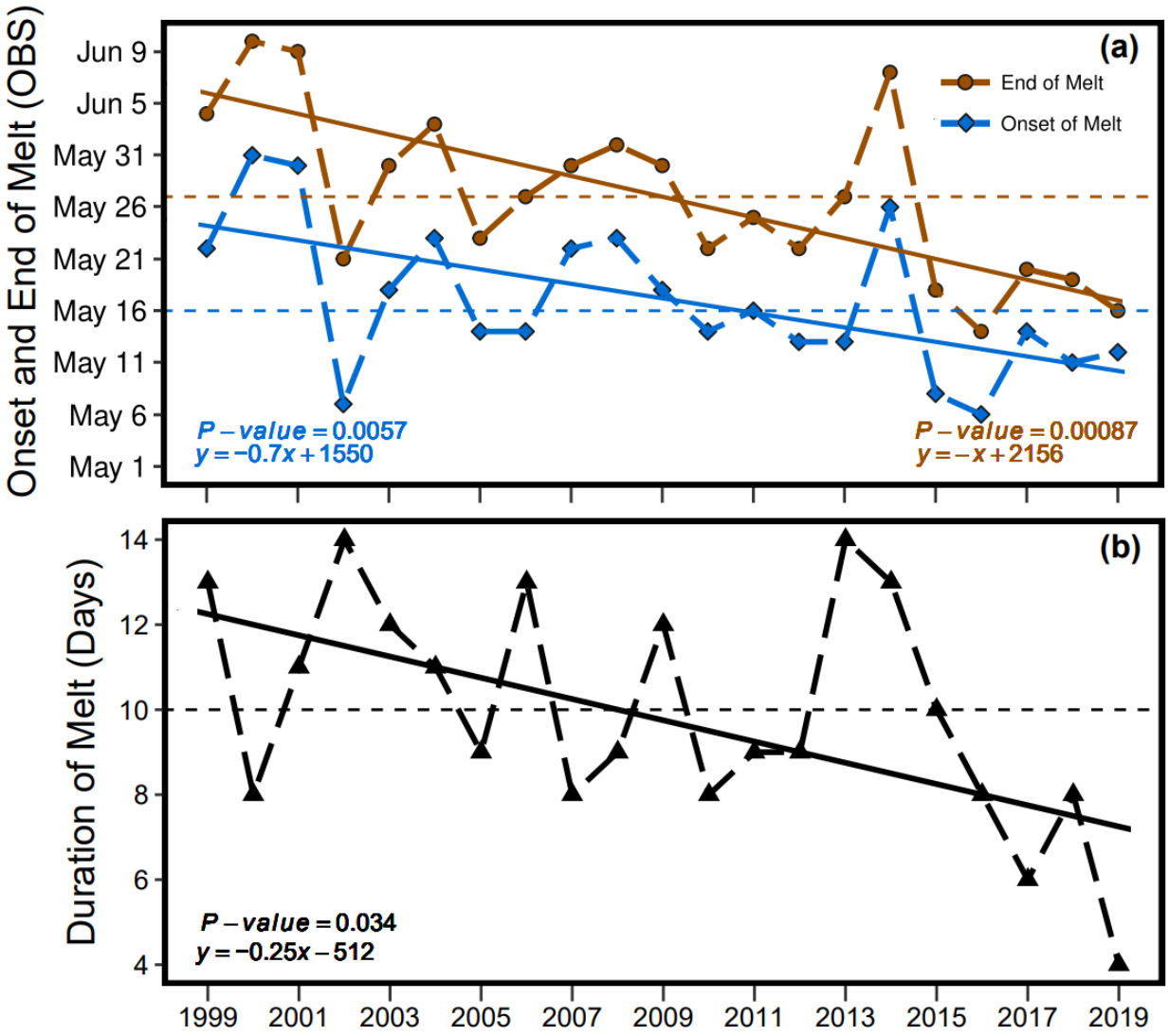

Figure 2.3: Over the study period 1999 to 2019, (a) the onset of snowmelt has occurred earlier by seven days/decade, and the end of melt has occurred earlier by 10 days/decade. As a result, (b) the duration of snowmelt in TMM has significantly shortened by 2.5 days/decade.

The average duration of the snowmelt period over the shallow snow, typical of TMM, was approximately 10 days. In 2019, the duration of snowmelt lasted only four days, while in

2002 and 2013, TMM experienced the longest 14-day duration of snowmelt. Five of the 21-year record had eight days of snowmelt. In the last five years, annual duration of snowmelt was never more than 10 days, with exceptional low in 2017 and 2019 of six days and four days, respectively. The standard deviation for the duration of melt was calculated to be 2.7 days or approximately 27 % of variation relative to the mean. The two-sided MK-trend analysis shows a significant monotonic downward trend at a significance level of 0.034, with the duration of melt decreasing by 2.5 days per decade as shown in Figure 2.3b.

2.3.3 Meteorological Conditions during the Snowmelt Period

Based on the above analysis of the start, end and duration of the melt period, the following considers the primary meteorological conditions during snowmelt. In addition to meteorological conditions, the end of winter SWE is another factor that controls the duration of the melt period. To allow consistency and comparison between years, over the study period between 1999 and 2019, this analysis will focus on the 10-day period (i.e. the average melt period duration) after the start of snowmelt in each year.

End of Winter SWE

The end of winter SWE over the footprint of TMM, averaged 112 mm over the record period, as shown in Figure 2.4. The lowest SWE (80 mm) was measured in 2016, and the highest SWE (181) was measured in 2006. The end of winter SWE varied quite significantly from year to year, with a standard deviation of 23.2 mm or approximately 21 % of the variation from the mean. In the last decade, only two years of measured SWE were higher than the mean. Despite a shallower end of winter snow cover, no trend was detected.

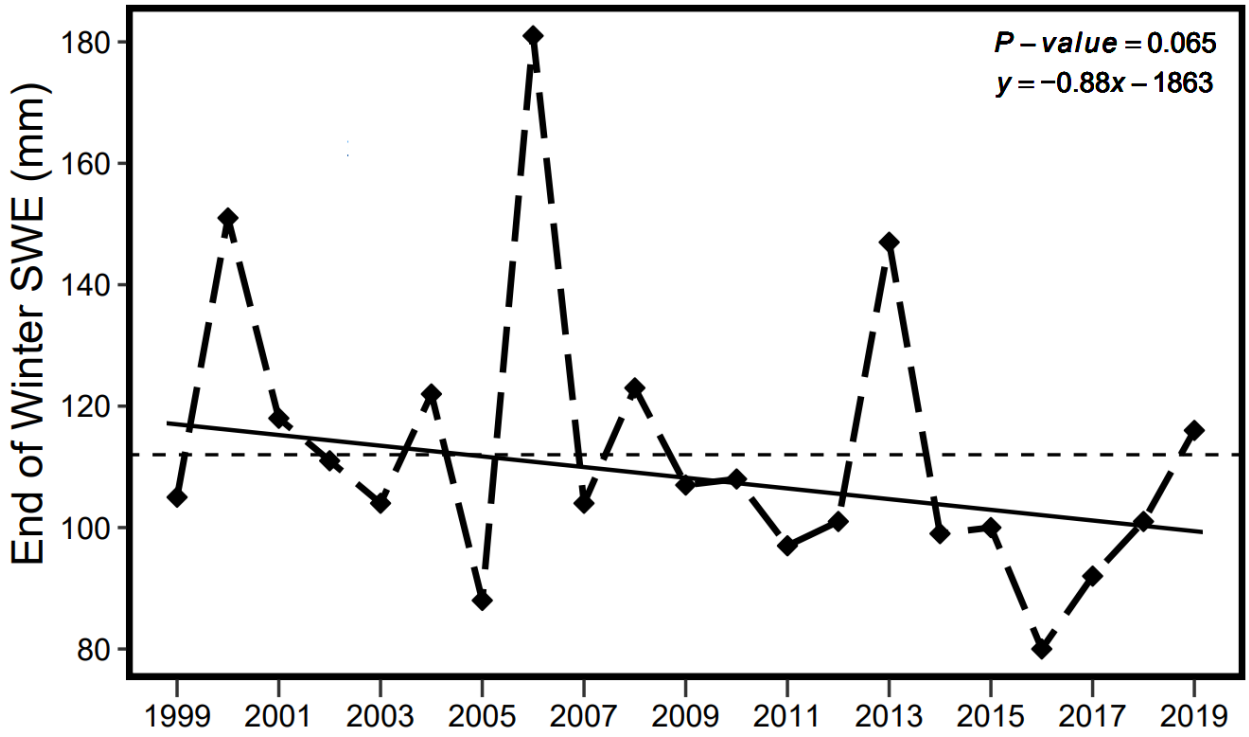

Figure 2.4: The end of winter SWE over the footprint of TMM snow survey measurements have no significant trend. The average SWE is indicated by the horizontal dotted line.

Air Temperature

The mean air temperature over the 63-year snowmelt period at TMM (Figure 2.5a) was 3.5 °C, warming by approximately 0.3 °C per decade. A 2.2 °C standard deviation, or approximately 63 % of variation relative to the mean was calculated, indicating a wide spread in air temperature from year to year. There were three years with average air temperature below freezing. The coldest snowmelt period was -0.4 °C in 1994 and 1980, while in 2013, the snowmelt period was approximately -0.1 °C. The warmest snowmelt period had an average air temperature of 10 °C in 2011, and on three other occasions mean air temperatures were above 7.5 °C. This monotonic upward trend is supported by the MK-trend test at a significance level of 0.046.

Refreezing events

Although an earlier rise in air temperature above 0 °C and rising air temperatures during the melt period suggest both earlier and increased rates of melt, an increase in the number of nighttime refreezing events could extend the melt period. This can occur if these nights are characterized by less cloud cover and greater longwave cooling. The mean number of refreeze days over the period of record was 0.58 days (Figure 2.5b). There was no significant change

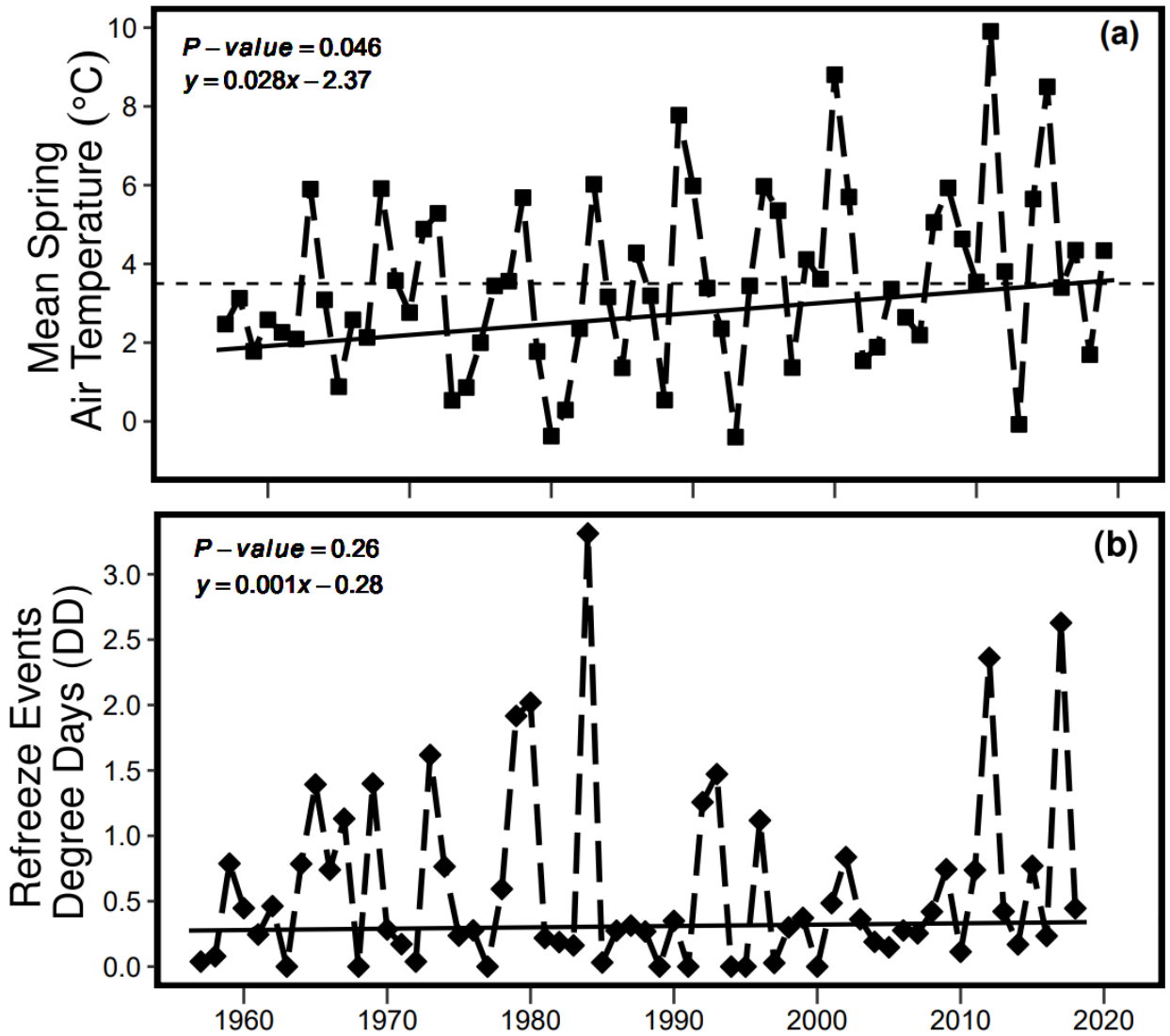

Figure 2.5: The meteorological conditions of (a) mean spring air temperature, and (b) refreeze days were averaged from 1957 to 2019 during the snowmelt period. Mean spring air temperature has increased by 0.3 °C/decade, while no significant changes were found in refreeze events.

found in melt period refreeze events at TMM over the 63-year period. The first half of the period of record (1957 to 1988) averaged 0.62 days, with a standard deviation of 0.76 days, of refreeze events, while the second half (1988 to 2019) averaged 0.53 days of refreeze events, and a standard deviation of 0.63 days. These differences between the two halves of the record reveals less refreeze events in the last 32 years, but fewer differences between years.

Relative Humidity

As air temperature has increased, relative humidity has also increased during the melt period (Figure 2.6a). This monotonic upward trend has a significance level of 0.037 and has increased at a rate of 4.3% per decade. Over the 21-year record period, humidity ranged between 63 % to 84 %, with an average of 76 % when the average temperature was 4.3 °C. In the last decade, seven of the 10 years experienced humidity higher than the mean. While in contrast to the first decade, with only four years above the mean. The dispersion to its mean is relatively small, a standard deviation of 6.1 or approximately 8 % of variation from the mean was calculated.

Wind Speed

The average wind speed during the melt period over the 21-year period of record was 3.4 m/s, with the lowest average wind speed of 2.7 m/s in 2012 (Figure 2.6b). Eight years, including 2012, had wind speeds below the average. Three years had average wind speed higher than 4 m/s, with the highest of 4.2 m/s in 2007. Wind speeds during the melt period varied year to year, but with a relatively small standard deviation of 0.5 m/s or approximately 14 % of the variation from the mean. Despite the year to year variations in wind speed, there were no trends was detected.

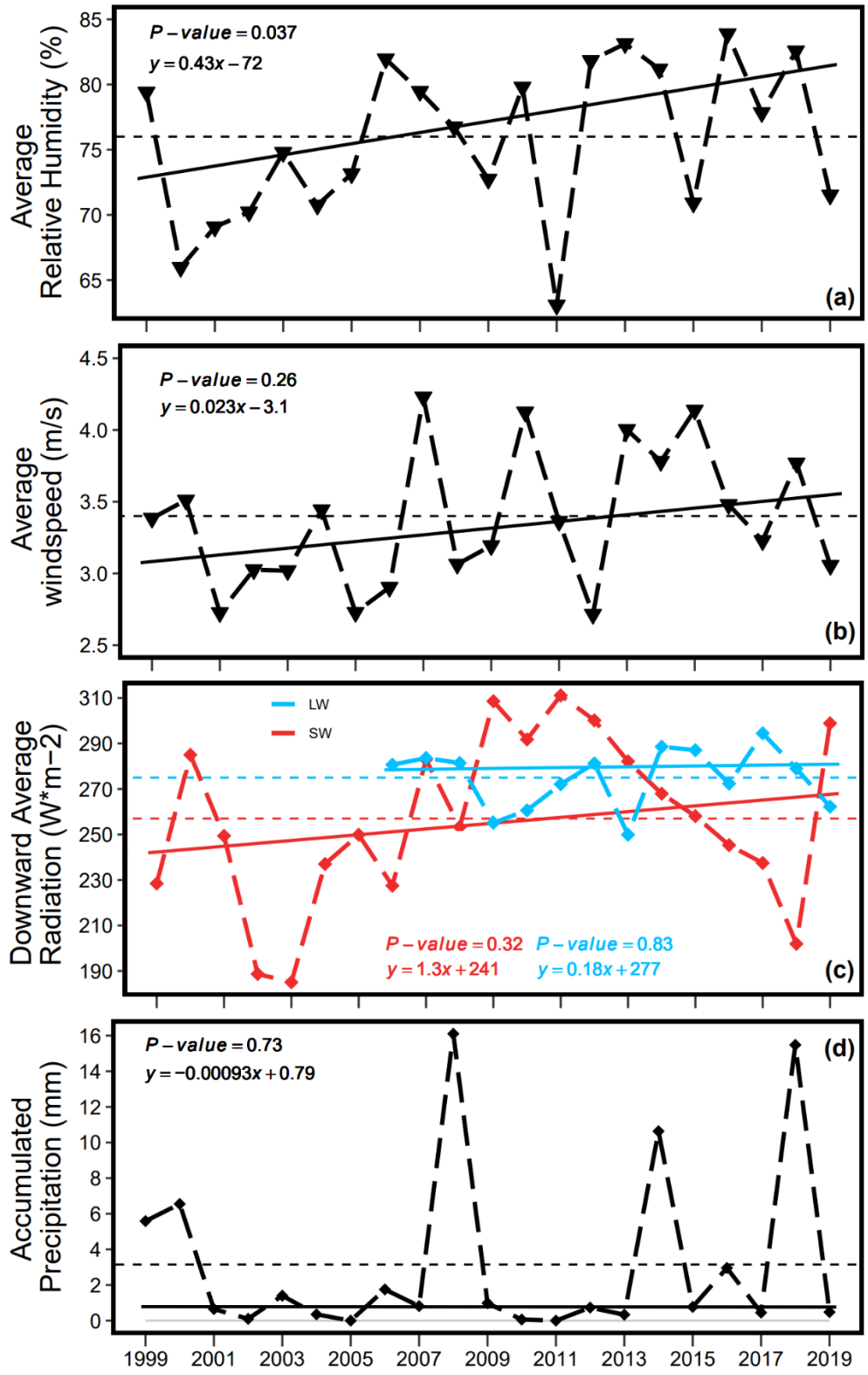

Figure 2.6: Over the melt period, additional meteorological conditions investigated includes (a) relative humidity, (b) wind speed, (c) downward shortwave and longwave radiation, and (d) precipitation. TMM has experienced more humid conditions by 4.3 %/decade. No trends were detected for the remaining four conditions.

Downward Radiation

Longwave radiation data is only available from 2006 onwards, and over this short period of record, the average downward longwave radiation was 275 Wm^{-2} (Figure 2.6c). In 2013, the lowest downward longwave radiation was averaged to be 249 Wm^{-2}, while the highest was seen in 2017 at 295 Wm^{-2}. The standard deviation of downward longwave radiation was calculated to be 13.4 Wm^{-2} or about 4.9 % of the variation relative to its mean. However, longwave radiation has no significant change during the melt period, with no trends detected by the MK-trend test.

Over the 21-year record period, the average downward shortwave radiation was 257 Wm^{-2}. In 2002 and 2003, the lowest averaged downward shortwave radiation of 189 Wm^{-2} and 185 Wm^{-2} was measured at TMM. The highest average value of 311 Wm^{-2} was observed in 2011. The standard deviation for downward shortwave radiation was found to be 37.6 Wm^{-2} or approximately 14.6 % of variation relative to its mean. The MK-trend analysis resulted in a non-monotonic trend at a significance level of 0.32. Over the 21-year record period, there were no trends was detected. Higher energy levels of downward shortwave radiation over the melt period would drive the earlier onset of melt.

Precipitation

The average air temperature was around 5 °C during the three high precipitation events, and as a result, over 95 % of these high precipitation events were mixed precipitation, as shown in Figure 2.7. Over the melt period, the distribution of precipitation consists of snow (2 %), mixed precipitation (97 %), and rain (1 %). Snowfall is typically very small during the melt period and only occurs during the earlier days of the melt period, when temperature is temporarily below freezing. The majority of the precipitation at TMM during the melt period is

mixed rain and snow, when air temperature hovers just under freezing or slightly above 0 °C. By late melt, when air temperature is well above 0 °C, beyond at this point precipitation falls as rain.

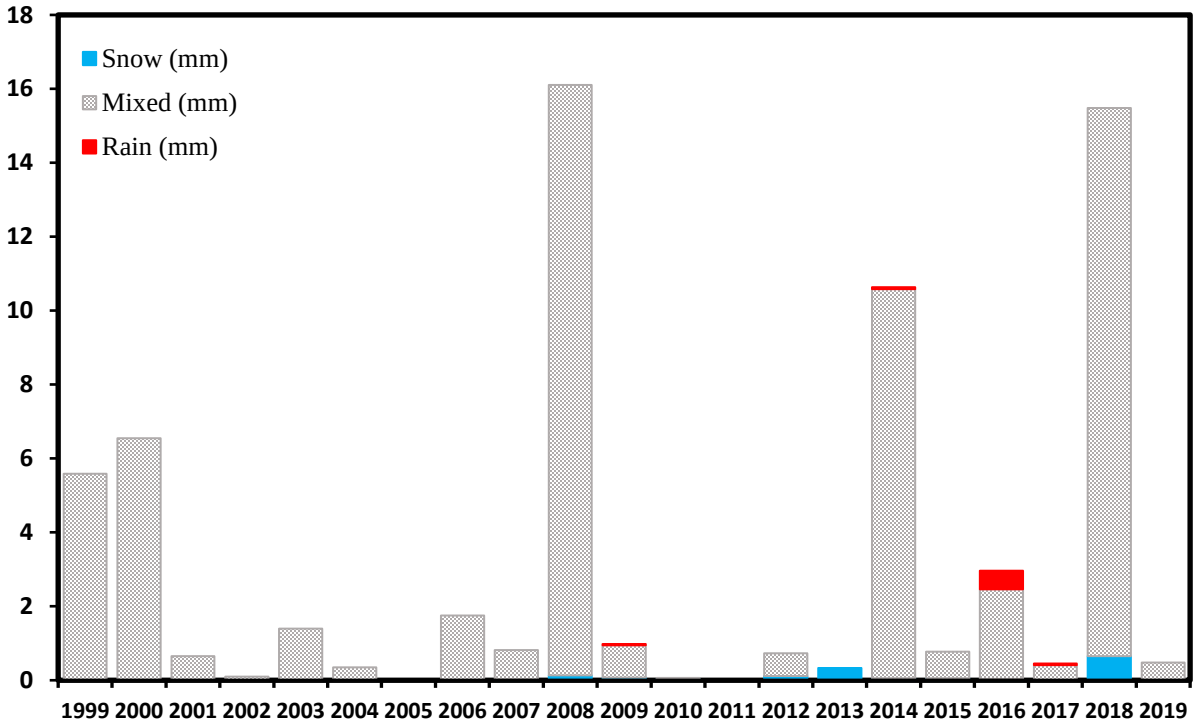

Figure 2.7: Precipitation phase partitioned based on Kienzle's (2008) method with the default values of hourly temperature threshold $T_t = 1.5\,°C$ and temperature range $T_r = 7.8\,°C$ over the study period from 1999 to 2019.

2.4 Summary and discussion

The detection of past trends and changes in meteorological variables (Table 2.1) are essential for the understanding of past changes. This paper has shown an earlier onset of melt, end of melt, and shorten duration of snowmelt. The start of melt is controlled only by meteorological conditions, while the end of melt is controlled by both meteorological conditions during the melt period and end of winter SWE. These changes are associated to significantly increased air temperature and humidity. On the other hand, end of winter SWE, refreeze events, wind speed, downward shortwave and longwave radiation, and precipitation have not changed

significantly. The differences in significance will require additional analysis of their impact to snowmelt timing and duration.

As shown in previous studies, TMM has experienced warming, and more pronounced warming in the spring (Lesack et al., 2014; Shi et al., 2015). The rising temperature induced greater surface melt, resulting in an earlier onset of snowmelt (Hamlet & Lettenmaier, 1999; Mioduszewski et al., 2014; Van Pelt et al., 2016). TMM has experienced an earlier onset of melt and end of melt, and therefore a shortened snowmelt period as snow was removed earlier in the year. As noted in section 2.3, snowmelt onset has occurred earlier at a rate of seven days per decade for the study period of 1999 to 2019. A similar trend was documented in Shi et al.'s (2015) study, an earlier snowmelt onset of 3.3 days per decade for the study period of 1985 to 2011. This drastic change can be critical to the timing and volume of the springtime streamflow. The end of snow-covered period has also experienced an earlier trend, at a rate of 10 days per decade. The year-to-year variation were found to be relatively similar to the onset of melt. In Alaska, Anttila et al. (2018) has documented an early end of melt by 4.3 days per decade for the study period of 1982 to 2015. Therefore, this led to a shorter snowmelt period, which could suggest higher melt rates during the spring period and are implications for possible flooding in flood prone areas. The shortened length of the snowmelt period was well documented across the pan-Arctic between 1979 to 2015 (Anttila et al., 2018; Tedesco et al., 2009). Although spring has occurred earlier, the removal of snow throughout snowmelt period was considerably earlier. And as such, the snowmelt period has shortened.

During the snowmelt period, TMM has experienced a significant warming by 0.3 °C per decade for the study period of 1957 to 2019. The comparison to Shi et al.'s (2015) warming of

0.84 °C per decade for the study period of 1985 to 2011, shows similar warming to other sites around the Arctic region. Krogh & Pomeroy (2018) had also documented a similar warming at a forest site near the Inuvik-A station. Over the last 60 years, northwestern Canada had also recorded an average spring warming of approximately 1.5 °C to 3 °C (Bonsal & Kochtubajda, 2009; Debeer et al., 2015; Pomeroy & Granger, 1997). The increased air temperature is important as it heavily influences the start of the spring melt season.

Table 2.1: A Summary of trends for the onset of snowmelt, end of the snow-covered period, duration of snowmelt and climate conditions. The MK trend test was used to detect for monotonic trends, accompanied by Theil Sen's slope estimator to calculate for the magnitude of the trend. Significant trends are noted with bolded p-values.

Summary Table	*Trend	**Slope (rate per decade)	P-value
SWE	↓	8.8 mm	0.065
Air Temperature	↑	**0.3 °C**	**0.046**
Refreeze Events	↑	0.01 degree days	0.26
Relative Humidity	↑	**4.3 %**	**0.037**
Windspeed	↑	0.2 m/s	0.26
downward LW	↑	1.8 W/m2	0.83
downward SW	↑	12.7 W/m2	0.32
Precipitation	↓	0.009 mm	0.73
Onset of Melt	**Earlier**	**7 days**	**0.0057**
End of Melt	**Earlier**	**10 days**	**0.00087**
Duration	↓	**2.5 days**	**0.034**

*Mann-Kendall Test was used to detect the monotonic trends

**Theil Sen's slope estimator

With warmer temperatures we would expect fewer nighttime refreeze events, however, no substantial changes in refreeze events were found over the years. There were years with increased refreeze days, but it was insufficient to influence an earlier onset of snowmelt and shortened melt period. Similarly, Bartsch et al. (2010) found no significant refreezing on the snow surface in the Eurasian Arctic.

Humidity had significantly changed during the snowmelt period, where TMM had experienced higher humidity at a rate of 4.3 % per decade, and therefore decreased latent heat flux as it changed the temperature gradient. Warmer temperatures and simultaneously increasing humidity would mean that the water vapour in the atmosphere is increasing at a higher rate, as warmer air has more capability to hold water vapour. Therefore, the importance of increases in humidity are associated with air temperature. A general significant increased trend in humidity was well documented by Willett et al. (2008) for the Northern Hemisphere region (20°-70° N). Vincent et al. (2007) had also shown an increase in humidity over northwestern Canada, however, the trend was not statistically significant.

Although increased wind conditions at TMM was not statistically significant, higher wind conditions during the snowmelt period would enhance sensible and latent energy (Van Mullem & Garen, 2004), and therefore contribute to the increase in the magnitude of snowmelt.

Shortwave radiation was observed to be usually positive (Russak, 2009), during the spring melt period. Many other studies have shown shortwave radiation controls on both the timing of snowmelt and the snowmelt rate (Granger & Gray, 1990; Kirnbauer et al., 1994). Despite, the increases in downward shortwave and longwave radiation at TMM, no trends were observed. The increase in downward longwave radiation is expected with significant warmer temperatures, increased cloud cover and atmospheric water vapour (Liang et al., 2012).

During the snowmelt period, the impact of precipitation was minimal and there were no significant changes in spring precipitation detected at TMM. However, in the likelihood of heavy precipitation, or increased precipitation during the snowmelt period, different types of precipitation were examined. While the majority of the precipitation that occurred was mostly mixed precipitation, a small fraction fell as snowfall or rainfall. This can be significant, as the

changes in precipitation during the snowmelt period can enhance or reduce spring snowmelt rates (Hamlet et al., 2005), depending on the precipitation phase (Musselman et al., 2017). However, precipitation at TMM does not show a significant role in enhancing or delaying snowmelt.

Therefore, these trends raise the question whether the changes in the timing and the duration of the snowmelt period, is controlled by the changes in meteorological conditions, the end of winter SWE, or a combination of changes in meteorological conditions and SWE. However, the changes in the duration of the snowmelt period cannot be explained solely by the end of winter SWE as TMM is getting warmer. Therefore, it is necessary to investigate the changes in the energy balance, using a physically based hydrological model.

References

Anttila, K., Manninen, T., Jääskeläinen, E., Riihelä, A., & Lahtinen, P. (2018). The role of climate and land use in the changes in surface albedo prior to snow melt and the timing of melt season of seasonal snow in northern land areas of 40°N-80°N during 1982-2015. *Remote Sensing*, *10*(10). https://doi.org/10.3390/rs10101619

Assmann, J. J., Myers-Smith, I. H., Phillimore, A. B., Bjorkman, A. D., Ennos, R. E., Prevéy, J. S., Henry, G. H. R., Schmidt, N. M., & Hollister, R. D. (2019). Local snow melt and temperature—but not regional sea ice—explain variation in spring phenology in coastal Arctic tundra. *Global Change Biology*, *25*(7), 2258–2274. https://doi.org/10.1111/gcb.14639

Balch, J. K., Bradley, B. A., Abatzoglou, J. T., Chelsea Nagy, R., Fusco, E. J., & Mahood, A. L. (2017). Human-started wildfires expand the fire niche across the United States. *Proceedings of the National Academy of Sciences of the United States of America*, *114*(11), 2946–2951. https://doi.org/10.1073/pnas.1617394114

Barnett, T. P., Adam, J. C., & Lettenmaier, D. P. (2005). Potential impacts of a warming climate on water availability in snow-dominated regions. *Nature*. Nature Publishing Group. https://doi.org/10.1038/nature04141

Bartsch, A., Kumpula, T., Forbes, B. C., & Stammler, F. (2010). Detection of snow surface thawing and refreezing in the Eurasian arctic with QuikSCAT: Implications for reindeer herding. *Ecological Applications*, *20*(8), 2346–2358. https://doi.org/10.1890/09-1927.1

Bjorkman, A. D., Elmendorf, S. C., Beamish, A. L., Vellend, M., & Henry, G. H. R. (2015). Contrasting effects of warming and increased snowfall on Arctic tundra plant phenology over the past two decades. *Global Change Biology*, *21*(12), 4651–4661. https://doi.org/10.1111/gcb.13051

Bonsal, B. R., & Kochtubajda, B. (2009). An assessment of present and future climate in the Mackenzie Delta and the near-shore Beaufort Sea region of Canada. *International Journal of Climatology*, *29*, 1780–1795. https://doi.org/10.1002/joc.1812

Brown, R. D., & Braaten, R. O. (1998). Spatial and temporal variability of Canadian monthly snow depths, 1946-1995. *Atmosphere - Ocean*, *36*(1), 37–54. https://doi.org/10.1080/07055900.1998.9649605

Brown, R., Derksen, C., & Wang, L. (2010). A multi-data set analysis of variability and change in Arctic spring snow cover extent, 1967-2008. *Journal of Geophysical Research Atmospheres*, *115*(16). https://doi.org/10.1029/2010JD013975

Burd, J. A., Peterson, P. K., Nghiem, S. V., Perovich, D. K., & Simpson, W. R. (2017). Snowmelt onset hinders bromine monoxide heterogeneous recycling in the Arctic Justine. *Journal of Geophysical Research: Atmospheres*, *122*, 8297–8309. https://doi.org/10.1002/2017JD026906

Burn, D. H., Cunderlik, J. M., & Pietroniro, A. (2004). Hydrological trends and variability in the Liard River basin. *Hydrological Sciences Journal*, *49*(1), 53–67. https://doi.org/10.1623/hysj.49.1.53.53994

Burns, D. A., Klaus, J., & McHale, M. R. (2007). Recent climate trends and implications for water resources in the Catskill Mountain region, New York, USA. *Journal of Hydrology*, *336*(1–2), 155–170. https://doi.org/10.1016/j.jhydrol.2006.12.019

Bush, E., & Lemmen, D. S. (2019). *Canada's Changing Climate Report*. Ottawa, ON. Retrieved from https://changingclimate.ca/CCCR2019

Cheng, C. L., Shalabh, & Garg, G. (2014). Coefficient of determination for multiple measurement error models. *Journal of Multivariate Analysis*, *126*, 137–152. https://doi.org/10.1016/j.jmva.2014.01.006

Colaizzi, P. D., O'Shaughnessy, S. A., Gowda, P. H., Evett, S. R., Howell, T. A., Kustas, W. P., & Anderson, M. C. (2010). Radiometer Footprint Model to Estimate Sunlit and Shaded Components for Row Crops. *Agronomy Journal*, *102*(3), 942–955. https://doi.org/10.2134/agronj2009.0393

Cortés, A. J., Waeber, S., Lexer, C., Sedlacek, J., Wheeler, J. A., Van Kleunen, M., Bossdorf, O., Hoch, G., Rixen, C., Wipf, S., & Karrenberg, S. (2014). Small-scale patterns in snowmelt timing affect gene flow and the distribution of genetic diversity in the alpine dwarf shrub Salix herbacea. *Heredity*, *113*(3), 233–239. https://doi.org/10.1038/hdy.2014.19

Debeer, C. M., Wheater, H. S., Quinton, W. L., Carey, S. K., Stewart, R. E., MacKay, M. D., & Marsh, P. (2015). The Changing Cold Regions Network: Observation, diagnosis and prediction of environmental change in the Saskatchewan and Mackenzie River Basins, Canada. *Science China Earth Sciences*, *58*(1), 46–60. https://doi.org/10.1007/s11430-014-5001-6

Dennison, P. E., Brewer, S. C., Arnold, J. D., & Moritz, M. A. (2014). Large wildfire trends in the western United States, 1984-2011. *Geophysical Research Letters*, *41*(8), 2928–2933. https://doi.org/10.1002/2014GL059576

Déry, S. J., & Brown, R. D. (2007). Recent Northern Hemisphere snow cover extent trends and implications for the snow-albedo feedback. *Geophysical Research Letters*, *34*(22), 2–7. https://doi.org/10.1029/2007GL031474

Environment and Climate Change Canada. (2019). Station Results - Historical Data - Climate - Environment and Climate Change Canada. Retrieved July 3, 2019, from https://climate.weather.gc.ca/historical_data/search_historic_data_stations_e.html?searchType=stnName&timeframe=1&txtStationName=inuvik+a&searchMethod=contains&optLimit=yearRange&StartYear=1840&EndYear=2021&Year=2021&Month=5&Day=5&selRowPerPage=25

Granger, R. J., & Gray, D. M. (1990). A net radiation model for calculating daily snowmelt in open environments. *Nordic Hydrology*, *21*(4–5), 217–234. https://doi.org/10.2166/nh.1990.0017

Hamed, K. H. (2008). Trend detection in hydrologic data: The Mann-Kendall trend test under the scaling hypothesis. *Journal of Hydrology*, *349*(3–4), 350–363. https://doi.org/10.1016/j.jhydrol.2007.11.009

Hamlet, A. F., & Lettenmaier, D. P. (1999). Effects of Climate Change on Hydrology and Water Resources in the Columbia River Basin. *Journal of the American Water Reources Association*, *35*(6), 1597–1623.

Hamlet, A. F., Mote, P. W., Clark, M. P., & Lettenmaier, D. P. (2005). Effects of Temperature and Precipitation Variability on Snowpack Trends in the Western United States. *Journal of Climate*, *18*(21), 4545–4561. https://doi.org/10.1175/JCLI3538.1

Harder, P., & Pomeroy, J. (2013). Estimating precipitation phase using a psychrometric energy balance method. *Hydrological Processes*, *27*(13), 1901–1914. https://doi.org/10.1002/hyp.9799

Hinzman, L. D., Bettez, N. D., Bolton, R. W., Chapin, F. S., Dyurgerov, M. B., Fastie, C. L., Griffith, B., Hollister, R. D., Hope, A., Huntington, H. P., Jensen, A. M., Jia, G. J., Jorgenson, T., Kane, D. L., Klein, D. R., Kofinas, G., Lynch, A. H., Lloyd, A. H., McGuire, A. D., Nelson, F. E., …, & Yoshikawa, K. (2005). Evidence and Implications of Recent Climate Change in Northern Alaska and Other Arctic Regions, Climatic Change. *Climatic Change*, *72*, 251–298. https://doi.org/10.1007/s10584-005-5352-2

Kendall, M. (1975). *Rank correlation methods*. London, UK: Griffin.

Kienzle, S. W. (2008). A new temperature based method to separate rain and snow. *Hydrological Processes*, *22*(October 2008), 5067–5085. https://doi.org/10.1002/hyp.7131

Kirnbauer, R., Bloschl, G., & Gutknecht, D. (1994). Entering the Era of Distributed Snow Models. *Nordic Hydrology*, *25*, 1–24.

Krogh, S. A., & Pomeroy, J. W. (2018). Recent changes to the hydrological cycle of an Arctic basin at the tundra-taiga transition. *Hydrology and Earth System Sciences*, *22*(7), 3993–4014. https://doi.org/10.5194/hess-22-3993-2018

Lesack, L. F. W., Marsh, P., Hicks, F. E., & Forbes, D. L. (2014). Local spring warming drives earlier river-ice breakup breakup in a large Arctic delta. *Geophysical Research Letters*, *41*, 1560–1566. https://doi.org/10.1002/2013GL058761

Lettenmaier, D. P., Wood, E. F., & Wallis, J. R. (1994). Hydro-Climatological Trends in the Continental United States , 1948 – 88. *Journal of Climate*, *7*(4), 586–607.

Liang, S., Li, X., & Wang, J. (2012). Surface Longwave Radiation Budget. In *Advanced remote sensing terrestrial information extraction and applications* (1st Ed., pp. 273–299). Oxford, UK: Elsevier/Academic Press. https://doi.org/10.1016/b978-0-12-385954-9.00009-5

Ling, F., & Zhang, T. (2007). Modeled impacts of changes in tundra snow thickness on ground thermal regime and heat flow to the atmosphere in Northernmost Alaska. *Global and Planetary Change*, *57*(3–4), 235–246. https://doi.org/10.1016/j.gloplacha.2006.11.009

Malik, M. J., Van Der Velde, R., Vekerdy, Z., & Su, Z. (2014). Improving modeled snow albedo estimates during the spring melt season. *Journal of Geophysical Research (Atmospheres)*, *119*(10), 7311–7331. https://doi.org/10.1002/ 2013JD021344

Mann, H. B. (1945). Nonparametric Tests Against Trend. *Econometrica*, *13*(3), 245–259.

Marsh, P., Bartlett, P., MacKay, M., Pohl, S., & Lantz, T. (2010). Snowmelt energetics at a shrub tundra site in the western Canadian Arctic. *Hydrological Processes*, *24*(25), 3603–3620. https://doi.org/10.1002/hyp.7786

Marsh, P., Onclin, C., & Neumann, N. (2002). Water and energy fluxes in the lower Mackenzie valley, 1994/95. *Atmosphere - Ocean*, *40*(2), 245–256. https://doi.org/10.3137/ao.400211

Marsh, P., & Pomeroy, J. (1996). Meltwater fluxes at an arctic forest-tundra site. *Hydrological Processes*, *10*(10), 1383–1400. https://doi.org/10.1002/(SICI)1099-1085(199610)10:10<1383::AID-HYP468>3.0.CO;2-W

Marsh, P., Pomeroy, J., & Quinton, B. (1995). Hydrological Processes and Runoff at the Arctic Treeline in Northwestern Canada. *10th Annual Northern Basins Symposium*, 368–397.

Marsh, P., Pomeroy, J., Pohl, S., Quiton, W., Onclin, C., Russel, M., Neumann, N., Pietroniro, A., Davison, B. & McCartney, S. (2008). Snowmelt Processes and Runoff at the Arctic Treeline: Ten Years of MAGS Research. *Cold Region Atmospheric and Hydrologic Studies. The Mackenzie GEWEX Experience*, *2*(January), 97–123. https://doi.org/10.1007/978-3-540-75136-6

Mioduszewski, J. R., Rennermalm, a K., Robinson, D. a, & Mote, T. L. (2014). Attribution of snowmelt onset in Northern Canada. *Journal of Geographical Sciences*, *119*, 9638–9653. https://doi.org/10.1002/2013JD021024

Moore, J. N., Harper, J. T., & Greenwood, M. C. (2007). Significance of trends toward earlier snowmelt runoff, Columbia and Missouri Basin headwaters, western United States. *Geophysical Research Letters*, *34*(16). https://doi.org/10.1029/2007GL031022

Musselman, K. N., Clark, M. P., Liu, C., Ikeda, K., & Rasmussen, R. (2017). Slower snowmelt in a warmer world. *Nature Climate Change*, *7*(3), 214–219. https://doi.org/10.1038/nclimate3225

Nicolaus, M., Haas, C., Bareiss, J., & Willmes, S. (2006). A model study of differences of snow thinning on Arctic and Antarctic first-year sea ice during spring and summer. *Annals of Glaciology*, *44*(November), 147–153. https://doi.org/10.3189/172756406781811312

Pohl, S., Marsh, P., & Bonsal, B. R. (2007). Modeling the impact of climate change on runoff and annual water balance of an arctic headwater basin. *Arctic*, *60*(2), 173–186. https://doi.org/10.14430/arctic242

Pohl, S., Marsh, P., & Liston, G. E. (2006). Spatial-temporal variability in solar radiation during spring snowmelt. *Arctic, Antarctic, and Alpine Research*, *38*(1), 136–146.

Pomeroy, J. W., & Granger, R. J. (1997). Sustainability of the western Canadian boreal forest under changing hydrological conditions. I. Snow accumulation and ablation. *IAHS-AISH Publication*, *240*, 237–242.

Quinton, W. L., & Marsh, P. (1999). A conceptual framework for runoff generation in a permafrost environment. *Hydrological Processes*, *13*(16), 2563–2581. https://doi.org/10.1002/(SICI)1099-1085(199911)13:16<2563::AID-HYP942>3.0.CO;2-D

Roux, M. J., Harwood, L. A., Zhu, X., & Sparling, P. (2015). Early summer near-shore fish assemblage and environmental correlates in an Arctic estuary. *Journal of Great Lakes Research*, *42*(2), 256–266. https://doi.org/10.1016/j.jglr.2015.04.005

Russak, V. (2009). Changes in solar radiation and their influence on temperature trend in Estonia (1955-2007). *Journal of Geophysical Research Atmospheres*, *114*(1), 1–6. https://doi.org/10.1029/2008JD010613

Sælthun, N. (1996). *The Nordic HBV model*. *Norwegian Water Resources and Energy …*. Retrieved from ftp://terra.uio.no/pub/dagrunv/HBVMOD.PDF

Shi, X., Déry, S. J., Groisman, P. Y., & Lettenmaier, D. P. (2013). Relationships between recent pan-arctic snow cover and hydroclimate trends. *Journal of Climate*, *26*(6), 2048–2064. https://doi.org/10.1175/JCLI-D-12-00044.1

Shi, X., Groisman, P. Y., Déry, S. J., & Lettenmaier, D. P. (2011). The role of surface energy fluxes in pan-Arctic snow cover changes. *Environmental Research Letters*, *6*(3). https://doi.org/10.1088/1748-9326/6/3/035204

Shi, X., Marsh, P., & Yang, D. (2015). Warming spring air temperatures, but delayed spring streamflow in an Arctic headwater basin. *Environmental Research Letters*, *10*(6), 064003. https://doi.org/10.1088/1748-9326/10/6/064003

Shook, K. (2016). CRHMr: pre- and post- processing for the Cold Regions Hydrological Modelling (CRHM) platform. Retrieved from https://github.com/CentreForHydrology/CRHMr

Souma, K., & Wang, Y. (2010). A comparison between the effects of snow albedo and infiltration of melting water of Eurasian snow on East Asian summer monsoon rainfall. *Journal of Geophysical Research Atmospheres*, *115*(D2). https://doi.org/10.1029/2009JD012189

Stewart, I. T., Cayan, D. R., & Dettinger, M. D. (2005). Changes toward earlier streamflow timing across western North America. *Journal of Climate*, *18*(8), 1136–1155. https://doi.org/10.1175/JCLI3321.1

Tedesco, M., Brodzik, M., Armstrong, R., Savoie, M., & Ramage, J. (2009). Pan arctic terrestrial snowmelt trends (1979 – 2008) from spaceborne passive microwave data and correlation with the Arctic Oscillation. *Geophysical Research Letters*, *36*(September), 1–6. https://doi.org/10.1029/2009GL039672

Theil, H. (1950). A rank-invariant method of linear and polynomial. *Series A Mathematical Sciences*, *53*, 387–392.

Theil, Henri. (1950). A Rank-Invariant Method of Linear and Polynomial Regression Analysis (pp. 345–381). Springer, Dordrecht. https://doi.org/10.1007/978-94-011-2546-8_20

Thompson, C., Beringer, J., Chapin, F. S., & McGuire, A. D. (2004). Structural complexity and land-surface energy exchange along a gradient from arctic tundra to boreal forest. *Journal of Vegetation Science*, *15*(3), 397–406. https://doi.org/10.1111/j.1654-1103.2004.tb02277.x

Tuttle, S. E., & Jacobs, J. M. (2019). Enhanced Identification of Snow Melt and Refreeze Events From Passive Microwave Brightness Temperature Using Air Temperature. *Water Resources Research*, *55*(4), 3248–3265. https://doi.org/10.1029/2018WR023995

Tsui, Matthew Y. T., & Marsh, Philip (2021). Hydrometeorological data and energy balance data, 1999-2019, Trail Valley Creek, Northwest Territories. https://doi.org/10.5683/SP3/MCDA2R.

Van Mullem, J. A., & Garen, D. (2004). Snowmelt. In *Hydrology National Engineering Handbook* (pp. 1–21). Portland, Oregon.

Van Pelt, W. J. J., Pohjola, V. A., & Reijmer, C. H. (2016). The changing impact of snow conditions and refreezing on the mass balance of an idealized svalbard glacier. *Frontiers in Earth Science*, *4*(November), 1–15. https://doi.org/10.3389/feart.2016.00102

Vincent, L. A., van Wijngaarden, W. A., & Hopkinson, R. (2007). Surface temperature and humidity trends in Canada for 1953-2005. *Journal of Climate*, *20*(20), 5100–5113. https://doi.org/10.1175/JCLI4293.1

Wang, L., Derksen, C., Brown, R., & Markus, T. (2013). Recent changes in pan-Arctic melt onset from satellite passive microwave measurements. *Geophysical Research Letters*, *40*, 522–528. https://doi.org/10.1002/grl.50098

Wheeler, J. A., Cortés, A. J., Sedlacek, J., Karrenberg, S., van Kleunen, M., Wipf, S., Hoch, G., Bossdorf, O., & Rixen, C. (2016). The snow and the willows: earlier spring snowmelt reduces performance in the low-lying alpine shrub Salix herbacea. *Journal of Ecology*, *104*(4), 1041–1050. https://doi.org/10.1111/1365-2745.12579

Wilcox, E. J., Keim, D., Jong, T. De, Walker, B., Sonnentag, O., Sniderhan, A. E., Mann, P., & Marsh, P. (2019). Tundra shrub expansion may amplify permafrost thaw by advancing snowmelt timing. *Arctic Science*, *5*, 202–217. https://doi.org/dx.doi.org/10.1139/as-2018-0028

Willett, K. M., Jones, P. D., Gillett, N. P., & Thorne, P. W. (2008). Recent changes in surface humidity: Development of the HadCRUH dataset. *Journal of Climate*, *21*(20), 5364–5383. https://doi.org/10.1175/2008JCLI2274.1

Yip, Q. K. Y., Burn, D. H., Seglenieks, F., Pietroniro, A., & Soulis, E. D. (2012). Climate impacts on hydrological variables in the Mackenzie River Basin. *Canadian Water Resources Journal*, *37*(3), 209–230. https://doi.org/10.4296/cwrj2011-899

Zhang, X., Vincent, L. A., Hogg, W. D., & Niitsoo, A. (2000). Temperature and precipitation trends in Canada during the 20th century. *Atmosphere - Ocean*, *38*(3), 395–429. https://doi.org/10.1080/07055900.2000.9649654

CHAPTER 3: Changing Snowmelt Energy Balance in the Western Canadian Arctic

Matthew Y. T. Tsui [a], Marsh Philip [a], and Shook Kevin [b]

[a] Cold Regions Research Centre, Wilfrid Laurier University, Waterloo, ON, Canada [b] Centre for Hydrology, University of Saskatchewan, Saskatoon, SK, Canada

Corresponding author: Matthew Y.T. Tsui tsui.myt@gmail.com Cold Regions Research Centre, Wilfrid Laurier University, Waterloo, ON, Canada.

Journal: Arctic, Antarctic, and Alpine Research

Abstract

The hydrology of the of the Arctic is dominated by the accumulation of snow over the long winter, and the rapid melt of this snow over a few weeks in the spring. This aspect of the Arctic water cycle is especially sensitive to a warming climate. The timing and the rate of snow melt during the spring period has implications for aquatic ecosystems and communities that depend on melt water. As shown in Chapter 2, the western Canadian Arctic has experienced an earlier onset of snowmelt compared to earlier decades, a warmer and shorter melt period. The changes in the energy balance components are tied to climate warming, and therefore, controlling the rate of snowmelt. In this paper we will use a physically based snowmelt model to investigate changes in the energy transfers between the snow surface and the atmosphere during the snowmelt period over the last 21 years. Model runs demonstrate that radiation plays a decisive role, followed by turbulent fluxes of sensible heat and latent heat. A shorter duration of melt is due to a combination of changes in the end of winter SWE and meteorological conditions. As net radiation and warmer air temperatures increased, we found an increase to the rate of snowmelt by 0.7 mm/day per decade.

Keywords: hydrological modelling, snowmelt, melt rate, climate change, energy balance

3.1 Introduction

Snow plays an important role in the hydrologic system as it largely affects both the water and energy fluxes of arctic regions through the high reflectivity of snow, surface roughness, surface temperature, and the sheer mass of water melting (Marsh & Pomeroy, 1996). The spring snowmelt period is a time with rapid changes in energy fluxes as the surface changes from snow covered to snow free. Spring snowmelt runoff is often the largest hydrological event of the year, with important biophysical controls and impacts on built infrastructure such as bridges, culverts, and roads. Numerous studies (Mioduszewski et al., 2014; Shi et al., 2015; Van Pelt et al., 2016) have shown that snowmelt is occurring earlier across the Arctic as the climate is warming. Chapter 2 also showed an earlier snowmelt with warmer and more humid conditions during melt period for a location in the western Canadian Arctic. However, understanding and predicting the rate of snowmelt requires a comprehensive interpretation of the energy transfers between the snow surface and the atmosphere that lead to changes in snowmelt (Cline, 1997) and runoff. Therefore, it is important for hydrological and climate predictions to properly estimate the surface energy balance during the spring snowmelt period, as snowmelt runoff events that follow the melt period, are the most important component of the hydrological cycle.

Snowmelt energy balance models include components that govern the full energy and mass conservation governing snowmelt (Kumar et al., 2013), including radiative fluxes, turbulent fluxes of sensible and latent heat, ground heat flux, changes in energy storage in the snowpack, and the energy transfer due to rainfall. During the early spring snowmelt period, snow cover in an arctic area is continuous and the rate of snowmelt is primarily dominated by higher levels of radiative energy (Shi et al, 2011), especially over the high latitudes (Ohmura, 2001; Zhang et al., 1997). Open tundra environments are known to react with incoming radiation in ways that

accelerate snow melt compared, for example, to boreal forest at the same latitude (Pomeroy & Granger, 1997). Next to radiation, sensible heat is the largest positive flux, while latent heat flux is negative on most days (Marsh & Pomeroy, 1996). Latent heat energy flux responds to the radiative fluxes with daytime evaporation and nighttime condensation (Granger & Male, 1978). The changes in turbulent heat fluxes are a result of increases of Arctic air temperature (Shi et al., 2011).

A warmer climate will cause earlier snowmelt, however, the temporal changes in the energy balance components are poorly understood. This study will provide a better understanding of the relative importance of the changes in each of the fluxes in the energy balance during the spring snowmelt period. The objectives of this paper are to (1) document the changes in the surface energy balance during the spring snowmelt period; and (2) estimate the magnitude of the resulting snowmelt.

3.2 Methods

3.2.1 Study Site

Meteorological observations were obtained from the Trail Valley Creek (TVC) Research Station (Quinton & Marsh, 1999), located in the taiga – tundra ecotone (68.7 °N, 133.5 °W; Figure 2.1). TVC is located in the uplands east of the Mackenzie River Delta and 50 km north of the Inuvik Airport (Inuvik-A), in the Northwest Territories (NWT). The total thickness of the ice-rich continuous permafrost is up to 500 m and is overlain by an active layer ranging from 0.5 m to 0.8 m (Wilcox et al., 2019). The topography is dominated by gently rolling hills and occasional steep sided river valleys, where the overall elevation ranges from 40 m to 187 m above sea level (a.s.l.) (Pohl et al., 2006), with an average of 99 m a.s.l. The TVC watershed

consists of shrub tundra, and sparse black spruce forest on hillslopes and in the valley bottoms, over an area of 57 km^2 (Marsh et al., 2002; Marsh et al., 2008).

The watershed has numerous meteorological stations, but we will focus on two of these here, that represent tundra snow cover. The TVC Main Meteorological station (TMM; 69.3 °N, 133.5°W) and the TVC Upper Plateau station (TUP; 68.7 °N, 133.7 °W). TMM is positioned at ~70 m a.s.l. and TUP is positioned at ~170 m a.s.l. (Pohl et al., 2006). The TVC landscape is comprised of 70 % tundra, 21 % shrub tundra, 8 % drift, and 1 % sparse forest (Marsh & Pomeroy, 1996). Both the TMM and TUP stations are situated over shallow tundra snow cover and have measurements of air temperature, relative humidity, wind speed, and downward and upward shortwave and longwave radiation, while TMM also measures precipitation. Missing data for TMM will be supplemented by data from TUP when available. Meteorological instrumentation details are outlined in Appendix A. Although observations began at TVC in 1991 and continues to this day, the data from 1991 to 1998 is not consistently available, and as a result we will only use data from TMM for the period 1999 to 2019.

The climate is characterized by short summers and long cold winters. Snowfall accumulates over eight to nine months and melts over a brief one to two week period from mid-May to early June (Pohl et al., 2007), with air temperature averaging -2.6 °C and an average precipitation of 3.1 mm at TMM. Near the end of winter, air temperatures gradually increase and rise above 0 °C for the first time in late April or early May. This rise above the freezing point is an important indicator of the start of the spring snowmelt period. Air temperature has increased over the study region in the spring, and as a result, the onset of snowmelt has occurred earlier (Shi et al., 2015).

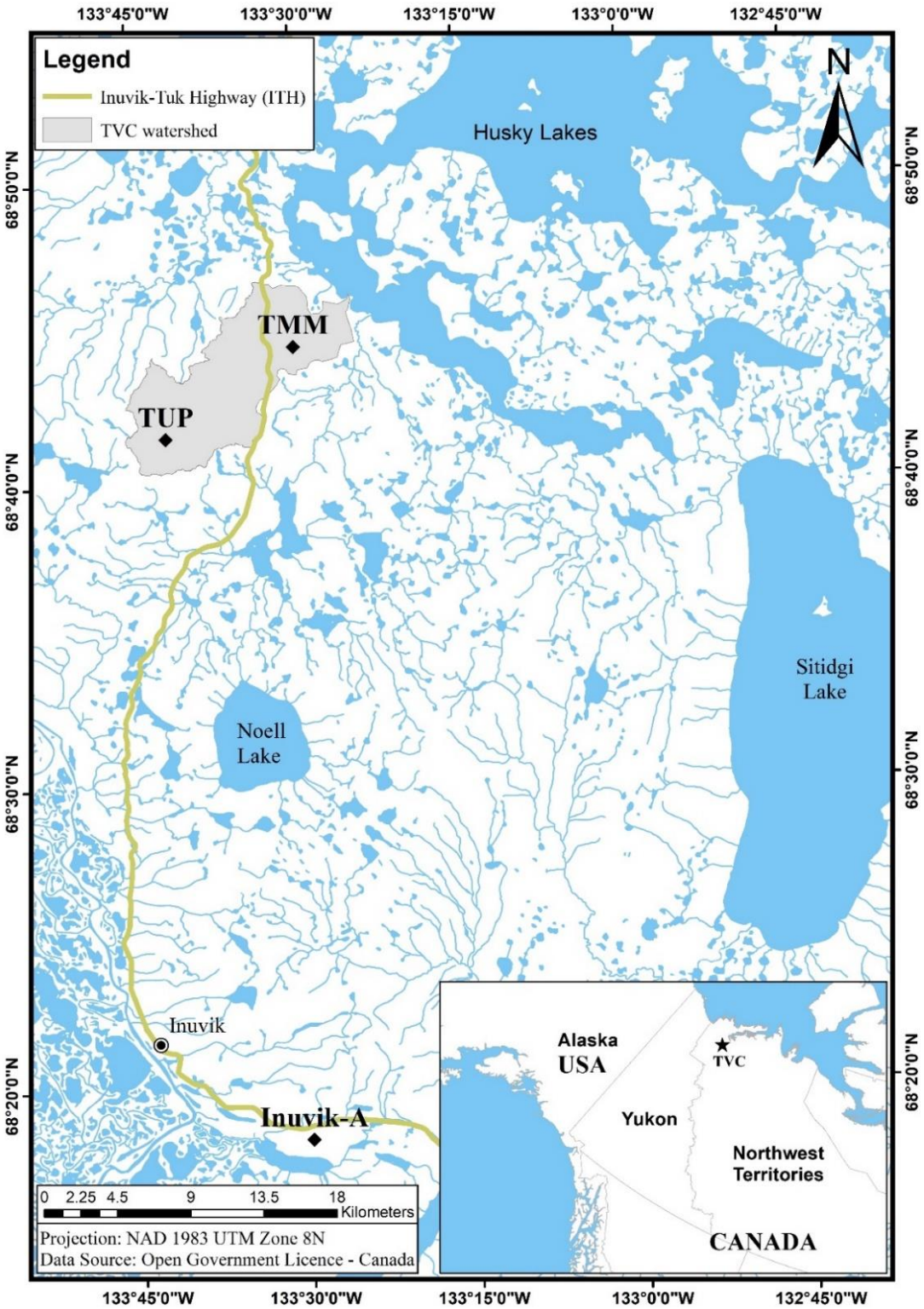

Figure 3.1: The location of the Trail Valley creek (TVC) main meteorological station (TMM) and upper plateau station (TUP), located 50 km north of Inuvik-A. TVC drains towards an Arctic estuary, the Husky Lakes (Roux et al., 2015).

3.2.2 Model Overview

Physically based hydrological models are effective approaches to examine the hydrological response to climate change and can better describe the complex hydrological processes (Fang & Pomeroy, 2020) like the Cold Regions Hydrological Model (CRHM). In contrast to many other hydrological models, CRHM is highly flexible and uses a modular object-oriented modeling framework (Leavesley et al. 2002; Pomeroy et al., 2007) that develop, support, and apply physically based representations of cold region hydrological processes, such as snow redistribution, precipitation interception, sublimation, energy balance snowmelt, evapotranspiration, soil moisture balance, infiltration into frozen and unfrozen soil, radiation exchange to complex surfaces, runoff, and frozen ground dynamics including active layer thaw, (Fang et al., 2013, 2010; Krogh & Pomeroy, 2018; Weber et al., 2016). CRHM has also been used to explore the hydrological effects of climate change (Dornes et al., 2008; Fang et al., 2013; Fang & Pomeroy, 2016). A detailed description of CRHM and its modules are available in Pomeroy et al. (2007). The watershed is discretized using hydrological response units (HRU), which are a spatial unit corresponding to biophysical landscape units. The HRU concept, introduced by Flügel (1995), is an areal unit described by similar hydrological characteristics. HRU are spatial units of mass and energy balance calculations that are normally defined by soil types, vegetation, slope, aspect, and elevation (Krogh et al., 2015).

This modelling approach makes CRHM suitable for use in many cold regions, and as a result it has been tested and applied in China (Zhou et al., 2014), Patagonia (Helsel & Hirsch, 1992; Krogh et al., 2015), Canada (Armstrong et al., 2010; Fang & Pomeroy, 2008; Krogh & Pomeroy, 2018; Krogh et al., 2017; Pomeroy et al., 2016; Rasouli et al., 2014), German Alps

(Weber et al., 2016), Spanish Pyrenees (Rasouli et al., 2014), and Svaldbard (Moreno et al., 2016).

CRHM operates through four main components: (1) forcing data, (2) parameters, (3) variables and states, and (4) modules. Parameters are based on measurable physiographic features. Initial states and variables include meteorological forcing variables and are specified within the appropriate module. Key modules in CRHM include the basin description, observations, radiation module, sunshine hours, prairie blowing snow module, albedo module, and the energy balance snowmelt module. The basin module holds commonly used physical and control parameters, which includes basin area, HRU area, latitude, and elevation. The observation module handles meteorological forcing variables (air temperature, vapour pressure, precipitation, wind speed, and radiation), as inputs to other modules. The global module estimates direct and diffuse solar radiation, maximum sunshine hours, and cloudiness effects that are based on latitude, elevation, ground slope and azimuth, providing radiation inputs to calcsun module and the energy budget snowmelt module. Calcsun module estimates actual sunshine hours from incoming shortwave radiation and maximum sunshine hours to generate inputs for the energy balance snowmelt module. Albedo was estimated based on snow depth, new and melting snow. The prairie blowing snow model (PBSM; Pomeroy & Li, 2000) estimates snow accumulation and simulates the end of winter snow water equivalent (SWE) that is available at the beginning of the spring season. The calculated end of winter SWE was generated as inputs for the energy balance snowmelt module.

The energy balance snowmelt model (EBSM) (Gray & Landine, 1988) estimates each components of the snow surface energy balance, including radiation, sensible heat, latent heat, ground heat, advection from rainfall, and the change in internal energy for snowpack layers.

Snowmelt, as the amount of water that is available to runoff from the bottom of the snowpack is then determined as the residual of the energy balance. Energy fluxes directed towards the snowpack are positive. The model uses the snowmelt energy Equation 3.1 as the physical framework.

$$\frac{dU}{dt} = Q_m + Q_n + Q_h + Q_e + Q_g + Q_d \quad (3.1)$$

Where Q_m is the energy available for snowmelt, Q_n is net radiation, Q_h is turbulent flux of sensible heat, Q_e is turbulent flux of latent energy, Q_g is ground heat flux, Q_d is the energy due to advection from rainfall, and $\frac{dU}{dt}$ is the rate of change of internal energy per unit surface area per unit time (all units are in Wm^{-2}). The net radiation, Q_n, is the sum of net longwave L* and net shortwave K* fluxes, and is calculated by:

$$Q_n = -0.53 + 0.47Q_0\left[0.52 + 0.52\left(\frac{n}{N}\right)\right](1 - A) \quad (3.2)$$

where Q_0 is the daily clear sky shortwave radiation incident to the surface (MJ/m^2*day), n is the number of hours of bright sunshine, N is the number of maximum hours of bright sunshine from the calcsun module, and A is the mean surface albedo over the footprint of TMM, which was estimated from the albedo module. Q_h, depends on wind speed and daily maximum air temperature, as shown in Equation 3.3:

$$Q_h = -0.92 + 0.076U + 0.19T_{Max}, \quad (3.3)$$

where U is the mean daily wind speed (m/s), T_{Max} is the daily maximum air temperature (°C). Application of the equation should be limited to days when T_{Max} is greater than – 5 °C. Sensible heat calculations yield a standard error of estimate of 0.55 MJ/m^2 per day. Latent energy, Q_e, is a function of wind speed and the difference between vapour pressure to actual vapour pressure of the air, as shown in Equation 3.4:

$$Q_e = 0.08(0.18 + 0.098U_{10})(e_s - e_2), \quad (3.4)$$

where e_s is the mean daily vapor pressure at the snow surface (mbar), and e_2 is the actual vapor pressure of the air at 2 m (mbar). The advection heat flux from rainfall is dependent on the temperature of rainfall, T_r and daily rainfall, P_r, and is calculated by Equation 3.5:

$$Q_p = 4.2T_rP_r. \quad (3.5)$$

The amount of daily melt rate, M (mm/day), is calculated from Q_m, as shown in Equation 3.6:

$$M = \frac{Q_m}{\rho_w B h_f}, \quad (3.6)$$

where the constants, ρ_w, is the density of water ($1000kg/m^3$), B, is the thermal quality of the snow, the fraction of ice in a unit mass of wet snow, ranging between 0.95 and 0.97 (corresponds to 3 % to 5% of liquid water (Mullem & Garen, 2004)), and h_f, is the latent heat of fusion of ice ($333.5\ kJ/kg^1$). This can be reduced to:

$$M = 0.27Q_m. \quad (3.7)$$

3.2.3 Model Implementation

A single HRU over the footprint of TMM was used, where parameters were set based on measured physiographic features (Appendix B). The end of winter SWE over the footprint of TMM, which replaced the estimated SWE from PBSM to eliminate snow accumulation errors generated by the model. SWE was measured with the ESC30 snow corer that was either plunged or twisted into the snow until it hits the ground. On average 40 to 50 depth measurements and six density cores were taken. SWE is related to snow depth by the local bulk density, and is calculated by Equation 3.8 equation:

$$SWE = h_s\left(\frac{\rho_b}{\rho_w}\right), \quad (3.8)$$

where h_s is the snow depth measured in centimeters (cm), ρ_b and ρ_w are the density in grams per

centimeters cubed (g/cm^3), and the density of water (g/cm^3). The ESC30 snow corer removes a snow core from the snowpack and weighed in the corer using a spring balance calibrated to read out directly. However, the uncertainty of these core related measurements is estimated to be approximate 7 % to 10 % (Sturm et al., 2010). Failure to retain a plug of soil, vegetation, and/or ice is a common source to the loss of snow in the core. This approach will be used in (Version: CRHM 01/17/18) this study. The energy balance and snowmelt rates by CRHM are accessible online at https://doi.org/10.5683/SP3/MCDA2R.

The end of the snowmelt period is defined by the removal of the snow cover. However, the Arctic snow cover is spatially variable in depth and SWE, and becomes patchy during the melt period (Marsh et al., 2008). As most snow depth sensors, such as the SR50A used at TVC, have a small footprint (0.45 m clearance radius), they do not provide a good estimation of when the snow cover disappears across a broad area. Instead, this study will rely on the measurement of ground albedo as radiometer sensors, generally have a larger footprint (Colaizzi et al., 2010). For example, the CNR1 has a clearance radius of 1.37 m. Using albedo is a robust way to estimate the removal of the snow cover given the large differences in albedo between snow-covered and snow-free tundra. The calculation of albedo, α, is given by Equation 3.9:

$$\alpha = \frac{K_{\uparrow}}{K_{\downarrow}} \tag{3.9}$$

where $K_{\uparrow}$ is the upward shortwave radiation, and $K_{\downarrow}$ is the downward shortwave radiation. At TMM, the end of winter albedo is typically near 0.8 when the ground is fully snow covered but with small amounts of shrubs extending above the snow surface, and 0.19 when completely snow free (Marsh et al., 2010). We will use an albedo value of 0.19, a value known to be when the ground at TVC is nearly snow free (Marsh et al., 2010; Thompson et al., 2004), to allow the

estimation of the end of the snow-covered period. The duration of snowmelt is defined by the difference between the onset of snowmelt and the end of the snow-covered period.

3.2.4 Model Performance Evaluation and Statistical Analyses

CRHM simulations were evaluated with the Nash-Sutcliffe efficiency coefficient (NSE) (Nash & Sutcliffe, 1970), root mean square error (RMSE), model bias index (MB), and Pearson correlation coefficient (R^2). Statistical analysis techniques were also implemented to examine the trends of a univariate timeseries. This includes a Mann Kendall (MK) trend test (Kendall, 1975; Mann, 1945) accompanied by Theil Sen's slope estimator (Theil, 1950) to determine the magnitudes of the trends (Lettenmaier et al., 1994) based on Kendall rank correlation. Biases in model reconstructions can be caused by errors in the measurement of meteorological variables, changes in observation instruments, model structural errors, and the selection of model parameter estimates (Shi et al., 2008), resulting to some degree of uncertainty.

The NSE is a measure for model efficiency to reproduce the time evolution of hydrological variables (Nash & Sutcliffe, 1970). NSE can vary from $-\infty$ to 1, where a value equal to 1 corresponds to a perfect model prediction with respect to the observed values. NSE values greater or equal to 0, but less than 1, suggests that the estimated values are not different from the observed values, and are considered acceptable (Moriasi et al., 2007). A higher positive value would indicate a progressively better model performance. On the other hand, negative NSE values are not an index of good fit. This would indicate the need for better understanding of hydrological responses. The NSE measure is calculated based on Equation 3.10:

$$NSE = 1 - \frac{\sum(X_s - X_o)^2}{\sum(X_o - \overline{X_o})^2}, \tag{3.10}$$

where X_s are the simulated values at time t, X_o are the observed values at time t, and $\overline{X_o}$ is the mean of the observed values.

The root mean square error is a weighted measure that represents the difference between the simulated and the observed values. The RMSE also integrates driving and evaluation of data errors. RMSE is calculated from the difference of squares between observations and simulations, as shown in Equation 3.11:

$$RMSE = \sqrt{\frac{1}{n}\sum(X_s - X_o)^2}, \tag{3.11}$$

where n is the total number of values in the data set.

The model bias index indicates the ability of the model to reproduce the variables of interest. MB assesses the ability of the model to estimate the duration of snowmelt and the snowmelt rate. MB values less than 1 represents an overall underprediction by the model, and values greater than 1 represents an overall overprediction by the model. This can be calculated by Equation 3.12:

$$MB = \frac{\sum X_s}{\sum X_o} - 1. \tag{3.12}$$

However, it is difficult to evaluate the performance of the model from overall statistical indices. This is due to their strong dependence on the distribution of the variable given the difficulty and the potential errors from measurements.

The non-parametric Mann Kendall (MK) test (Kendall, 1975; Mann, 1945) and Theil Sen's slope estimator (Theil, 1950) has been extensively used to test for randomness against trends in climatology and hydrology (Lettenmaier et al., 1994; Zhang et al., 2000), and for identifying linear trends in hydrological and meteorological variables (Burn et al., 2004; Déry & Brown, 2007; Hamed, 2008; Krogh & Pomeroy, 2018; Lettenmaier et al., 1994; Shi et al., 2013, 2011; Yip et al., 2012). Tests were applied with a probability level (p-value) of 0.05 (two-sided test). MK estimates are used instead of least square estimates, as it is less inclined to be affected

by extreme values or outliers in the data and less sensitive to non-normally distributed variables (Moore et al., 2007). According to Mann (1945), the null hypothesis of randomness H_0 states that the data $(x_1, \dots, x_n)$ are independently and identically distributed (IID) random variables, as shown in Equation 3.13.

$$S = \sum_{k=1}^{n-1} \sum_{j=k+1}^{n} \text{sgn}(X_j - X_k), \text{ where} \tag{3.13}$$

$$\text{sgn}(x) = \begin{cases} 1 & if\ x > 0 \\ 0 & if\ x = 0. \\ -1 & if\ x < 0 \end{cases}$$

The alternate hypothesis H_a of a two-sided test is that the distribution of x_j and x_i are not identical for all $j, i \leq n\ with\ j \neq i$. The power of the MK test is the probability to reject the null hypothesis, detecting a monotonic (single direction) trend over time.

Theil Sen's slope method is a robust non-parametric slope estimator, used for the determination of trend magnitudes (Lettenmaier et al., 1994) based on Kendall's rank correlation, τ, a common application of Kendall's test for correlation (Kendall, 1975). This magnitude for monotonic trends are based on the associated Kendall-Theil robust lines (Theil, 1950). The slope estimator is calculated based on Equation 3.14:

$$\text{d} = \frac{\text{x}_\text{j} - \text{x}_\text{i}}{\text{j} - \text{i}}, \tag{3.14}$$

where $1 \leq \text{i} < \text{j} \leq \text{n}$.

The coefficient of determination, also known as the R-squared (R^2) value is a statistical measure that represents the proportion of the variance for a dependent variable that is explained by an independent variable (Cheng et al., 2014). The correlation is statistically significant at a level of p-value of < 0.05. This is a good indicator of how much variation of a dependent variable is explained by the independent variable in a regression model, and how close the data are fitted to the regression line. The R^2 values range from 0 to 1 and is calculated from Equation 3.15:

$$R^2 = 1 - \frac{RSS}{TSS} = 1 - \frac{\sum_{i=1}^{n}(y_i - \hat{y})^2}{\sum_{i=1}^{n}(y_i - \bar{y})^2} \quad (3.15)$$

where the residual sum of squares (RSS) and the total sum of squares (TSS) can be calculated given, the actual value, y_i, the predicted value of y_i, $\hat{y}$, and the mean of the y_i values, $\bar{y}$. However, R^2 is unable to show whether the chosen model is good or bad, nor will it show whether the predictions and estimations are biased. Therefore, the R^2 value should be evaluated in conjunction with NSE measure.

3.3 Results and Discussion

End of Winter SWE

The end of winter SWE over the footprint of TMM, averaged 112 mm over the record period, as shown in Figure 2.4. The lowest SWE (80 mm) was measured in 2016, and the highest SWE (181) was measured in 2006. The end of winter SWE varied quite significantly from year

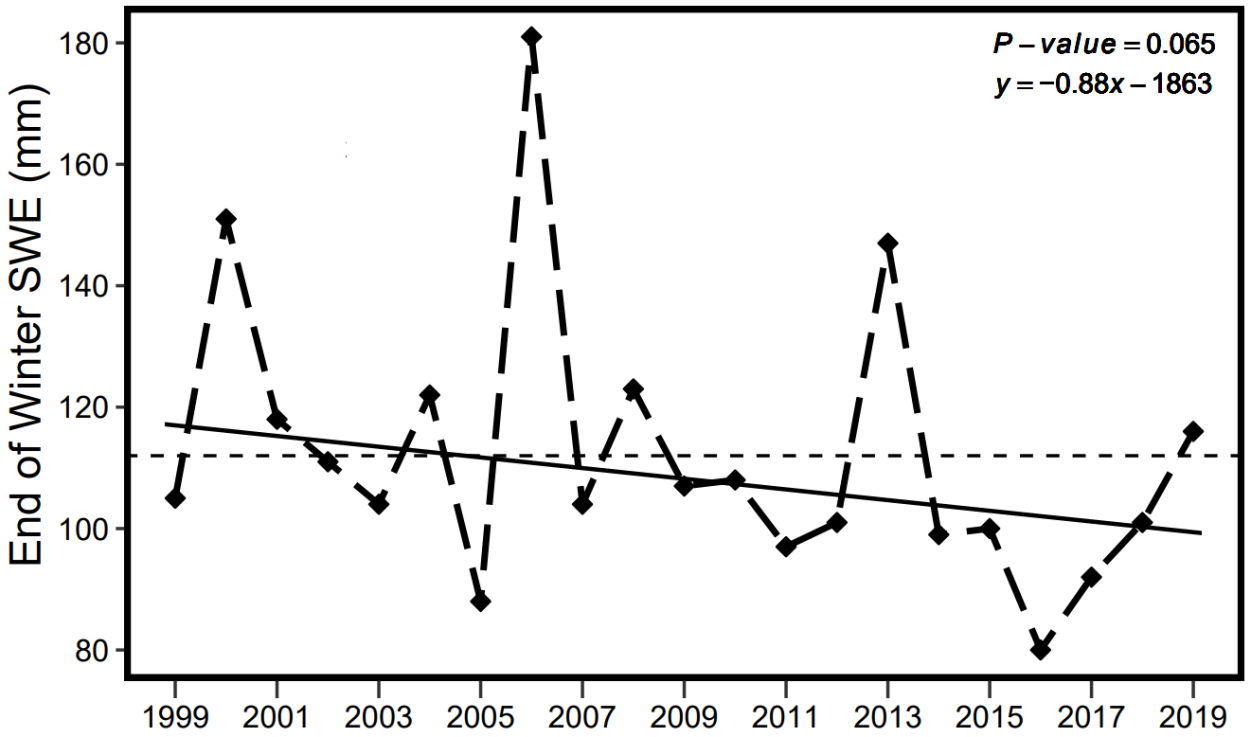

Figure 3.2: The end of winter SWE over the footprint of TMM snow survey measurements have no significant trend. The average SWE is indicated by the horizontal dotted line

to year, with a standard deviation of 23.2 mm or approximately 21 % of the variation from the mean. In the last decade, only two years of measured SWE were higher than the mean. Despite a shallower end of winter snow cover, no trend was detected. This is also due to a significant year to year variation over time.

Changes in Duration of Snowmelt

As shown in Chapter 2, TMM air temperature has increased by 2.1 °C over the spring snowmelt period from 1957 to 2019 (Figure 2.5a), resulted in earlier onset of snowmelt at a significant rate of seven days per decade (Figure 2.3a). Similarly, the snowmelt period ended earlier by ten days per decade. CRHM has effectively estimated the end of the melt period, as shown in Figure 3.3a. The end of melt, when snow cover is completely removed, occurs eight days later on average. The earliest end of snow-covered period was estimated to be on May 12th in 2015 and 2016, and the latest end of snow-covered period was estimated to be on June 11th in 2000. The end of melt has occurred earlier by approximately 8.5 days per decade. The MK-trend analysis shows a significant monotonic downward trend, evaluated by a significance level of 0.0083. The end of melt also yields a large variation over time with a standard deviation of 8.1 days relative to its mean on May 25th.

The trend of earlier snowmelt onset (Adam et al., 2009; Brown & Braaten, 1998; Burd et al., 2017; Burn, 2008; Gleason et al., 2019; Moore et al., 2007; Shi et al., 2015), and earlier end of melt, has led to a shorter snowmelt period (Anttila et al., 2018; Tedesco et al., 2009), suggesting an increase in melt rates during the spring melt period. The average estimated duration of the snowmelt period over shallow snow at a tundra site was approximately eight days. Similar to the observed measurements in Figure 2.3a, the magnitude of the simulated end of the snow-covered period is noticeably higher than that of the observed onset of snowmelt.

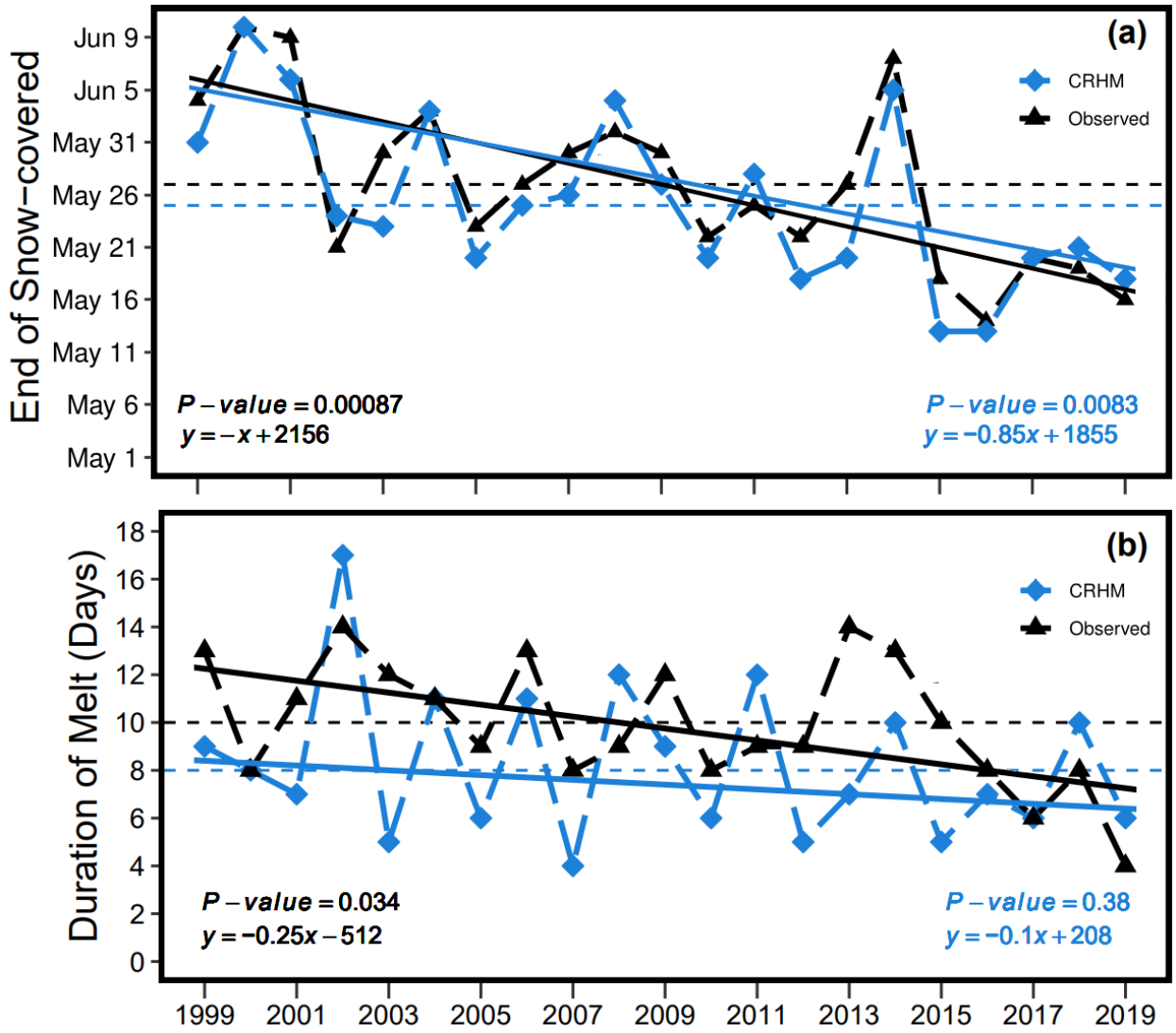

Figure 3.3: (a) The estimated end of melt has occurred earlier by 8.5 days/decade. (b) The estimated duration of the snowmelt period in TMM has significantly shortened by 2.5 days/decade. However, no trends were detected for the simulated duration of snowmelt [CRHM].

This reflects to a shorter snowmelt period over the last 21 years, as illustrated in Figure 3.3b. The standard deviation for the duration of melt is calculated to be 3.2 days or approximately 38.5 % of variation relative to the mean. The MK-trend analysis does not show a significant monotonic trend, evaluated by a significance level of 0.38. As the onset of snowmelt and the end of the snow-covered period vary year to year, the snowmelt period also adapts to the same variation. However, the timeseries does indicate a decrease in the snowmelt period by one day per decade. To allow for consistency and comparison between years, this analysis will focus on the 10-day

period (i.e. the observed average duration of the snowmelt period) after the start of snowmelt in each year. The estimated duration of melt will not be considered as no trends were detected.

Validation of the End and Duration of Snowmelt

The simulated end of melt albedo and duration of melt was compared to the observations. For the end of the snow-covered period, the simulation showed good timing for estimating the end of melt (Figure 3.4a). The observed end of melt occurred earlier by 10 days per decade, which is very comparable to the predicted end of melt that occurred earlier by 8.5 days per decade. The model explains approximately 86 % of variability of the observed data around its mean, with an R^2 value of 0.86. The NSE value of 0.8 also indicates that the model predictions were exceptionally good to the observed (Figure 3.4a). MB listed in Table 3.1 for the simulation was -0.01, suggesting that the model underestimated the end of melt by approximately 1 %. This result suggests predicting the end of snowmelt process at TMM watershed is possible with sufficient calibration.

For the duration of melt, the observed onset of melt was used to calculate the observed duration of melt and the simulated duration of melt. The simulated duration of melt predicted the same shortened trend as the observation. The observed duration of melt shortened by 2.5 days per decade, while the predicted duration of melt shortened by one day per decade. However, approximately 26 % of the observed variation was explained by the model, with an R^2 value of 0.26 (Figure 3.4b). A negative NSE value of -0.28 also indicated that the observed mean is a better predictor than the model. This is likely due to the year to year variation of the onset of melt. The MB listed in Table 3.1 for the simulation was -0.14, suggesting that the model underestimated the duration of melt by approximately 14 %. The results indicate that the variations of the onset of melt greatly influences the duration of melt. The accurate simulation of

the duration of snowmelt requires the consideration of the energy balance control of snowmelt, including radiative and turbulent fluxes.

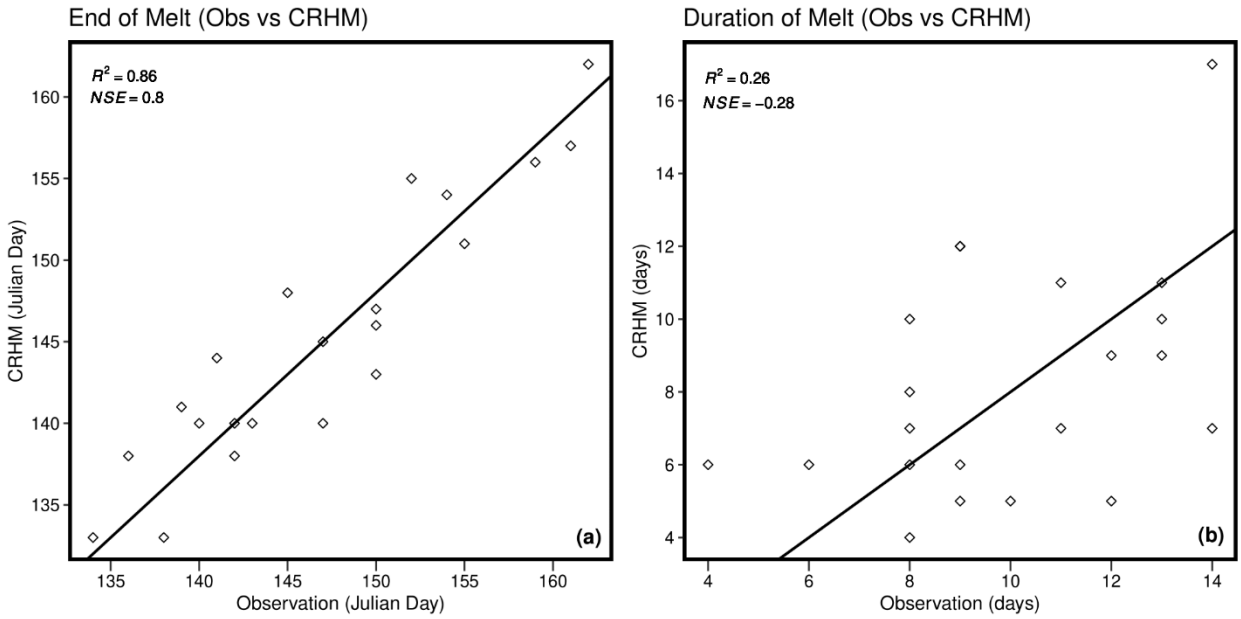

Figure 3.4: The comparison for (a) end of the snow-covered period albedo and (b) the duration of snowmelt between observation values and CRHM estimations, based on observed onset of melt. CRHM is evaluated using the coefficient of determination, and complemented by the NSE measure of 0.8 and -0.28 which explains the predictability and sensitivity of the estimation values for albedo and duration of melt, respectively.

Energy Balance

On average 77 % of the energy balance is net radiative flux over the snowmelt period, while approximately 21 % is sensible heat flux (Figure 3.5). Previous studies have shown also shown a similar dominance of radiative energy control snowmelt in open tundra environments (Mioduszewski et al., 2014; Pomeroy & Granger, 1997). Large positive net radiative energy, followed by smaller sensible heat flux was also documented at TVC (Marsh et al., 2010), with latent heat flux being negative on most days (Marsh & Pomeroy, 1996). It was noted in Figure 2.7 that most of the energy in the system in May and June, are from these increase in shortwave radiation and is primarily associated with the increasing net radiation in the energy balance, as shown in Figure 3.6. Sensible heat flux is almost always positive during the spring once the air

temperature does not go below freezing at night (Marks & Dozier, 1992), with exception in (2013 and 2018). Latent heat fluxes are much smaller and generally do not contribute more than 5 % of the overall energy balance. During the spring snowmelt period, at times, latent heat mirrors sensible heat neutralizing their effects on the overall snow surface energy balance (Pohl et la., 2006), as a result, reducing the amount of melt energy available from turbulent fluxes (Datt et al., 2008). However, for example, the melt period between 2001 and 2006 do not reflect this mirroring effect. In 2012, the air was near saturation vapour pressure at 0 °C, and so the latent heat flux was near, or at zero, during the snowmelt period. While in 2014, slightly negative latent heat flux would indicate condensation, which was reflected with higher humidity (Figure 2.6a). This was not always the case, other years such as 2000 and 2011 did not agree with this association, showing much lower humidity. On the contrary, ground heat flux makes a negligible contribution to the energy balance during the snowmelt period, and can safely be ignored (Granger & Male, 1978). For this reason, ground heat flux is not shown in Figure 3.5. Similarly,

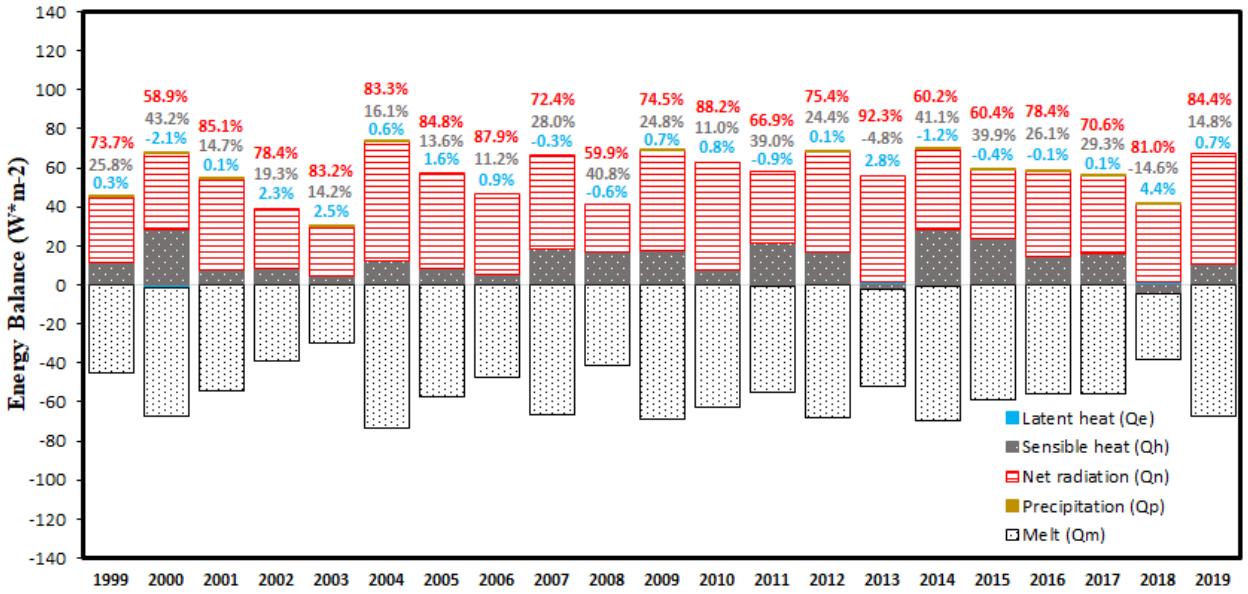

Figure 3.5: The sum of the energy balance from 1999 to 2019 of net radiation (red), sensible heat flux (grey), latent heat flux (blue), and heat from rainfall (yellow) as a percentage of the total energy required for snowmelt (white) during the snowmelt period.

the energy transferred to the snowpack from precipitation is relatively small. Although rain on snow has an important influence on the water retention characteristics of snow (Male & Granger, 1981), it has low effects compared to energy fluxes. The heat content of precipitation over the snowmelt period ranged between 0 to 0.1 %. While high volume of mixed precipitation was seen in 2008, 2014 and 2018 (Figure 2.5d), the mean spring temperature ranged from 2 °C to 5 °C, which was not significantly greater than 0 °C to greatly influence melt over the snowmelt period.

The changes to each individual energy balance component over the snowmelt period are shown in Figure 3.6. No previous studies have attempted to understand the multidecadal changes in energy balance components during the melt period in the Arctic. The average Q_n was estimated to be 43.1 Wm^{-2}, with the highest radiation value of 61.4 Wm^{-2} in 2004, and the lowest radiation value of 24.4 Wm^{-2} in 2008. The standard deviation for Q_n was found to be 10.2 Wm^{-2} or approximately 23.7 % of variation relative to its mean. Q_h was averaged at 12.7 Wm^{-2}, with the highest value of 28.6 Wm^{-2} in 2014 and the lowest value of -4.9 Wm^{-2} in

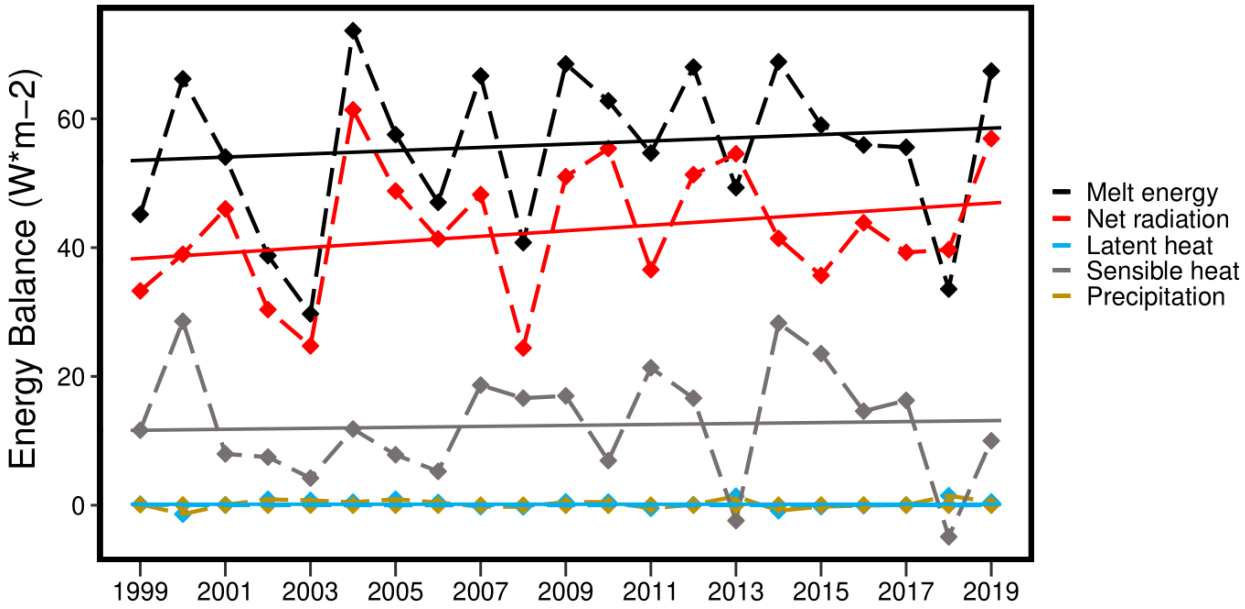

Figure 3.6: The changes to the energy balance during the snowmelt period from 1999 to 2019. No trends were detected from radiative fluxes, and turbulent fluxes of sensible and latent heat, while the energy from precipitation had no apparent changes.

2018. The standard deviation for Q_h was found to be 8.9 Wm^{-2} or approximately 70 % of variation relative to its mean. Q_e was averaged at 0.2 Wm^{-2}, with the highest value of 1.5 Wm^{-2} in 2018 and the lowest value of -1.4 Wm^{-2} in 2000. The standard deviation for Q_e was found to be 0.1 Wm^{-2} or approximately 46 % of variation relative to its mean. The average Q_m was estimated to be 55.4 Wm^{-2}, with the highest value of 74.7 Wm^{-2} in 2004 and the lower value of 29.7 Wm^{-2} in 2003. The standard deviation for Q_m was found to be 12.5 Wm^{-2} or approximately 22.6 % of variation relative to its mean. However, no significant trends were detected for each of the energy balance components. The minimal influence of heat content from precipitation has not changed during the snowmelt period.

Rate of melt

The average rate of snow melt over the period of record was 13.8 mm/day (Figure 3.7). The standard deviation for the rate of melt was about 5.4 mm/day or approximately 39 % of variation relative to the mean, indicating wide spread in the rate of melt from year to year. Given this variability, the MK-trend test resulted in a non-monotonic trend at a significance level of 0.49, no significant trends were detected. Lower snowmelt rates echoes the conditions of lower available energy of each year, for example, a lower net radiative flux in 2003 would reflect to one of the lowest melt rate calculated. In contrast, the highest melt rate of 20 mm/day was estimated in 2004, with one of the highest levels of radiative energy was estimated. The changes in meteorological conditions are likely to be closely linked to changes in melt rates. Warm and humid conditions would suggestively influence the changes in melt rate. Despite no trends were detected from TMM downward radiation, Dornes et al. (2008) have shown a direct correlation between downward radiation to an increase in melt rates.

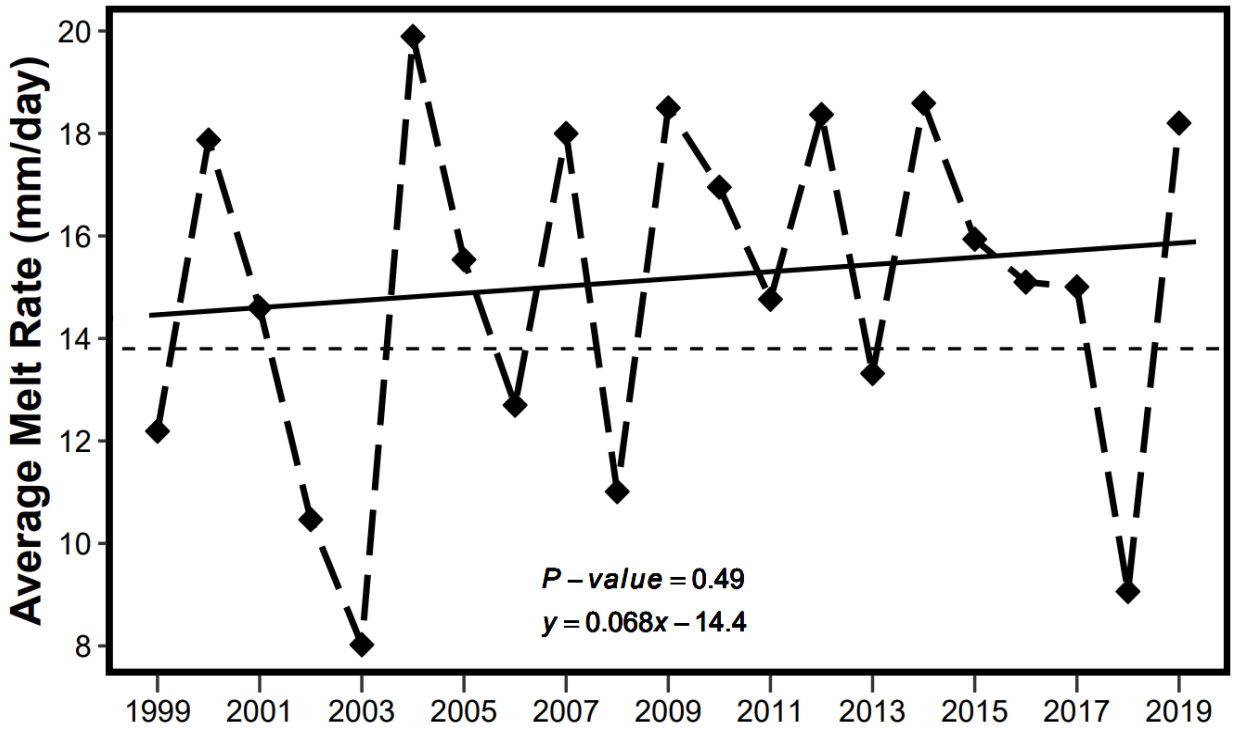

Figure 3.7: The average rate of snowmelt (dotted line) estimated from a physically based energy balance snowmelt model in CRHM over a 10-day snowmelt period. There were no significant trends found.

Atmospheric controls on surface Energy Balance

In order to investigate the effects of changes in atmospheric conditions on energy balance terms and melt rate, we set the end of winter SWE to be sufficiently high that it would not melt during the brief 10-day melt period. For this example, we set the end of winter SWE at 370 mm, an amount typical of a shrub patch controlled snow drift (Jitnikovitch, 2019), located approximately 100 m north of TMM. Similar to Figure 3.5, the energy balance with high end of winter SWE (h-SWE), was primarily composed of net radiative fluxes (Figure 3.8). Sensible heat fluxes were mostly positive, with exception, in 2018 with a substantial negative flux of 5.3 Wm^{-2}. Latent heat fluxes do not contribute more than 8 % of the overall energy balance during the snowmelt period. In the same year, the snow surface was exceptionally warmer than the air leading to an upward evaporation of 1.6 Wm^{-2}. As latent heat is released, this warms the snow

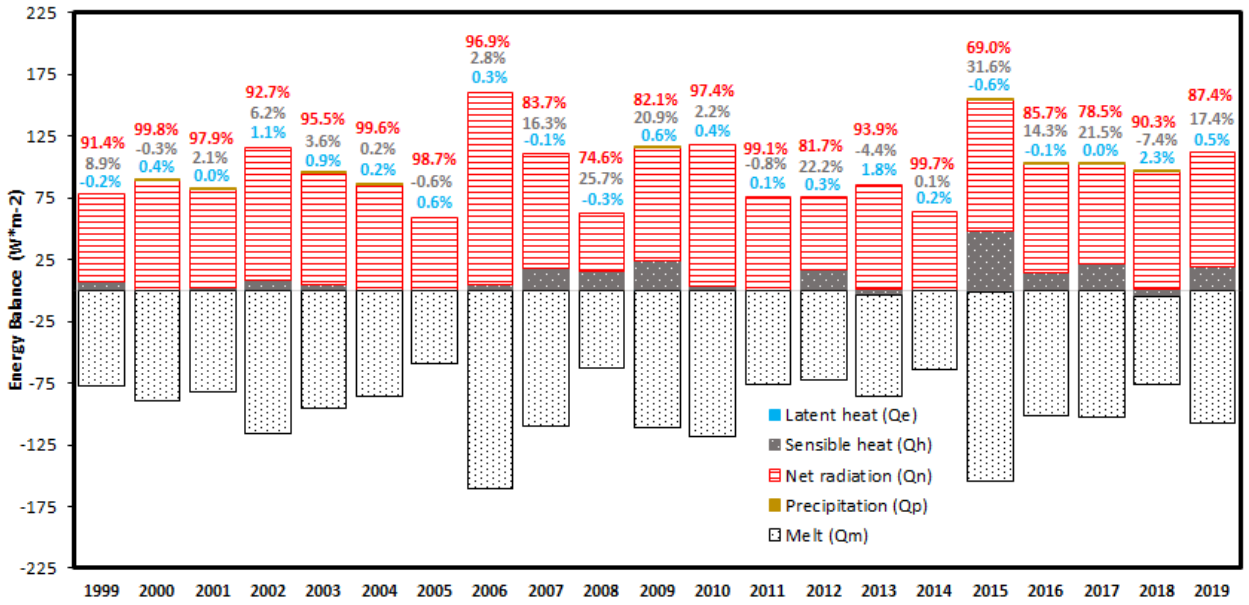

Figure 3.8: The energy balance with a high end of winter SWE (h-SWE) of net radiation (h-Qn), sensible heat flux (h-Qh), latent heat flux (h-Qe), and heat from rainfall (h-Qp) as a percentage of the total energy required for melt (h-Qm), with a SWE of 370 mm over a large drift in TMM.

surface which would result in melt. The heat content of precipitation over the record period ranged between 0 to 0.01 %. With the abundance of SWE to initiate snowmelt, higher levels of energy are available for melt. We can see that, despite the differences in atmospheric conditions of each year, the end of winter SWE positively drives the energy that is available for melt, with an R^2 value of 0.82 (Figure 3.9a). This would suggest that with a decrease in the end of winter SWE, the rate of melt would respectively decrease. However, this is not always the case, the increase in melt rate is also a direct result of the changes in atmospheric controls such as air temperature, humidity, and solar radiation that influence the energy available for melt. In fact, various years (1999 – 2001, 2011, 2014, 2018) driven by big drift that have lower Q_m, as shown in Figure 3.9b. Therefore, the end of winter SWE is not the only factor that control the changes in the snowmelt period. The combination of other factors like meteorological controls must also be considered.

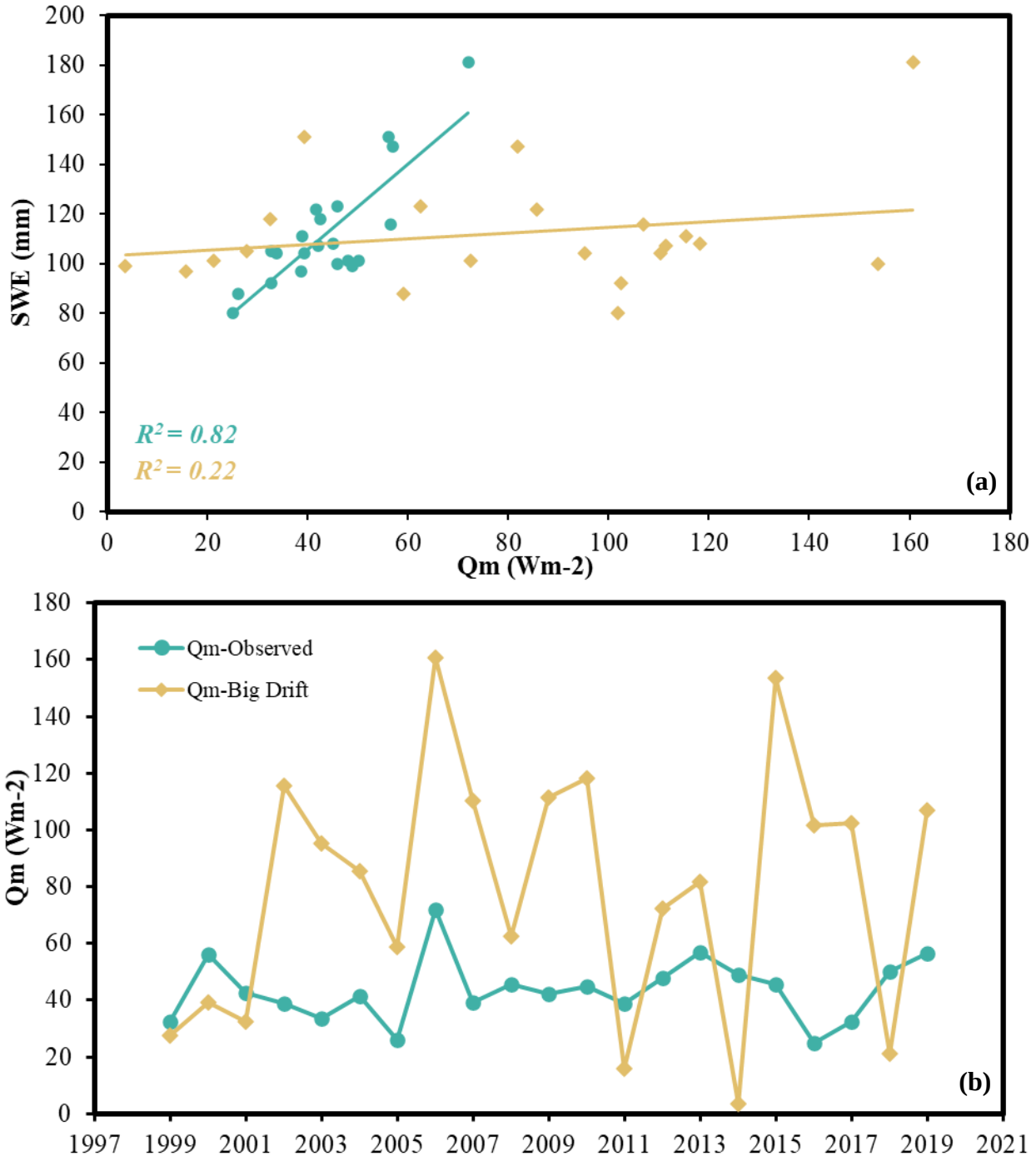

Figure 3.9: (a) A positive relationship between the end of winter SWE and Qm over the snowmelt period. (b) The comparison between the energy available for melt from the observed SWE and h-SWE of a nearby big drift site.

Table 3.1: A summary of trends for the onset of snowmelt, end of the snow-covered period, duration of snowmelt and energy balance components. The MK trend test was used to detect for monotonic trends, accompanied by Theil Sen's slope estimator to calculate for the magnitude of the trend. The NSE, MB, and coefficient of determination were used to test the model. Significant trends are noted with bolded p-values.

Summary Table	*Trend	**Slope (rate per decade)	P-value	NSE	R^2	MB
SWE	↓	8.8 mm	0.065			
Qn	↑	4.3 W/m2	0.29			
Qh	↑	0.8 W/m2	0.43			
Qe	-	-	0.17			
Qp	-	-	0.22			
Qm	↑	2.5 W/m2	0.49			
Melt Rate	↑	0.7 mm/day	0.49			
Onset of Melt	**Earlier**	**7 days**	**0.0026**			
End of Melt (Obs)	**Earlier**	**10 days**	**0.00087**			
Duration (Obs)	↓	**2.5 days**	**0.034**			
End of Melt (CRHM)	**Earlier**	**8.5 days**	**0.0083**	0.8	0.86	-0.01
Duration (CRHM)	↓	1 day	0.38	-0.28	0.26	-0.14

*Mann-Kendall Test was used to detect the monotonic trends

**Theil Sen's slope estimator

3.4 Conclusion

To conclude, snow plays an important role in the energy fluxes of arctic regions (Marsh & Pomeroy, 1996). This spring snowmelt period has shown a rapid and dramatic change in the surface energy fluxes. It is critical to continue with hydrological and climate predictions to properly understand the surface energy balance during the snowmelt period. The robust physically based hydrological modelling can confidently perform better, unlike the simple temperature index models, which are not a reliable method in open environments to estimate the energy balance and snowmelt rates. Despite no trends detected for each of the energy balance components, net radiative flux and sensible heat flux have shown signs of increase. There were no changes from latent heat flux and heat flux from rainfall during the snowmelt period. With the abundance of SWE from a big snow drift, the changes in the snowmelt period are composed of a

combination of the end of winter SWE and the changes in atmospheric controls. The energy balance enabled this study to investigate the changes in melt rate during the snowmelt period. The melt rate at TMM has increased by 1.4 mm/day at a rate of 0.7 mm/day per decade. It is difficult to conclude whether meteorological conditions or the end of winter SWE have greater impacts to the changes in snowmelt rates. An in-depth examination of the correlation between each meteorological condition and the changes in the timing and duration of snowmelt will be required. However, the shifts in timing and rate of snowmelt in a warmer spring will have major implications to the changes in spring snowmelt runoff, leading to flood risks, and increased wildfire severity (Westerling et al., 2006). Flood risks may increase if warming temperatures persist, triggering more rain-on-snow events, which will be important considerations for water resource management. Delayed runoff can lead to an earlier and longer dry season, providing greater opportunities for large fires.

A shift towards earlier onset of snowmelt has led to a shorter snowmelt period as climate conditions, like warming temperature or increased radiation, has amplified the melt rate. The end of the snow-covered period was well described by the simulated albedo values. The albedo estimations had a significant decreased by 8.5 days per decade. The negative model bias of simulated albedo indicates an underestimation by approximately 1 %. However, the observed duration of melt were better predictors than the estimated values from CRHM. No trend was detected for the simulated duration of the snowmelt period. This is due to the collection variability from the onset of snowmelt and the end of melt. The negative model bias of the simulated duration of melt indicates an underestimation by approximately 14 %. The methodological nature and limited time span of this study cannot directly address the issue of data set quality, but could provide further insight, given that at least part of the discrepancy

among data sets is likely rooted in the combination of surface and atmosphere interactions during the snowmelt period.

References

Adam, J. C., Hamlet, A. F., & Lettenmaier, D. P. (2009). Implications of global climate change for snowmelt hydrology in the twenty-first century. *Hydrological Processes*, *23*, 962–972. https://doi.org/10.1002/hyp

Anttila, K., Manninen, T., Jääskeläinen, E., Riihelä, A., & Lahtinen, P. (2018). The role of climate and land use in the changes in surface albedo prior to snow melt and the timing of melt season of seasonal snow in northern land areas of 40°N-80°N during 1982-2015. *Remote Sensing*, *10*(10). https://doi.org/10.3390/rs10101619

Armstrong, R. N., Pomeroy, J. W., & Martz, L. W. (2010). Estimating evaporation in a prairie landscape under drought conditions. *Canadian Water Resources Journal*, *35*(2), 173–186. https://doi.org/10.4296/cwrj3502173

Brown, R. D., & Braaten, R. O. (1998). Spatial and temporal variability of Canadian monthly snow depths, 1946-1995. *Atmosphere - Ocean*, *36*(1), 37–54. https://doi.org/10.1080/07055900.1998.9649605

Burd, J. A., Peterson, P. K., Nghiem, S. V., Perovich, D. K., & Simpson, W. R. (2017). Snowmelt onset hinders bromine monoxide heterogeneous recycling in the Arctic Justine. *Journal of Geophysical Research: Atmospheres*, *122*, 8297–8309. https://doi.org/10.1002/2017JD026906

Burn, D. H. (2008). Climatic influences on streamflow timing in the headwaters of the Mackenzie River Basin. *Journal of Hydrology*, *352*(1–2), 225–238. https://doi.org/10.1016/j.jhydrol.2008.01.019

Burn, D. H., Cunderlik, J. M., & Pietroniro, A. (2004). Hydrological trends and variability in the Liard River basin. *Hydrological Sciences Journal*, *49*(1), 53–67. https://doi.org/10.1623/hysj.49.1.53.53994

Cheng, C. L., Shalabh, & Garg, G. (2014). Coefficient of determination for multiple measurement error models. *Journal of Multivariate Analysis*, *126*, 137–152. https://doi.org/10.1016/j.jmva.2014.01.006

Cline, D. W. (1997). Snow surface energy exchanges and snowmelt at a continental, midlatitude Alpine site. *Water Resources Research*, *33*(4), 689–701. https://doi.org/10.1029/97WR00026

Colaizzi, P. D., O'Shaughnessy, S. A., Gowda, P. H., Evett, S. R., Howell, T. A., Kustas, W. P., & Anderson, M. C. (2010). Radiometer Footprint Model to Estimate Sunlit and Shaded Components for Row Crops. *Agronomy Journal*, *102*(3), 942–955. https://doi.org/10.2134/agronj2009.0393

Datt, P., Srivastava, P. K., Negi, P. S., & Satyawali, P. K. (2008). Surface energy balance of seasonal snow cover for snow-melt estimation in N-W Himalaya. *Journal of Earth System Science*, *117*(5), 567–573. https://doi.org/10.1007/s12040-008-0053-7

Déry, S. J., & Brown, R. D. (2007). Recent Northern Hemisphere snow cover extent trends and implications for the snow-albedo feedback. *Geophysical Research Letters*, *34*(22), 2–7. https://doi.org/10.1029/2007GL031474

Dornes, P. F., Pomeroy, J. W., Pietroniro, A., Carey, S. K., & Quinton, W. L. (2008). Influence of landscape aggregation in modelling snow-cover ablation and snowmelt runoff in a sub-arctic mountainous environment. *Hydrological Sciences Journal*, *53*, 725–740. https://doi.org/10.1623/hysj.53.4.725

Fang, X., & Pomeroy, J. W. (2008). Drought impacts on Canadian prairie wetland snow hydrology. *Hydrological Processes*, *22*, 2858–2873.

Fang, X., Pomeroy, J. W., Ellis, C. R., MacDonald, M. K., Debeer, C. M., & Brown, T. (2013). Multi-variable evaluation of hydrological model predictions for a headwater basin in the Canadian Rocky Mountains. *Hydrology and Earth System Sciences*, *17*(4), 1635–1659. https://doi.org/10.5194/hess-17-1635-2013

Fang, X., Pomeroy, J. W., Westbrook, C. J., Guo, X., Minke, A. G., & Brown, T. (2010). Prediction of snowmelt derived streamflow in a wetland dominated prairie basin. *Hydrology and Earth System Sciences*, *14*, 1–16. https://doi.org/10.5194/hess-14-1-2010

Fang, Xing, & Pomeroy, J. (2020). Diagnosis of future changes in hydrology for a Canadian Rocky Mountain headwater basin. *Hydrology and Earth System Sciences Discussions*, *d*(January), 1–40. https://doi.org/10.5194/hess-2019-640

Fang, Xing, & Pomeroy, J. W. (2016). Impact of antecedent conditions on simulations of a flood in a mountain headwater basin. *Hydrological Processes*, *30*(16), 2754–2772. https://doi.org/10.1002/hyp.10910

Flügel, W. A. (1995). Delineating hydrological response units by geographical information system analyses for regional hydrological modelling using PRMS/MMS in the drainage basin of the River Bröl, Germany. *Hydrological Processes*, *9*(3–4), 423–436. https://doi.org/10.1002/hyp.3360090313

Gleason, K. E., McConnell, J. R., Arienzo, M. M., Chellman, N., & Calvin, W. M. (2019). Four-fold increase in solar forcing on snow in western U.S. burned forests since 1999. *Nature Communications*, *10*(1), 1–8. https://doi.org/10.1038/s41467-019-09935-y

Granger, R. J., & Male, D. H. (1978). Melting of a Prairie Snowpack. *Journal of Applied Meteorology*, *17*, 1833–1842.

Gray, D. M., & Landine, P. G. (1988). An energy-budget snowmelt model for the Canadian Prairies. *Canadian Journal of Earth Sciences*, *25*(8), 1292–1303. https://doi.org/10.1139/e88-124

Hamed, K. H. (2008). Trend detection in hydrologic data: The Mann-Kendall trend test under the scaling hypothesis. *Journal of Hydrology*, *349*(3–4), 350–363. https://doi.org/10.1016/j.jhydrol.2007.11.009

Helsel, D. R., & Hirsch, R. M. (1992). Statistical methods in water resources. *Statistical Methods in Water Resources*, *49*(February), 1–510. https://doi.org/10.2307/1269385

Jitnikovitch, A. (2019). *Cosmic ray sensors for the continuous measurement of Arctic snow accumulation and melt*. Wilfrid Laurier University.

Kendall, M. (1975). *Rank correlation methods*. London, UK: Griffin.

Krogh, S. A., & Pomeroy, J. W. (2018). Recent changes to the hydrological cycle of an Arctic

basin at the tundra-taiga transition. *Hydrology and Earth System Sciences*, *22*(7), 3993–4014. https://doi.org/10.5194/hess-22-3993-2018

Krogh, S. A., Pomeroy, J. W., & Marsh, P. (2017). Diagnosis of the hydrology of a small Arctic basin at the tundra-taiga transition using a physically based hydrological model. *Journal of Hydrology*, *550*, 685–703. https://doi.org/10.1016/j.jhydrol.2017.05.042

Krogh, S. A., Pomeroy, J. W., & McPhee, J. (2015). Physically based mountain hydrological modeling using reanalysis data in Patagonia. *Journal of Hydrometeorology*, *16*(1), 172–193. https://doi.org/10.1175/JHM-D-13-0178.1

Kumar, M., Marks, D., Dozier, J., Reba, M., & Winstral, A. (2013). Evaluation of distributed hydrologic impacts of temperature-index and energy-based snow models. *Advances in Water Resources*, *56*, 77–89. https://doi.org/10.1016/j.advwatres.2013.03.006

Leavesley, G. H., Markstrom, S. L., Restrepo, P. J., & Viger, R. J. (2002). A modular approach to addressing model design, scale, and parameter estimation issues in distributed hydrological modelling. *Hydrological Processes*, *16*(2), 173–187. https://doi.org/10.1002/hyp.344

Lettenmaier, D. P., Wood, E. F., & Wallis, J. R. (1994). Hydro-Climatological Trends in the Continental United States , 1948 – 88. *Journal of Climate*, *7*(4), 586–607.

López-Moreno, J. I., Boike, J., Sanchez-Lorenzo, A., & Pomeroy, J. W. (2016). Impact of climate warming on snow processes in Ny-Ålesund, a polar maritime site at Svalbard. *Global and Planetary Change*, *146*, 10–21. https://doi.org/10.1016/j.gloplacha.2016.09.006

Male, D. H., & Granger, R. J. (1981). Snow surface energy exchange. *Water Resources Research*, *17*(3), 609–627. https://doi.org/10.1029/WR017i003p00609

Malik, M. J., Van Der Velde, R., Vekerdy, Z., & Su, Z. (2014). Improving modeled snow albedo estimates during the spring melt season. *Journal of Geophysical Research (Atmospheres)*, *119*(10), 7311–7331. https://doi.org/10.1002/ 2013JD021344

Mann, H. B. (1945). Nonparametric Tests Against Trend. *Econometrica*, *13*(3), 245–259.

Marks, D., & Dozier, J. (1992). Climate and energy exchange at the snow surface in the Alpine Region of the Sierra Nevada: 2. Snow cover energy balance. *Water Resources Research*, *28*(11), 3043–3054. https://doi.org/10.1029/92WR01483

Marsh, P., Bartlett, P., MacKay, M., Pohl, S., & Lantz, T. (2010). Snowmelt energetics at a shrub tundra site in the western Canadian Arctic. *Hydrological Processes*, *24*(25), 3603–3620. https://doi.org/10.1002/hyp.7786

Marsh, P., Onclin, C., & Neumann, N. (2002). Water and energy fluxes in the lower Mackenzie valley, 1994/95. *Atmosphere - Ocean*, *40*(2), 245–256. https://doi.org/10.3137/ao.400211

Marsh, P., & Pomeroy, J. (1996). Meltwater fluxes at an arctic forest-tundra site. *Hydrological Processes*, *10*(10), 1383–1400. https://doi.org/10.1002/(SICI)1099-1085(199610)10:10<1383::AID-HYP468>3.0.CO;2-W

Marsh, P., Pomeroy, J., & Quinton, B. (1995). Hydrological Processes and Runoff at the Arctic Treeline in Northwestern Canada. *10th Annual Northern Basins Symposium*, 368–397.

Marsh, P., Pomeroy, J., Pohl, S., Quiton, W., Onclin, C., Russel, M., Neumann, N., Pietroniro, A., Davison, B. & McCartney, S. (2008). Snowmelt Processes and Runoff at the Arctic Treeline: Ten Years of MAGS Research. *Cold Region Atmospheric and Hydrologic Studies. The Mackenzie GEWEX Experience*, *2*(January), 97–123. https://doi.org/10.1007/978-3-540-75136-6

Mioduszewski, J. R., Rennermalm, a K., Robinson, D. a, & Mote, T. L. (2014). Attribution of snowmelt onset in Northern Canada. *Journal of Geographical Sciences*, *119*, 9638–9653. https://doi.org/10.1002/2013JD021024

Moore, J. N., Harper, J. T., & Greenwood, M. C. (2007). Significance of trends toward earlier snowmelt runoff, Columbia and Missouri Basin headwaters, western United States. *Geophysical Research Letters*, *34*(16). https://doi.org/10.1029/2007GL031022

Moriasi, D. N., Arnold, J. G., Van Liew, M. W., Binger, R. L., Harmel, R. D., & Veith, T. L. (2007). Model evaluation guidelines for systematic quantification of accuracy in watershed simulations. *Transactions of the ASABE*, *50*(3), 885–900.

Nash, J. E., & Sutcliffe, J. V. (1970). River flow forecasting through conceptual models part I - A discussion of principles. *Journal of Hydrology*, *10*(3), 282–290. https://doi.org/10.1016/0022-1694(70)90255-6

Ohmura, A. (2001). Physical Basis for the Temperature-Based Melt-Index Method. *Journal of Applied Meteorology*, *40*(4), 753–761. https://doi.org/10.1175/1520-0450(2001)040<0753:PBFTTB>2.0.CO;2

Pohl, S., Marsh, P., & Bonsal, B. R. (2007). Modeling the impact of climate change on runoff and annual water balance of an arctic headwater basin. *Arctic*, *60*(2), 173–186. https://doi.org/10.14430/arctic242

Pohl, S., Marsh, P., & Liston, G. E. (2006). Spatial-temporal variability in solar radiation during spring snowmelt. *Arctic, Antarctic, and Alpine Research*, *38*(1), 136–146.

Pomeroy, J. W., & Granger, R. J. (1997). Sustainability of the western Canadian boreal forest under changing hydrological conditions. I. Snow accumulation and ablation. *IAHS-AISH Publication*, *240*, 237–242.

Pomeroy, J. W., & Li, L. (2000). Prairie and arctic areal snow cover mass balance using a blowing snow model. *Journal of Geophysical Research: Atmospheres*, *105*, 26619–26634. https://doi.org/10.1029/2000JD900149

Pomeroy, J W, Gray, D. M., Brown, T., Hedstrom, N. R., Quinton, W. L., & Granger, R. J. (2007). The Cold Regions Hydrological Model , a Platform for Basing Process Representation and Model Structure on Physical Evidence. *Hydrological Processes*, *21*(19), 2650–2667. https://doi.org/10.1002/hyp.6787

Pomeroy, John W., Fang, X., & Marks, D. G. (2016). The cold rain-on-snow event of June 2013 in the Canadian Rockies — characteristics and diagnosis. *Hydrological Processes*, *30*(17), 2899–2914. https://doi.org/10.1002/hyp.10905

Quinton, W. L., & Marsh, P. (1999). A conceptual framework for runoff generation in a permafrost environment. *Hydrological Processes*, *13*(16), 2563–2581. https://doi.org/10.1002/(SICI)1099-1085(199911)13:16<2563::AID-HYP942>3.0.CO;2-D

Rasouli, K., Pomeroy, J. W., Janowicz, J. R., Carey, S. K., & Williams, T. J. (2014). Hydrological sensitivity of a northern mountain basin to climate change. *Hydrological Processes*, *28*(14), 4191–4208. https://doi.org/10.1002/hyp.10244

Roux, M. J., Harwood, L. A., Zhu, X., & Sparling, P. (2015). Early summer near-shore fish assemblage and environmental correlates in an Arctic estuary. *Journal of Great Lakes Research*, *42*(2), 256–266. https://doi.org/10.1016/j.jglr.2015.04.005

Shi, X., Déry, S. J., Groisman, P. Y., & Lettenmaier, D. P. (2013). Relationships between recent pan-arctic snow cover and hydroclimate trends. *Journal of Climate*, *26*(6), 2048–2064. https://doi.org/10.1175/JCLI-D-12-00044.1

Shi, X., Groisman, P. Y., Déry, S. J., & Lettenmaier, D. P. (2011). The role of surface energy fluxes in pan-Arctic snow cover changes. *Environmental Research Letters*, *6*(3). https://doi.org/10.1088/1748-9326/6/3/035204

Shi, X., Marsh, P., & Yang, D. (2015). Warming spring air temperatures, but delayed spring streamflow in an Arctic headwater basin. *Environmental Research Letters*, *10*(6), 064003. https://doi.org/10.1088/1748-9326/10/6/064003

Shi, X., Wood, A. W., & Lettenmaier, D. P. (2008). How essentialis hydrologic model calibration to seasonal stream flow forecasting? *Journal of Hydrometeorology*, *9*(6), 1350–1363. https://doi.org/10.1175/2008JHM1001.1

Sturm, M., Taras, B., Liston, G. E., Derksen, C., Jonas, T., & Lea, J. (2010). Estimating snow water equivalent using snow depth data and climate classes. *Journal of Hydrometeorology*, *11*(6), 1380–1394. https://doi.org/10.1175/2010JHM1202.1

Tedesco, M., Brodzik, M., Armstrong, R., Savoie, M., & Ramage, J. (2009). Pan arctic terrestrial snowmelt trends (1979 – 2008) from spaceborne passive microwave data and correlation with the Arctic Oscillation. *Geophysical Research Letters*, *36*(September), 1–6. https://doi.org/10.1029/2009GL039672

Theil, H. (1950). A rank-invariant method of linear and polynomial. *Series A Mathematical Sciences*, *53*, 387–392.

Theil, Henri. (1950). A Rank-Invariant Method of Linear and Polynomial Regression Analysis (pp. 345–381). Springer, Dordrecht. https://doi.org/10.1007/978-94-011-2546-8_20

Thompson, C., Beringer, J., Chapin, F. S., & McGuire, A. D. (2004). Structural complexity and land-surface energy exchange along a gradient from arctic tundra to boreal forest. *Journal of Vegetation Science*, *15*(3), 397–406. https://doi.org/10.1111/j.1654-1103.2004.tb02277.x

Tsui, Matthew Y. T., & Marsh, Philip (2021). Hydrometeorological data and energy balance data, 1999-2019, Trail Valley Creek, Northwest Territories. https://doi.org/10.5683/SP3/MCDA2R.

Van Mullem, J. A., & Garen, D. (2004). Snowmelt. In *Hydrology National Engineering Handbook* (pp. 1–21). Portland, Oregon.

Van Pelt, W. J. J., Pohjola, V. A., & Reijmer, C. H. (2016). The changing impact of snow conditions and refreezing on the mass balance of an idealized svalbard glacier. *Frontiers in Earth Science*, *4*(November), 1–15. https://doi.org/10.3389/feart.2016.00102

Weber, M., Bernhardt, M., Pomeroy, J. W., Fang, X., Härer, S., & Schulz, K. (2016). Description of current and future snow processes in a small basin in the Bavarian Alps. *Environmental Earth Sciences*, *75*(17). https://doi.org/10.1007/s12665-016-6027-1

Westerling, A. L., Hidalgo, H. G., Cayan, D. R., & Swetnam, T. W. (2006). Warming and earlier spring increase Western U.S. forest wildfire activity. *Science*, *313*(5789), 940–943. https://doi.org/10.1126/science.1128834

Wilcox, E. J., Keim, D., Jong, T. De, Walker, B., Sonnentag, O., Sniderhan, A. E., Mann, P., & Marsh, P. (2019). Tundra shrub expansion may amplify permafrost thaw by advancing snowmelt timing. *Arctic Science*, *5*, 202–217. https://doi.org/dx.doi.org/10.1139/as-2018-0028

Yip, Q. K. Y., Burn, D. H., Seglenieks, F., Pietroniro, A., & Soulis, E. D. (2012). Climate impacts on hydrological variables in the Mackenzie River Basin. *Canadian Water Resources Journal*, *37*(3), 209–230. https://doi.org/10.4296/cwrj2011-899

Zhang, T., Bowling, S. A., & Stamnes, K. (1997). Impact of the atmosphere on surface radiative fluxes and snowmelt in the Arctic and Subarctic. *Journal of Geophysical Research*, *102*(D4), 4287–4302.

Zhang, X., Vincent, L. A., Hogg, W. D., & Niitsoo, A. (2000). Temperature and precipitation trends in Canada during the 20th century. *Atmosphere - Ocean*, *38*(3), 395–429. https://doi.org/10.1080/07055900.2000.9649654

Zhou, J., Pomeroy, J. W., Zhang, W., Cheng, G., Wang, G., & Chen, C. (2014). Simulating cold regions hydrological processes using a modular model in the west of China. *Journal of Hydrology*, *509*, 13–24. https://doi.org/10.1016/j.jhydrol.2013.11.013

CHAPTER 4: Conclusion and Recommendations

4.1 Summary

Previous studies have demonstrated that the arctic is warming (Bonsal & Kochtubajda, 2009; Fouché et al., 2017; White et al., 2007) and snowmelt is occurring earlier (Brown & Braaten, 1998; Shi et al., 2015). This has led to a shorter period of melt (Bavay et al., 2013), which would partly suggest higher melt rates during the spring period. However, little is known about the changes in the details of the snowmelt period. This study has investigated the changes to the onset and the duration of snowmelt, the influences of the meteorological conditions, the changes in melt rates and surface energy balance during the snowmelt period for our research site in northwestern Canada.

Chapter 2 has shown an early onset and end of snowmelt which defined a shorter snowmelt period at Trail Valley Creek (TVC). The changes in temperature and albedo had a considerable impact on spring snowmelt. Spring air temperature and relative humidity were key conditions that had significantly increased during the spring snowmelt period. On the other hand, SWE, precipitation, wind speed, refreeze events, incoming shortwave and longwave radiation did not result to any significant trend. Nonetheless, the end of winter SWE has decreased, and with less snow at the start of melt, this presents major changes to the duration and rate of melt.

Chapter 3 examined the changes to rate of snowmelt and the energy balance during the snowmelt period. The energy balance has shown the dominance of radiative fluxes in comparison to turbulent and advective fluxes during the snowmelt period. On average, 77 % of the total energy for snowmelt is due to net radiation. The model estimated end of melt albedo with considerable success, with an NSE value of 0.8, indicates that the model predictions were exceptional good to the observed albedo. Although the simulated end of snowmelt albedo was

underestimated at an average of approximately two days, a significant trend has demonstrated the ability to estimated surface albedo over the TVC watershed. This has also led to an underestimated duration of snowmelt, solely due to the simulated albedo values. However, the estimated duration of melt indicates that the observed mean is a better predictor than the model. Under a warming climate and increased radiative energy to the snow surface, the end of winter SWE has decreased by 8.8 mm per decade and the rate of snowmelt has increased by 0.7 mm/day per decade over the last 21 years. The combination of low SWE and higher melt rate, in conjunction with interannual variability in the meteorological conditions is resulting in shorter duration of the melt period.

4.2 Future Implications

There is increasing evidence that environmental changes have reached an unprecedented level. Many of these changes are related to the hydrological cycle and can result from both the direct and indirect impacts of human activities. Global change are results of anthropogenic causes that stimulated a variety of research focused on predicting future climate and its effects on the Earth. The consequence of climate warming and earlier snowmelt has increased the intensity, duration and frequency of forest fires (Balch et al., 2017; Dennison et al., 2014) and snowmelt floods in many regions of Canada (Stadnyk et al., 2016). In Canada, floods occur five times as often as other natural disasters and damage estimates are billions of dollars (Fang & Pomeroy, 2016; Sandink et al., 2010). These environmental changes will likely continue in the future, representing challenges for water resources managers throughout the Canada.

Shi et al. (2015) has shown that an earlier start of melt but delayed runoff may be due to a longer melt period, decreasing fluxes during the melt period, and more end of winter SWE. However, this study has shown opposite trends, with warmer temperatures that led to an earlier

start of melt resulted in a shorter melt period, increasing fluxes, and decreased end of winter SWE. Therefore, other factors like deeper active layer that can store more meltwater or increased shrubs resulting in more drift needs to be considered before it is possible to unequivocally attribute the observed trends and variability to climatic changes. Further study is warranted to investigate the effects of variations in forcing variables, such as wind direction and cloud cover, which affects both surface radiative and turbulent heat fluxes. The use of remote sensing approach to detect melt-refreeze events will provide an improved estimation, in particular to refreeze events over the spring snowmelt. This may include microwave backscatter measurements from the SeaWinds instrumentation on the QuikSCAT satellite. The dependence and correlation between each meteorological conditions during the snowmelt period can be better understood utilizing multiple regression models. Stepwise multiple regression can be used to assess the relative importance of the explanatory variables in determining the response of snowmelt onset. There are many uncertainties in the study of onset of snowmelt and the influences of temporal variability from meteorological conditions, these would potentially be remarkable research opportunities for the hydrometeorological community.

References

Balch, J. K., Bradley, B. A., Abatzoglou, J. T., Chelsea Nagy, R., Fusco, E. J., & Mahood, A. L. (2017). Human-started wildfires expand the fire niche across the United States. *Proceedings of the National Academy of Sciences of the United States of America*, *114*(11), 2946–2951. https://doi.org/10.1073/pnas.1617394114

Bavay, M., Grünewald, T., & Lehning, M. (2013). Response of snow cover and runoff to climate change in high Alpine catchments of Eastern Switzerland. *Advances in Water Resources*, *55*(2013), 4–16. https://doi.org/10.1016/j.advwatres.2012.12.009

Bonsal, B. R., & Kochtubajda, B. (2009). An assessment of present and future climate in the Mackenzie Delta and the near-shore Beaufort Sea region of Canada. *International Journal of Climatology*, *29*, 1780–1795. https://doi.org/10.1002/joc.1812

Brown, R. D., & Braaten, R. O. (1998). Spatial and temporal variability of Canadian monthly snow depths, 1946-1995. *Atmosphere - Ocean*, *36*(1), 37–54. https://doi.org/10.1080/07055900.1998.9649605

Dennison, P. E., Brewer, S. C., Arnold, J. D., & Moritz, M. A. (2014). Large wildfire trends in the western United States, 1984-2011. *Geophysical Research Letters*, *41*(8), 2928–2933. https://doi.org/10.1002/2014GL059576

Fang, X., & Pomeroy, J. W. (2016). Impact of antecedent conditions on simulations of a flood in a mountain headwater basin. *Hydrological Processes*, *30*(16), 2754–2772. https://doi.org/10.1002/hyp.10910

Fouché, J., Lafrenière, M. J., Rutherford, K., & Lamoureux, S. (2017). Seasonal hydrology and permafrost disturbance impacts on dissolved organic matter composition in High Arctic headwater catchments. *Arctic Science*, *3*(2), 378–405. https://doi.org/10.1139/as-2016-0031

Sandink, D., Kovacs, P., Oulahen, G., & McGillivray, G. (2010). *Making Flood Insurable for Canadian Homeowners: A Discussion Paper*. Toronto, Canada: Institute for Catastrophic Loss Reduction & Swiss Reinsurance Company Ltd.

Shi, X., Marsh, P., & Yang, D. (2015). Warming spring air temperatures, but delayed spring streamflow in an Arctic headwater basin. *Environmental Research Letters*, *10*(6), 064003. https://doi.org/10.1088/1748-9326/10/6/064003

Stadnyk, T., Dow, K., Wazney, L., & Blais, E. L. (2016). The 2011 flood event in the Red River Basin: Causes, assessment and damages. *Canadian Water Resources Journal*. Taylor and Francis Ltd. https://doi.org/10.1080/07011784.2015.1008048

White, D., Hinzman, L., Alessa, L., Cassano, J., Chambers, M., Falkner, K., Francis, J., Gutowski, W. J., Holland, M., Holmes, R. M., Huntington, H., Kane, D., Kliskey, A., Lee, C., McClelland, J., Peterson, B., Rupp, T. S., Straneo, F., Steele, M., Woodgate, R., Yang, D., Yoshikawa, K., & Zhang, T. (2007). The arctic freshwater system: Changes and impacts. *Journal of Geophysical Research: Biogeosciences*, *112*(G4), n/a-n/a. https://doi.org/10.1029/2006jg000353

Appendix

Appendix A: *A catalog of meteorological instruments used at TMM and TUP, followed by descriptive specifications of each parameter. For this study, data began recording on August 1998 with the Campbell 21X datalogger. In 2006, the datalogger was updated to a CR23X and again to a CR1000 in 2017. Each parameter were measured every half-hour.*

TMM Meteorological Instruments				
Parameter	Unit	Instrument Name	Height	Accuracy
Air Temperature	°C	HMP35CF	1.5 m a.g.s.	• +/- 0.4 °C over the range of –24 °C to +48 °C • +/- 9 °C over the range of –38 °C to +53 °C
Relative Humidity	%	HMP35CF	1.5 m a.g.s.	• +/-2 % RH from 0 to 90 % • +/-3 % RH from 90 to 100 %
Precipitation	mm	Tipping bucket	1.25 m a.g.s.	• +/- 3 % when rainfall range from 10 to 20 mm/hr • +/- 5 % when rainfall range from 20 to 30 mm/hr
		Geonor T200B (added in 2006)	1.9 m a.g.s.	• +/- 0.1 mm per 30 minutes
Wind Speed	m/s	NRG40	2.55 m a.g.s.	• +/-0.45 m/s at 10 m/s
		05103-10 RM Young (added in 2008)	5.5 m a.g.s.	• +/- 0.3 m/s
Downward Solar	W/m^2	REBS PDS 7.1 Radiometer	2.85 m a.g.s.	
		CNR1 Radiometer (added in 2006)	2.37 m a.g.s.	• +/-10% expected accuracy for daily sums
Downward Infrared		CNR1 Radiometer (added in 2006)	2.37 m a.g.s.	• +/-10% expected accuracy for daily sums
Upward Solar		REBS PDS 7.1 Radiometer	2.85 m a.g.s.	
		CNR1 Radiometer (added in 2006)	2.37 m a.g.s.	• +/-10% expected accuracy for daily sums
Upward Infrared		CNR1 Radiometer (added in 2006)	2.37 m a.g.s.	• +/-10% expected accuracy for daily sums

TUP Meteorological Instruments				
Parameter	Unit	Instrument Name	Height	Accuracy
Air Temperature	°C	HMP35CF	1.5 m a.g.s.	• +/- 0.4 °C over the range of –24 °C to +48 °C • +/- 9 °C over the range of –38 °C to +53 °C
		HMP45C212 (added in 2012)	1.5 m a.g.s.	
Relative Humidity	%	HMP35CF	1.5 m a.g.s.	• +/-2 % RH from 0 to 90 % • +/-3 % RH from 90 to 100 %
		HMP45C212 (added in 2012)		
Precipitation	mm	TE525M Tipping bucket	1.2 m a.g.s.	• +/- 3 % when rainfall range from 10 to 20 mm/hr • +/- 5 % when rainfall range from 20 to 30 mm/hr
Wind Speed	m/s	NRG40	1.21 m a.g.s.	• +/-0.45 m/s at 10 m/s
		05103-10 RM Young (added in 2008)	3.25 m a.g.s.	• +/- 0.3 m/s
Downward Solar	W/m^2	Eppley B&W Radiometer	1.32 m a.g.s.	• <10 Wm^{-2}
		CNR1 Radiometer (added in 2006)	1.15 m a.g.s.	• +/-10% expected accuracy for daily sums
Downward Infrared		CNR1 Radiometer (added in 2006)	1.15 m a.g.s.	• +/-10% expected accuracy for daily sums
Upward Solar		Eppley B&W Radiometer	1.32 m a.g.s.	• <10 Wm^{-2}
		CNR1 Radiometer (added in 2006)	1.15 m a.g.s.	• +/-10% expected accuracy for daily sums
Upward Infrared		CNR1 Radiometer (added in 2006)	1.15 m a.g.s.	• +/-10% expected accuracy for daily sums

Appendix B: *Model parameter values used for the albedo, PBSM, and EBSM module.*

HRU parameters	
area	2 km^2
elevation	87 m
Latitude	69.3161
New snowfall albedo	0.85
Bare ground albedo	0.19
Vegetation height	0.1 m